

DOCTORATE SCHOOL IN BIOLOGY

Cycle XXXIV



*Angiogenin-like proteins from Vertebrate
Superfamily RNases: novel functional features*



Ph.D. student

Rosanna Culurciello

Supervisor

Prof. Eliodoro Pizzo

Coordinator

Prof. Sergio Esposito

ACADEMIC YEAR 2020/2021

Riassunto	1
Summary	3
PART 1. Human angiogenin involvement in the stress response of skin cells	5
1.1. Introduction	6
1.1.1. Cellular stress response and stress-induced proteins	7
1.1.2. Human angiogenin (ANG)	15
1.1.3. ANG involvement in cell stress response	16
1.1.4. Stress granules (SGs)	18
1.1.5. Aims	22
1.2. Materials and Methods	23
1.2.1. Plasmid vectors	24
1.2.2. Heterologous proteins production and purification	24
1.2.3. Circular Dichroism analysis	25
1.2.4. Ribonucleolytic activity assays	25
1.2.5. Cell culture and treatments	26
1.2.6. Cellular extracts	27
1.2.7. Western blot analysis	27
1.2.8. Densitometric analysis	27
1.2.9. Cell viability assay	28
1.2.10. DCFH-DA assay	28
1.2.11. Real-Time quantitative PCR (RT-qPCR)	29

1.2.12. Immunofluorescence	29
1.2.13. Cell cycle analysis	30
1.2.14. Statistical analysis	30
1.3. Results	31
1.3.1. Expression of endogenous ANG and its localization in HaCaT cells	32
1.3.2. Effects of rANG on viability and homeostasis of HaCaT cells	36
1.3.3. Design, production and characterization of two new rANG variants	41
1.4. Discussion and Conclusions	52
1.5. Bibliography	57
Figure index Part 1	
Figure 1.1. Schematic view of the cellular stress response	7
Figure 1.2. Cellular Stress Response	8
Figure 1.3. Cap-dependent translation initiation	9
Figure 1.4. General translation inhibition by stress	10
Figure 1.5. 3D structure of human angiogenin	15
Figure 1.6. The biogenesis of tiRNAs	17
Figure 1.7. Structure overview of SGs	19
Figure 1.8. Mechanism of translation arrest and stress granule formation	21
Figure 1.9. ANG analysis in HaCaT cells cultured in different growth conditions	33

Figure 1.10. Immunofluorescence analysis in HaCaT cells cultured in different growth conditions	34
Figure 1.11. Immunofluorescence analysis in HaCaT cells cultured in different growth conditions	35
Figure 1.12. Amino acid sequence of rANG (PDB: 1ANG) and its predictive protein model obtained with the molecular visualization system PyMOL	36
Figure 1.13. Conformational and biocompatibility analysis of rANG	37
Figure 1.14. Immunofluorescence analysis of HaCaT treated with 2 μ M of rANG	38
Figure 1.15. Real-Time qPCR analysis of the expression of HSPA6 gene	39
Figure 1.16. DCFH-Da assay performed in HaCaT cells subjected to oxidative stress	39
Figure 1.17. Cell cycle analysis	40
Figure 1.18. Amino acid sequence of rANG _{6xHis} and its predictive protein model obtained with the molecular visualization system PyMOL	42
Figure 1.19. Amino acid sequence of rANG(Q ₃₁ Q ₃₂) _{6xHis} and its predictive protein model obtained with the molecular visualization system PyMOL	43
Figure 1.20. Structural analysis of rANG and of its variants	45
Figure 1.21. Thermal unfolding curves	45
Figure 1.22. Reversible thermal denaturation analysis	46
Figure 1.23. rANG variants biocompatibility with HaCaT cells	47
Figure 1.24. Internalization in HaCaT cells of rANG _{6xHis} tested by immunofluorescence (A) and Z-stack analysis (B)	48

Figure 1.25. Internalization in HaCaT cells of rANG(Q ₃₁ Q ₃₂) _{6xHis} tested by immunofluorescence (A) and Z-stack analysis (B)	49
Figure 1.26. Effects of ANG variants on HSPA6 gene expression in HaCaT cells subjected to oxidative stress by sodium arsenite	50
Figure 1.27. Determination of cellular ROS by DCFH-DA assay in HaCaT cells, pre-treated rANG _{6xHis} or rANG(Q ₃₁ Q ₃₂) _{6xHis} and then subjected to oxidative stress by sodium arsenite	51
Figure 1.28. Immunofluorescence analysis of HaCaT cells subjected to oxidative stress with sodium arsenite	55
Table index	
Table 1.1. Primer sequences of selected genes	29
Table 1.2. Catalytic efficiency of rANG	37
Table 1.3. Catalytic efficiency of rANG and of its two variants	44
Table 1.4. Denaturation temperatures of rANG and of its two variants	46
PART 2. The structural features of an ancient ribonuclease from <i>Salmo salar</i> reveal an intriguing case of auto-inhibition	
2.1. Introduction	69
2.1.1. Vertebrate-secreted RNase Superfamily	70
2.1.2. Fish RNases	72
2.1.3. Mechanisms of RNases enzymatic regulation	73
2.1.4. Salmon RNases	75
2.1.5. Aims	80

2.2. Materials and Methods	82
2.2.1. Design of two mutants of SS2	83
2.2.2. Production of RNases from <i>Salmo salar</i>	84
2.2.3. Sequence analysis of SS2 from <i>Salmo salar</i> tissue	85
2.2.4. Circular Dichroism analysis	85
2.2.5. Ribonucleolytic activity assays	86
2.3. Results	87
2.3.1. SS2 gene expression analysis in <i>Salmo salar</i> muscle tissue	88
2.3.2. CD and thermal stability of SS2 and its mutants	88
2.3.3. Catalytic activity assays	90
2.3.4. Crystal structure of SS2-des116–120	91
2.4. Discussion and Conclusions	94
2.5. Bibliography	98
List of Publications	104
Appendix	105
Figure index Part 2	
Figure 2.1. Crystal structure of wild-type bovine pancreatic Ribonuclease A (PDB. 3DH5)	71
Figure 2.2. Phylogenetic tree documenting relationships among various vertebrate secretory (RNase A) ribonucleases	72

Figure 2.3. Crystal structure of SS2	77
Figure 2.4. Electron density map of SS2	78
Figure 2.5. Stereo view of SS2 superposed on RNase A (pdb: 1KF5)	78
Figure 2.6. Drawing of SS2 selected regions	79
Figure 2.7. Schemes of the possible SS2 activation mechanisms	80
Figure 2.8. pET-22b(+) vector map and corresponding multiple cloning site region (MCS)	83
Figure 2.9. Multiple alignment between coding sequence of parent SS2 and SS2 variants	84
Figure 2.10. A. Far-UV CD spectra recorded at 10 °C B. thermal denaturation profiles	89
Figure 2.11. Superimposition of the CD spectra, registered at 10 °C before heating (plane line), at 90 °C (dotted line) and at 10 °C after cooling	89
Figure 2.12. Electron density map at the P1 subsite of the mutant SS2-des116–120	92
Figure 2.13. Cartoon representation of the four SS2-des116-120 molecules (A, B, C and D) in the asymmetric unit	93
Table index Part 2	
Table 2.1. Denaturation temperature of SS2 and its two mutants	90
Table 2.2. Ribonucleolytic activity of SS2 and its two mutants	91

To all the fantastic people who accompanied me
along this incredible journey, which I hope is just
the first stop on a longer one,
thank you!



Riassunto

La Superfamiglia delle RNasi da vertebrati comprende enzimi che, oltre all'attività idrolitica necessaria alla regolazione del *turnover* dell'RNA, presentano numerose funzioni biologiche addizionali tra cui proprietà immunomodulatorie, citotossiche, neuroprotettive e stress indotte.

Fatta eccezione per alcune peculiarità strutturali, le RNasi da vertebrati sono piuttosto divergenti in termini di identità di sequenza, che variano dal 20% a quasi il 100%, e tali differenze sono alla base dell'acquisizione di nuove ed interessanti caratteristiche strutturali e funzionali.

Il presente elaborato di tesi si basa infatti sullo studio di due RNasi, filogeneticamente molto distanti, che condividono alcune caratteristiche quali la ridotta attività catalitica, la presenza di tre ponti disolfuro, la stimolazione della proliferazione cellulare (angiogenesi), ma che sono state prese in esame per due diversi aspetti, che le rendono particolarmente interessanti: la risposta allo stress in cellule della pelle (RNasi 5 umana anche nota come angiogenina) e un meccanismo di auto-regolazione dell'attività enzimatica (RNasi 2 da salmone anche nota come SS2).

La pelle rappresenta l'organo più esteso del corpo umano e allo stesso tempo anche quello più esposto a fattori stressogeni. Ad oggi non esistevano evidenze riguardo il ruolo dell'angiogenina (ANG) come RNasi stress-indotta nella pelle: nel presente lavoro è stato evidenziato per la prima volta che ANG è espressa in cellule dell'epidermide (HaCaT) ed è abile a modificare la propria localizzazione in funzione delle condizioni di crescita. Inoltre, il trattamento delle medesime cellule con ANG e sue varianti (prodotte in forma ricombinante), ha evidenziato un incremento significativo nella risposta allo stress, lasciando supporre per questa proteina un ipotetico e al tempo stesso intrigante potenziale terapeutico.

La seconda parte del presente lavoro ha riguardato invece lo studio della RNasi 2 da *Salmo salar*, nota anche come SS2, un enzima caratterizzato da un'atipica sequenza pentapeptidica addizionale nella regione C-terminale, assente in tutte le altre RNasi della Superfamiglia. Tale caratteristica strutturale ha

permesso di supporre un ipotetico meccanismo di auto-inibizione dell'attività catalitica.

La produzione e caratterizzazione di due mutanti di delezione di SS2, nonché l'analisi della struttura cristallografica di uno dei due, ha permesso di aggiungere nuove informazioni sulla ricostruzione strutturale di un sito attivo funzionale, permettendo di validare l'ipotesi di un nuovo meccanismo di auto-inibizione, mai descritto prima nella superfamiglia delle RNasi da Vertebrati.

Summary

The vertebrate RNase Superfamily includes enzymes which, in addition to the hydrolytic activity necessary for the RNA turnover regulation, have many additional biological functions including immunomodulatory, cytotoxic, neuroprotective and stress induced properties.

Except for some structural peculiarities, vertebrate RNases are quite divergent in terms of sequence identity, ranging from 20% to 100%, and these differences are the basis for the development of new and interesting structural and functional characteristics.

This work is in fact based on the study of two RNases, phylogenetically very distant, which share some characteristics such as the reduced catalytic activity, the presence of three disulphide bridges, the stimulation of cell proliferation (angiogenesis), but which here have been considered for two further different aspects, which make them particularly interesting: the contribution to stress response in skin cells (human RNase 5 also known as angiogenin) and a mechanism of self-regulation of enzymatic activity (salmon RNase 2 also known as SS2).

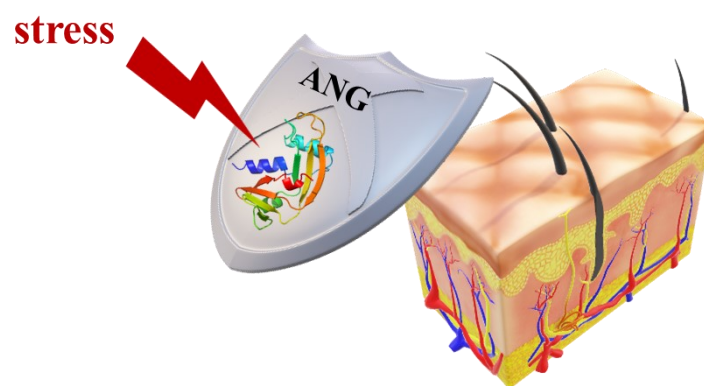
The skin is the largest organ in the human body and at the same time also the most exposed to stressful agents. To date, there was no evidence regarding the role of angiogenin (ANG) as a stress-induced RNase in the skin: in the present work it was shown for the first time that ANG is expressed in epidermal cells (HaCaT cells) and is able to modify its localization as a function of altered growth conditions. Furthermore, the treatment of the same cells with ANG and its variants (produced in recombinant form), has shown a significant increase in the stress response, suggesting a hypothetical and at the same time intriguing therapeutic potential for this protein.

The second part of this work instead concerned the study of RNase 2 from *Salmo salar*, also known as SS2, an enzyme characterized by an atypical additional pentapeptide sequence in the C-terminal region, absent in all the other RNases of the Superfamily. This structural feature has allowed us to suppose a hypothetical mechanism of auto-inhibition of the catalytic activity.

The production and characterization of two SS2 deletion mutants, as well as the analysis of the crystallographic structure of one of them, made it possible to add new information on the structural reconstruction of a functional active site, allowing to validate the hypothesis of a new mechanism of auto-inhibition, never described before in the vertebrate RNase Superfamily.

Part 1

Human angiogenin involvement in the stress response of skin cells



Chapter 1.1. Introduction

1.1.1. Cellular stress response and stress-induced proteins

At the cellular level, the term homeostasis refers to the maintenance of a relatively constant state essential to ensure maximum efficiency of physiological processes. However, different stimuli can occur and upset this balance, so the cell can put into effect different responses to overcome them and restore a new functional balance to environmental conditions (Nakagawa et al., 2016).

Cellular stress response is characterized by a wide range of molecular changes that cells carry out in response to environmental stressors, exposure to toxins and mechanical damage, triggering a universal mechanism of extraordinary physiological/pathophysiological significance (Fulda et al., 2010).

Many aspects of the cellular stress response can be not stressor specific because cells monitor stress based on macromolecular damage without regard to the type of stress that causes such damage, while other cellular responses directed at re-establishing homeostasis are stressor specific and often activated in parallel to the non-specific stress response (Kültz, 2005; Fulda et al., 2010).

In general, the cell response takes place at two different levels: a slow response, which provides for a transcriptional regulation and leads to the production of proteins useful for overcoming or adapting to stress; a faster response, based on translational regulation, in which the response to stress occurs starting from pre-existing mRNA and proteins (**Figure 1.1**).

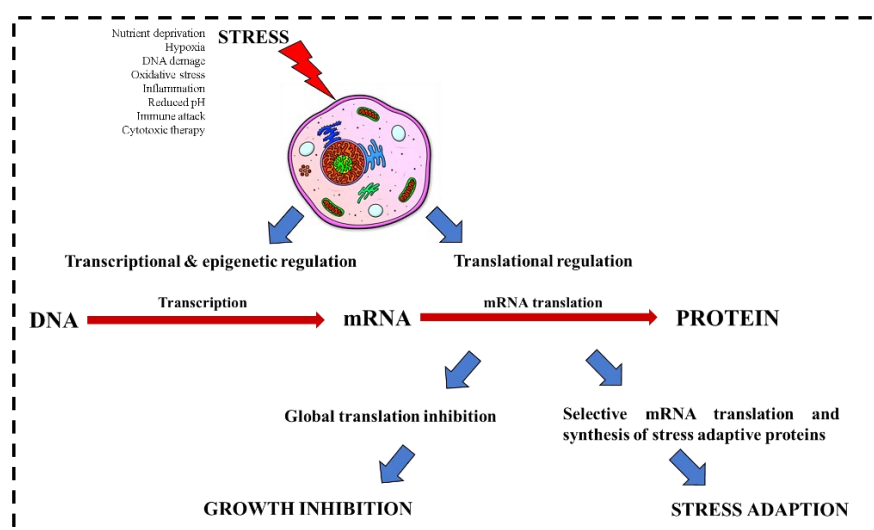


Figure 1.1. Schematic view of the cellular stress response.

Reprogramming of transcription is strictly related to the induction of cyto-protective genes and the repression of housekeeping ones (Himanen & Sistonen, 2019). The induction of transcription is mediated from the activation of stress-responsive transcription factors (TFs), as for instance the heat-shock factor 1 (HSF1) or the nuclear factor erythroid 2-related factor 2 (Nrf2 or even known as NFE2L2), both able to regulate transcription during thermal and oxidative stress respectively (Cox et al., 2011; Himanen & Sistonen, 2019). Basically, these transcriptional factors facilitate the release of stalled RNA polymerase II and so allow for transcriptional elongation (**Figure 1.2**).

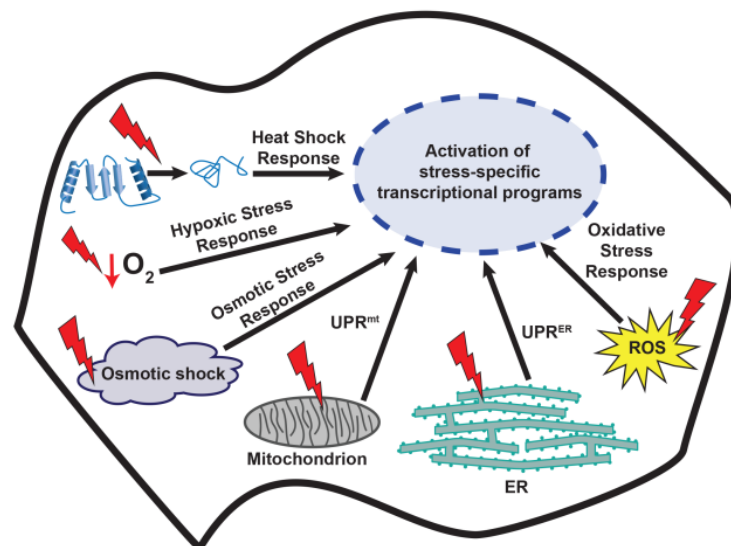


Figure 1.2. Cellular Stress Response. To maintain their function under stress condition, cells activate specific transcriptional programs (<https://sistonenlab.com/>).

In addition to the gene expression regulation, the stress response requires the trigger of mechanisms of dynamic reprogramming of on-going protein synthesis, targeting specifically components of the translation machine (both proteins and RNAs) and by directing specific mRNAs to sites of translation, storage, or decay. These mechanisms redirect mRNAs encoding non-essential ‘housekeeping’ proteins from polysomes to transient storage aggregates (e.g stress granules - SGs) and simultaneously allow the selective translation of mRNAs

encoding proteins directly involved in rescue operations (Liu & Qian, 2014; Yamasaki & Anderson, 2008).

Although stress influences each step of the translation, the initiation phase is the major target of stress-induced translational silencing (Katz et al., 2016), consisting in the modification of components of the translational machinery.

In physiological conditions, translation is initiated when the preinitiation complex (composed of the 40S ribosomal subunit bound by the initiation factors eIF1, eIF1A, eIF3, and the eIF2-Met-tRNA^{Met}-GTP ternary complex) binds to capped mRNA in association with the eIF4E cap-binding protein, the eIF4A RNA helicase, and the eIF4G scaffold protein (see **Figure 1.3**). The interaction of eIF4G with polyA-binding protein (PABP) promotes the circularization of the mRNA. The association of the 43S to the mRNA leads to the formation of the 48S initiation complex (Jackson et al., 2010).

The resulting 48S preinitiation complex scans the 5'- untranslated region until the Met-tRNA^{Met} anticodon recognizes the initiation codon to trigger the release of early initiation factors, recruits the large ribosomal subunit and activates the peptidyltransferase reaction (McCormick & Khaperskyy, 2017).

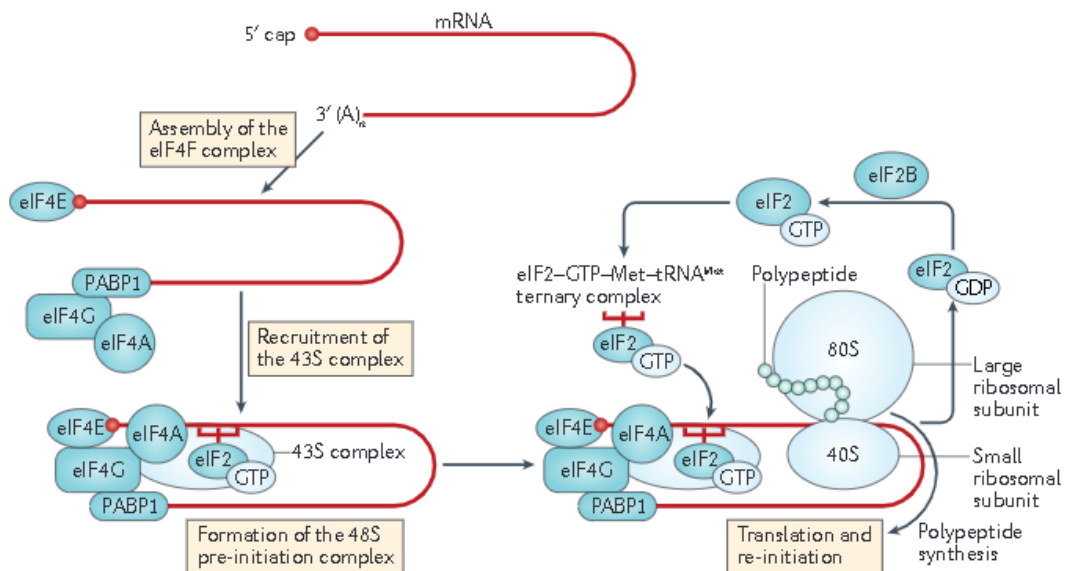


Figure 1.3. Cap-dependent translation initiation (McCormick & Khaperskyy, 2017).

Several stress-activated signalling pathways inhibit protein synthesis by disabling this initiation program. General events in these pathways include: 1) phosphorylation of eIF2 α ; 2) phosphorylation of eIF4E-binding proteins; 3) phosphorylation of ribosomal protein S6; 4) inosine modification of double-stranded RNA; 5) endonucleolytic cleavage of ribosomal RNA. Combinations of these stress-activated inhibitory pathways play a major role in reprogramming protein translation in stressed cells (**Figure 1.4**).

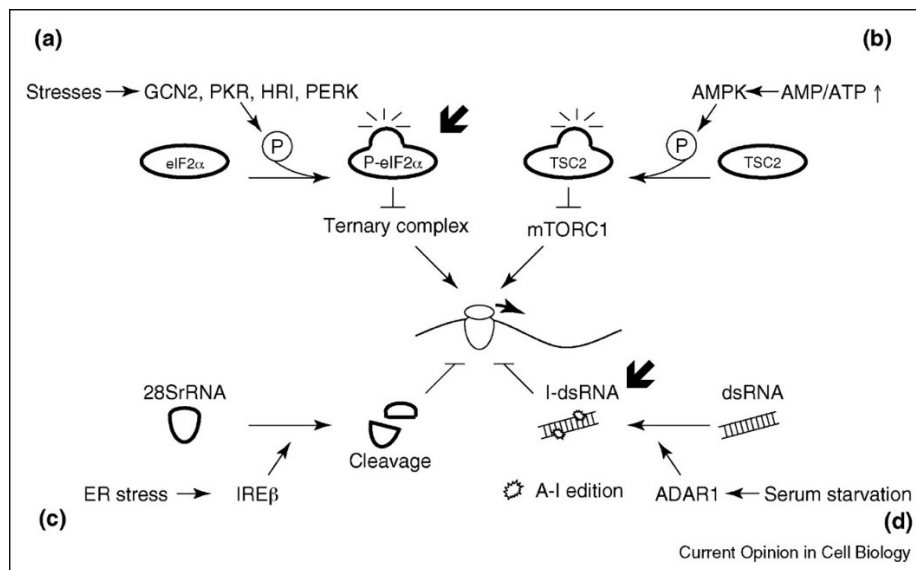



Figure 1.4. General translation inhibition by stress. (a) Phosphorylation of eIF2 α (P-eIF2 α) is induced by GCN2 (amino acid starvation, UV), PKR (dsRNA), HRI (low heme, arsenite, osmotic stress, heat stress), or PERK (ER stress). P-eIF2 α blocks translation initiation by inhibiting the eIF2/GTP/tRNA $_{i}^{met}$ ternary complex. (b) Energy starvation elevates the AMP/ATP ratio activating the AMPK-TSC pathway. This in turn attenuates mTORC1 activity to inhibit phosphorylation of 4E-BP and S6K. (c) 28S rRNA cleaved by IRE β . The resulting structural alteration inhibits translation by an unknown mechanism. (d) Hyper-edited inosine containing dsRNA (I-dsRNA) is produced by ADAR1 whose protein expression is up-regulated by serum starvation. I-dsRNA inhibits translation at initiation probably by nucleating the assembly of SGs. The localization of ADAR1 in SGs has not been confirmed, however, APOBEC3G, a C to U RNA editing enzyme, is found in SGs.  indicates possible SG-related mechanisms (Yamasaki & Anderson, 2008).

1.1. Introduction

One of the most potent translation inhibitory pathways is mediated by phosphorylation of the α subunit of eIF2 (at serine 51) that converts the eIF2-GTP-tRNA_i^{Met} active ternary complex into a competitive inhibitor of the GDP/ GTP exchange factor eIF2B, resulting in the inhibition of 48S preinitiation complexes formation (Yamasaki & Anderson, 2008). Phosphorylation of eIF2 α is mediated by a family of kinases that are activated by different types of environmental stress (Donnelly et al., 2013), such as:

1. GCN2 (general control non-depressible-2), activated by the accumulation of uncharged tRNAs in cells experiencing nutrient deprivation;
2. PKR (double-stranded RNA dependent protein kinase) activated by double-stranded RNA replication intermediates produced during virus infection;
3. HRI (heme-regulated inhibitor kinase) activated by during erythrocyte maturation and by arsenite;
4. PERK (PKR-like endoplasmic reticulum (ER) kinase) activated when unfolded proteins accumulate in the ER, a consequence of secretory or membrane protein overload. Direct consequence of eIF2 α -phosphorylation is the disassembly of polysomes resulting in the accumulation of untranslated mRNPs, containing aggregation-prone proteins (e.g. TIA-1, TIAR, G3BP, Lsm4) that nucleate the assembly of SGs (Park et al., 2020; Sack et al., 2005; Tello-Montoliu et al., 2006) (see **Figure 1.4a**).

SGs play an important role in reprogramming mRNA metabolism by directing incoming transcripts to sites of storage, re-initiation, or decay (see later).

Another important regulatory pathway involves mTOR (mammalian target of rapamycin), a member of the phosphatidylinositol kinase-related kinase (PIKK) family. mTOR is a serine/threonine kinase and it is a core component of two distinct complexes: mTOR complex 1 (mTORC1) and mTOR complex 2 (mTORC2). mTORC1 includes raptor and G protein β -subunit-like protein (mLST8/GbL), known to phosphorylate eIF4E-binding proteins (4E-BPs) and the ribosomal kinase

1.1. Introduction

S6K1/S6K2, both resulting in the promotion of protein translation (Hay & Sonenberg, 2004; Wullschleger et al., 2006; Yamasaki & Anderson, 2008).

Adverse environmental conditions, including nutrient depletion, hypoxia, metabolic stress, osmotic stress, DNA damage and heat shock can reduce the activity of mTORC1 (Hay & Sonenberg, 2004; Reiling & Sabatini, 2006; Wullschleger et al., 2006). In cells subjected to metabolic stress, the AMP-activated protein kinase (AMPK) is activated in response to the elevated AMP/ATP ratio (Yamasaki & Anderson, 2008). AMPK phosphorylates tuberous sclerosis complex 2 (TSC2) allowing it to complex with TSC1. The corresponding complex converts Ras-homolog enriched in brain (Rheb) from an active GTP-bound form to an inactive GDP-bound form. As Rheb positively regulates mTORC1, the activation of AMPK-TSC1 kinase signalling by metabolic stress results in inhibition of protein translation (Hardie, 2007; Y. Li et al., 2004). AMPK is also activated by hypoxia, osmotic stress, low glucose, and impaired mitochondrial function (Hardie, 2007). Thus, the AMPK/mTOR pathway contributes to translational arrest in cells exposed to a variety of environmental stresses (**see Figure 1.4b**).

Endogenous dsRNAs derived from inverted repeat sequences found in untranslated RNAs are subject to RNA editing, a post-transcriptional modification that converts cytosine to uridine or adenosine to inosine (Slotkin & Nishikura, 2013), that may contribute to host defense against viruses that assemble a dsRNA replicative intermediate (Keegan et al., 2001). Surprisingly, hyperedited dsRNA has recently been shown to inhibit protein synthesis by nucleating the assembly of SGs (Scadden, 2007). The putative mechanism involves the adenosine deaminase, an enzyme that converts adenosine to inosine within dsRNA targets, that is induced by interferon and serum starvation, so that inosine-modified dsRNAs may trigger stress-induced translational arrest (**see Figure 1.4c**) (Samuel, 2001; Wang et al., 2004).

ER stress dramatically induces activation of IREb, an ER resident transmembrane kinase/ribonuclease, that cleaves XBP1 transcripts at intron/ exon junctions to initiate a cytoplasmic splicing reaction required for the production of mature XBP1 transcripts (Yoshida et al., 2001). Remarkably, IREb also cleaves 28S

ribosomal RNA, a modification that inhibits global protein synthesis (see **Figure 1.4d**) (Iwawaki et al., 2001).

Since protein synthesis is an energy-intensive process (Good & Stoffers, 2020), translational activity must be strictly regulated, especially in cells subjected to adverse environmental conditions (Harding et al., 2000; P. D. Lu et al., 2004).

Furthermore, reprogramming of protein synthesis by a combination of these stress-induced pathways can promote cell survival by selectively translating repair enzymes. The key to this regulation, in addition to the selective translation block, is the selective exclusion from the SGs, of heat shock proteins and other protein factors involved in the stress response. This is accomplished through additional mechanisms that promote translation of selected mRNAs in response to stress, including IRES-mediated and miRNA-mediated translation control (Baird et al., 2006; Bushati & Cohen, 2007).

In addition to mechanisms of stress induced protein synthesis inhibition, notable is the targeting of RNA components of the translational machinery, in particular of tRNAs, by specific ribonucleases (RNases).

RNases are ancient enzymes that catalyze the degradation of RNA into smaller fragments and regulate various aspects of RNA metabolism, including the cleavage of tRNA during a variety of stress responses (S. Li & Hu, 2012). Housekeeping RNases play key roles in the maturation, quality control and turnover of cellular RNA, other RNases are instead activated in response to stress conditions (stress-induced RNases).

In physiological conditions, stress-induced RNases are inactivated by several mechanisms including physical compartmentalization within membrane-bound organelles such as vacuoles or nuclei, secretion into the extracellular environment or binding to RNase inhibitor (L. Lu et al., 2018). Upon stress, these enzymes are activated into the cytoplasm and cleave different RNA substrates that can profoundly affect cellular physiology (Ivanov et al., 2011).

RNases activation is an intriguing new aspect of cellular stress responses, with a potential impact on apoptosis, cancer and disease progression. Among the RNases, particularly relevant is human RNase 5, also known as angiogenin, a member of the Vertebrate RNase Superfamily (better described later in Part 2) with

different physiological functions and involved in stress response mediated by tRNA cleavage (Emara et al., 2010).

1.1.2. Human angiogenin (ANG)

ANG is a member of Vertebrate RNase Superfamily and, in contrast to most members of this group, it exhibits relatively low ribonuclease activity but essential for its proliferative properties (Sheng & Xu, 2016).

ANG is a cationic single-chain protein with a molecular weight of about 14 kDa, characterized by three α -helices, seven β -strands and a 3_{10} helix (at the C-terminus) and until recently reputed to be a protein secreted into the extracellular environment to stimulate formation of new blood vessels and cell growth (Thiyagarajan & Acharya, 2012).

ANG is widely characterized from a structural point of view (PDB code 1ANG – see **Figure 1.5**). Some of the most relevant structural properties are listed below:

1. a consensus sequence C-K-x-x-N-T-F, shared by all members of the Superfamily;
2. six cysteine residues involved in the formation of three disulphide bridges;
3. a conserved catalytic triad, containing two histidines and one lysine (His13, Lys40, His114), at the level of which the enzyme recognizes and hydrolyses the phosphodiester bond of target RNA;
4. a nuclear localization sequence composed by residues RRRGL and which allows its import into the nucleus;
5. specific phosphorylation sites (S28, Y36, S37 and S87), determining in regulating the dissociation from its inhibitor (RNH1) (Palmer et al., 1986; Shapiro et al., 1986).

Although its ribonucleolytic activity is about 10^6 orders lower than that of RNase A, the prototype of Superfamily, this is essential for angiogenesis and a few other functions. Chemical modifications or site-directed mutagenesis on catalytic residues, turn off both the ribonucleolytic and the angiogenic activity (Shapiro & Vallee, 1987).



Figure 1.5. 3D structure of human angiogenin (PDB entry: 1ANG). The three disulphide bonds are shown in yellow and the catalytic triad in orange.

ANG was originally isolated from the conditioned medium of HT-29 human colon adenocarcinoma cells as a tumour angiogenic factor (Fett et al., 1985); afterwards, many others additional roles were detected in a huge number of both physiological and pathological conditions (Sheng et al., 2014). Indeed, just to name a few, it is known that ANG is involved in cancer progression by stimulating both tumour angiogenesis and cancer cell proliferation and it possesses neurogenic and neuroprotective activity (S. Li et al., 2013). Relatively to the latter, ANG deficiency has been related to pathogenesis underlying neurodegenerative diseases including amyotrophic lateral sclerosis (S. Li et al., 2013) and Parkinson's disease (van Es et al., 2011). Studies in various animal models have shown that ANG inhibitors and activators are effective therapeutics for cancer (Ibaragi, Yoshioka, Kishikawa, et al., 2009; Ibaragi, Yoshioka, Li, et al., 2009) and for ALS (Kieran et al., 2008), respectively. Mechanistic studies indicate also that nuclear localization is necessary for ANG to exert the above indicated biological activities (Moroianu & Riordan, 1994; Tsuji et al., 2005).

ANG is also involved in the innate immune system and inflammatory disease (Park et al., 2020). It has been shown that ANG, as a circulating protein induced during inflammation, exhibits microbicidal activity against bacterial and

fungal systemic pathogens, suggesting that it can contribute also to systemic responses to infection (Hooper et al., 2003).

1.1.3. ANG involvement in cell stress response

ANG is also a paracrine agent that can be taken up by endocytosis into the cytoplasm of target cells (Prehn & Jirström, 2020; Skorupa et al., 2012). Nevertheless, beyond the autocrine or paracrine origin, stress-induced ANG cellular activity is critically regulated by the endogenous inhibitor, RNH1, both in the nucleus and cytosol.

In physiological growth conditions, ANG undergoes nuclear translocation and accumulates in the nucleolus where it stimulates rRNA transcription (Sheng et al., 2014). When cells are subject to a stress, ANG drastically changes its intracellular localization, mediating the cleavage of cytoplasmic mature tRNAs with the subsequent release of a novel class of small noncoding RNAs that act as stress response transducers: the tRNA-derived stress-induced RNAs known also as tiRNAs (Tao et al., 2020).

Generated tiRNA contributes to the cell stress response and has potential cell protective effects mainly via reprogramming translation, inhibiting apoptosis, degrading mRNA and contributing SG recruitment (Elkordy et al., 2019; Pizzo et al., 2013; Wen et al., 2021).

The RNA turnover plays a key role in the intricate signalling network of stress response and in particular tRNA cleavage is considered to be an essential paradigm in promoting cell survival when drastic environmental switches occur (Elkordy et al., 2018; Thompson et al., 2008) (**Figure 1.6**).

The ribonucleolytic activity and cellular localization of ANG are essential for both pro-proliferative and stress response processes. In this context a key role is played by ribonuclease/angiogenin inhibitor 1 (RNH1), that controls both the localization and activity of ANG (Pizzo et al., 2013). In physiological conditions, nuclear and cytosolic ANG are totally sequestered by RNH1 except at the nucleolar level, where the ribonucleolytic activity of the protein is protected to ensure rRNA transcription (Kishimoto et al., 2004).

Although RNHI strongly binds ANG (femtomolar K_d) possible events can induce the loss of this interaction and promote the stress-induced role of ANG (Pizzo et al., 2013).

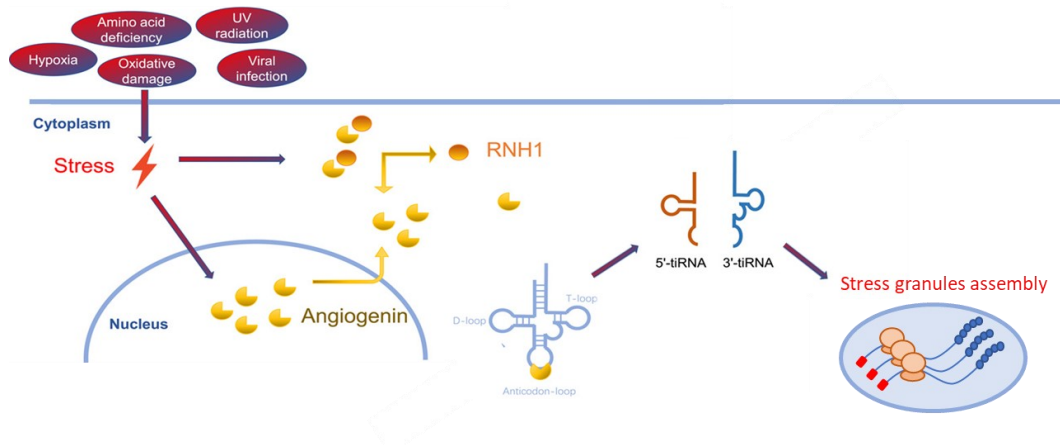


Figure 1.6. The biogenesis of tiRNAs. Under specific stress conditions, ANG is accumulated in the cytoplasm via translocating from the nucleus into the cytoplasm and activated by disassociating RNHI. Then, ANG binds and cleaves the anticodon region of tRNA, generating 5'-tiRNAs and 3'- tiRNAs. ANG, angiogenin; RNHI, ribonuclease/angiogenin inhibitor 1; tiRNA, tRNA-derived stress-induced RNA; tRNA, transfer RNA-modified image adapted from: (Tao et al., 2020).

Based on this it is evident that RNHI plays a delicate task because, inhibiting the activity of ANG, prevents the random cleavage of cellular RNA and consequently ensures the continuation of life processes. Nevertheless, under stressful conditions, such as oxidative stress, disruption of proteostasis or withdrawal of trophic factors (Emara et al., 2010; Ivanov et al., 2011), ANG is mainly localized in the cytoplasm where evades the inhibition of RNHI and actively contributes to the recruitment of SGs on which it is enzymatically active and thus able to produce tiRNAs (Emara et al., 2010). At the same time, in order to save precious anabolic energy, residual nuclear ANG remains associated with RNHI to prevent that its enzymatic activity could allow unnecessary rRNA production (Pizzo et al., 2013).

1.1.4. Stress granules (SGs)

As above mentioned, tiRNAs fragments exerts multiple cellular functions (e.g. inhibition of ribosome biogenesis, inhibition of protein translation, inhibition of apoptosis, etc.) which culminate in the assembly of the SGs.

SGs are cytoplasmic foci, ~100 nm–1 µm in diameter, that are nucleated by the aggregation of untranslated messenger ribonucleoproteins (mRNPs), which accumulate as a result of stress-induced translation arrest. These transient, non-membrane-bound organelles are hubs that orchestrate stress responses and cell fate, containing mainly mRNAs stalled in translation initiation and various translation initiation factors, a variety of RNA-binding proteins, and many non-RNA-binding proteins, through interactions between mRNA-binding proteins that link together populations of mRNPs (Mahboubi & Stochaj, 2017; Protter & Parker, 2016).

Interactions promoting SGs formation include conventional protein–protein interactions as well as interactions involving intrinsically disordered regions of proteins (Protter & Parker, 2016). Assembly and disassembly of SGs are modulated by various post-translational modifications as well as numerous ATP-dependent ribonucleoproteins or protein remodelling complexes, illustrating that SGs represent an active liquid wherein energy input maintains their dynamic state (Protter & Parker, 2016).

These aggregates also contain key components of signalling pathways proving thereby how the formation of this aggregates can alter significantly also signalling networks of the cells (Buchan & Buchan, 2014; Jain et al., 2016). Structurally, they are not uniform, and contain internal substructures which define two distinct layers: a core structure surrounded by a less concentrated and potentially more dynamic shell (Jain et al., 2016). These two regions may have different components, functions, and dynamics (see **Figure 1.7**).

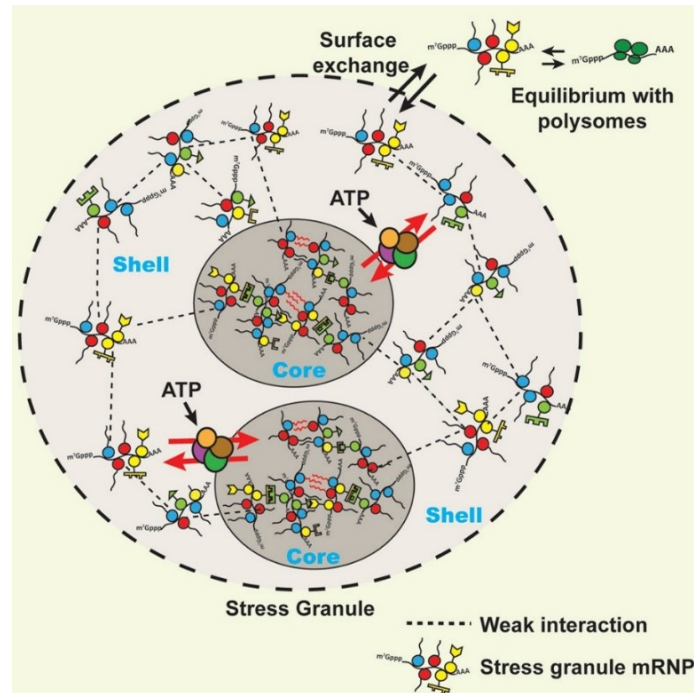


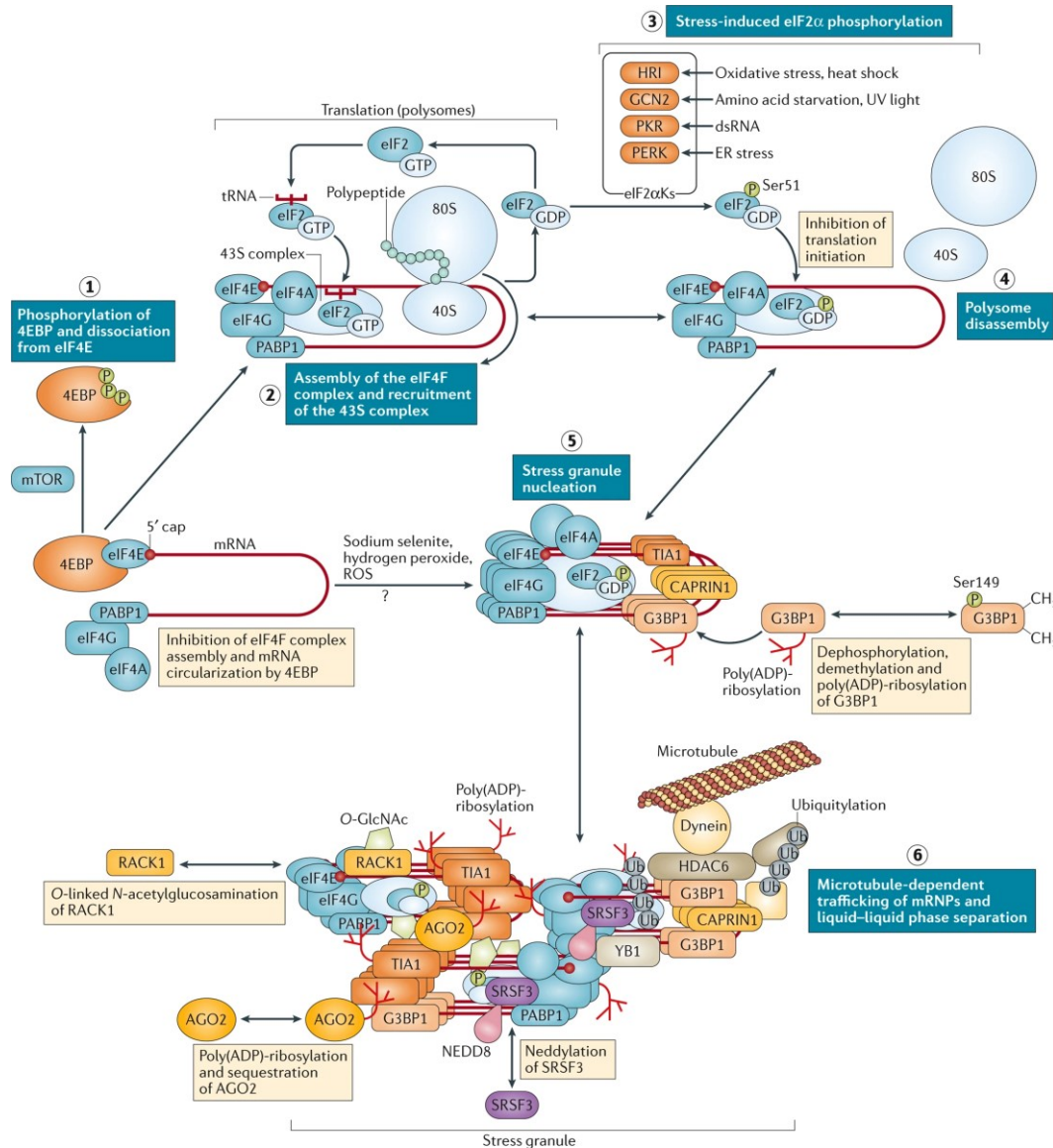
Figure 1.7. Structure overview of SGs. SGs contain a stable core structure surrounded by a dynamic shell with assembly, disassembly, and transitions between the core and shell modulated by numerous protein and RNA remodelling complexes (Jain et al., 2016).

As shown in **Figure 1.8**, the formation of SGs is an articulated and complex process, that requires participation of several protein and non-protein components involved in various subsequent steps summarized below:

- Step 1. Canonical SGs formation begins with the phosphorylation of eIF4E (eukaryotic translation initiation factor 4E)-binding proteins (referred to collectively as 4EBPs) by mTOR (mammalian target of rapamycin), that is required for the dissociation of 4EBPs from the mRNA cap-binding protein eIF4E. This enables the association of eIF4E with eIF4G and eIF4A to form the eIF4F complex.
- Step 2. The eIF4F complex recruits the 43S small ribosomal subunit complex. Upon recognition of the initiation codon, eIF2–GTP is hydrolysed and eIF2–GDP is released.
- Step 3. One of four eIF2 α kinases (eIF2 α Ks) that include HRI (heme-regulated inhibitor), GCN2 (general control non-derepressible protein 2),

PKR (double-stranded RNA (dsRNA)-activated protein kinase) and PERK (PKR-like endoplasmic reticulum (ER) kinase), phosphorylate the eIF2 α subunit of eIF2 in response to various types of stress. This prevents GDP–GTP exchange and the regeneration of the initiation-competent 43S complex.

- Step 4. Ribosomes complete elongation and dissociate upon termination (a process known as ribosome ‘run off’), which exposes polysome-free RNA to RNA-binding proteins.
- Step 5. After the RNA-binding proteins G3BP1 (RAS GTPase-activating protein SH3 domain-binding protein 1) and TIA1 (T cell-restricted intracellular antigen 1) bind polysome-free mRNAs and aggregate to nucleate stress granule formation (Gilks et al., 2004; Tourrière et al., 2003).
- Step 6. Large SGs aggregate from smaller foci are formed in a process that requires microtubule-dependent retrograde trafficking that is mediated by dynein motors and HDAC6 (histone deacetylase 6), which binds to G3BP1, microtubules and polyubiquitin chains that are enriched in SGs (Kwon et al., 2007). SGs are also rich in post-translational modifications such as poly (ADP)-ribosylation (Leung et al., 2011) and O-linked N-acetylglucosamination (Ohn et al., 2008), which regulate the recruitment of various proteins. The O-linked N-acetylglucosamination-dependent recruitment of receptor for activated protein C kinase 1 (RACK1) to SGs (Ohn et al., 2008) causes its sequestration and the inhibition of RACK1-mediated pro-apoptotic signalling (Arimoto et al., 2008). Poly (ADP)-ribosylation controls the sequestration of Argonaute 2 (AGO2) in SGs and hence the inhibition of microRNA-mediated regulation of gene expression by the AGO2-containing RNA-induced silencing complex (RISC) (Leung et al., 2011).



Nature Reviews | Immunology

Figure 1.8. Mechanism of translation arrest and stress granule formation. (McCormick & Khapersky, 2017).

1.1.5. Aims

As above described, the involvement of ANG in the stress cell response is linked to its activity as a stress-induced RNase, which targets tRNAs, and leads to the generation of tiRNAs in turn involved in the recruitment of SGs.

Although newly identified, SGs have been described in different types of human cells (Aulas et al., 2017). However, studies on SGs in skin cells have not yet been reported, despite this organ is extremely broad and particularly exposed to various types of stresses given the role it plays as the body's first defense barrier. Equally interesting is the surprising lack of, or at least partial, experimental evidence regarding expression and localization of ANG in cells of the epidermis, the most superficial non-vascularized layer of the skin.

For this reason, it seemed interesting to launch a pilot study that first of all would confirm the presence of ANG in skin cells and then the potential effects that this unconventional enzyme could exert when these cells are strongly disturbed.

To accomplish this strategy, human keratinocytes (HaCaT cells) were chosen as model system and the following approaches were applied:

- Analysis of expression of ANG and its intracellular localization in HaCaT cells subjected to different growth conditions;
- Production of recombinant ANG and analysis of its effects on HaCaT cells subjected to different growth conditions;
- Production and characterization of two new variants of recombinant ANG;
- Analysis of possible internalization in HaCaT cells of these variants;
- Analysis of effects of these variants in HaCaT cells subjected to different growth conditions.

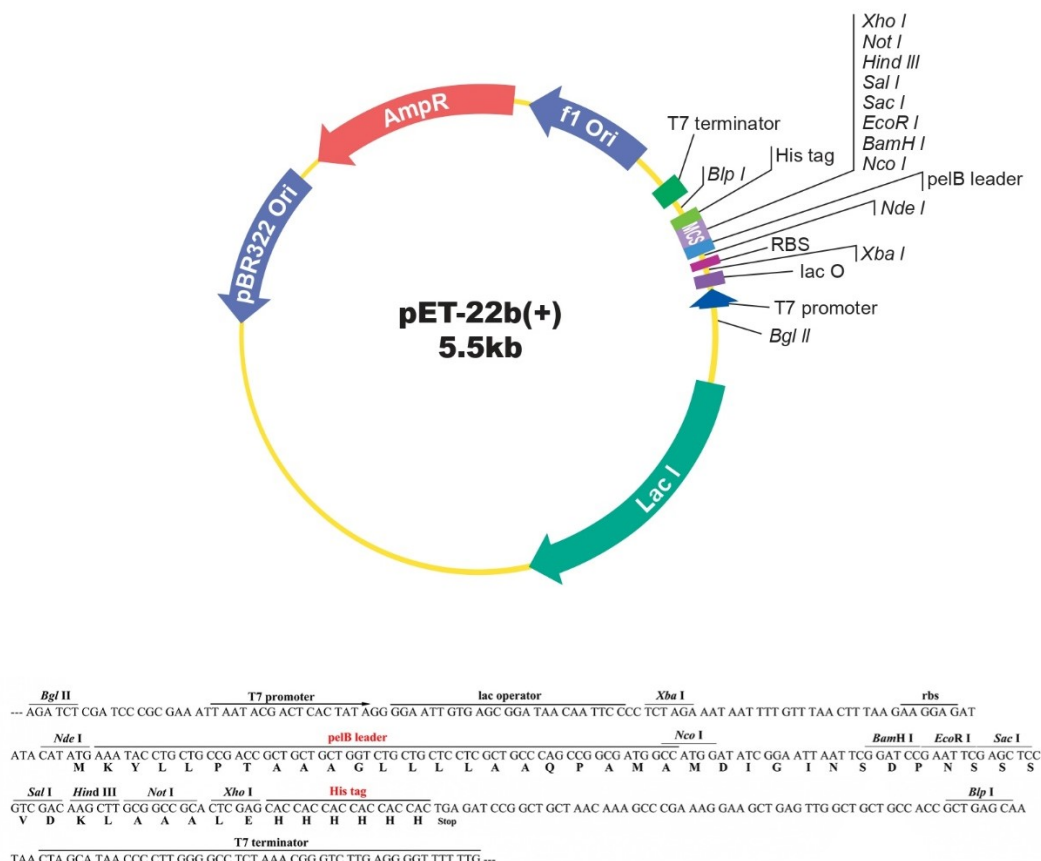
The details of this experimental scheme will be deeply described in the results section (Chapter 1.3).

The present work therefore opens a new curtain in the study of the stress-induced role of ANG, and above all its potential involvement in the stress response of skin cells, a very interesting combination never studied before.

Chapter 1.2. Materials and Methods

1.2.1. Plasmid vectors

rANG, rANG_{6xHis} and rANG(Q₃₁Q₃₂)_{6xHis} were cloned into pET-22b (+) (the figure below indicates map and multiple coding sequence) by the Custom Cloning service of GenScript®.



1.2.2. Heterologous proteins production and purification

The expression plasmids pET-22b(+) encoding rANG, rANG_{6xHis} or rANG(Q₃₁Q₃₂)_{6xHis}, were used to transform competent *E. coli* strain BL21(DE3) (Invitrogen®). Cells were grown at 37 °C to an A₆₀₀ nm = 0.6, then induced with 0.4 mM IPTG (isopropyl-1-thio-d-galactopyranoside) and grown overnight.

Expressed recombinant proteins were purified by inclusion bodies, the latter isolated after sonication and centrifugation of bacterial lysates. Inclusion bodies were first washed and then denatured in 7.0 M guanidine hydrochloride, 100 mM Tris-HCl pH 7.4, 0.1 M reduced glutathione and then renatured in 0.1 M Tris acetate pH 8.4, 0.5 M L-Arginine and 0.001 M oxidized glutathione diluting 20-fold the

denaturing mixture. Finally, all three RNases were purified by RP-HPLC by using a C4 column (Phenomenex®) (Pizzo et al., 2008).

1.2.3. Circular Dichroism analysis

Circular dichroism (CD) spectra were recorded with a Jasco J-715 spectropolarimeter equipped with a Peltier temperature controller. Far-UV measurements were carried out at protein concentration of 0.2 mg/ml in 10 mM Tris-HCl pH 7.4, at 10 °C, using a cell with an optical path length of 0.1 cm. Spectra, registered with 50 nm min⁻¹ scanning speed, 2 s response time, 1 nm data pitch, and 2.0 nm bandwidth, were obtained averaging three scans. Thermal unfolding curves were obtained by following the CD signal at 222 nm, in the 10–90 °C range, at heating rate of 1.0 °C min⁻¹. The denaturation temperatures (Td) were determined through analysis of the first derivative of the melting profiles. The reversibility of the transition was checked by lowering the temperature to 10 °C and re-scanning.

1.2.4. Ribonucleolytic activity assays

Ribonucleolytic activity studies were performed according to the method described in (Ferguson et al., 2019). RNase A was purchased from Sigma-Aldrich and the fluorogenic substrate 5'-FAM-(dA)₂U(dA)₃-TAM-3' was synthesized by Eurofins genomics.

Fluorescence measurements were performed in a low volume quartz cuvette with 1 cm optical path length under magnetic stirring at 20 °C using a Fluoromax-4 spectrofluorometer equipped with a Peltier thermostatic cell holder. The variation of the emission signal induced by substrate cleavage was monitored at $\lambda_{em} = 520$ nm (slit width = 3 nm) using an excitation wavelength $\lambda_{ex} = 495$ nm (slit width = 2 nm) with an acquisition time of 0.5 s. Each measurement was performed in triplicate in 10 mM Tris-HCl pH 7.4 containing 0.001% w/v Tween-20, 100 nM 5'-FAM-(dA)₂U(dA)₃-TAM-3', 200 pM RNase A or 45 nM ANG (rANG or its variants with His 6xtag). To obtain a stable signal in the absence of the enzyme, fluorescence was preliminarily recorded during an equilibration period (5 min).

1.2. Materials and Methods

The catalytic reactions were initialized upon the addition of the enzymes and then were monitored for ~15 min until the complete cleavage of the substrate. The quantum yield increase registered upon the phosphodiester bond cleavage is due to the contemporary removal from the substrate of a quencher group. The variation of the emission intensity with time was used to calculate the k_{cat}/K_M value by the following equation:

$$\frac{k_{cat}}{K_M} = \left(\frac{\left(\frac{\Delta F}{\Delta t} \right)}{(F_{max} - F_0)} \right) 1/[E]$$

where $\Delta F/\Delta t$ is the slope of the straight line that fits the initial velocity of the enzymatic activity with $R^2 \geq 0.99$, F_{max} and F_0 are the fluorescence acquired after the complete cleavage of the substrate and in the absence of enzyme, respectively, and $[E]$ is the concentration of the enzyme used during the experiment.

1.2.5. Cell culture and treatments

HaCaT cells were maintained in Dulbecco's modified Eagle medium (DMEM) supplemented with 10% fetal bovine serum (FBS), 1mM L-glutamine, 1% v/v penicillin/streptomycin solution (100 Unit/ml) and grown at 37°C in 5% CO₂.

Oxidative stress was induced chemically by 500 µM sodium arsenite (SA) (Sigma Aldrich) for 1 hour or 1 mM hydrogen peroxide (Sigma Aldrich) for 2 hours, each prepared in stock aqueous solutions and added to medium. UV irradiation was obtained by using the ULTRAVEKL UV-A/UV-C LED lamp (EKTRACOM) (irradiance $7,8 \cdot 10^{-4}$ mW/m²), exposing cells in PBS at a distance of 60 cm from the source for 1 hour, and then incubating them in DMEM for an additional 1 hour at 37°C in 5% CO₂.

Thermal stress was obtained exposing cells for 1 hour to 45°C in 5% CO₂. Recombinant proteins were administrated for the biocompatibility assay at increasing concentrations (0,1, 1 and 10 µM) for 24 hours at 37°C in 5% CO₂. For the following experiments, pre-treatments were carried out by using 2 µM of rANG, rANG_{6xHis} or rANG(Q31Q32)_{6xHis}, for 1 hour at 37°C in 5% CO₂.

1.2. Materials and Methods

1.2.6. Cellular extracts

Cytosolic extracts were prepared as follows: cells were collected in ice cold phosphate buffered saline (PBS) and lysed in RIPA Buffer (50 mM Tris-HCl buffer at pH 8 containing 150 mM NaCl, 1 mM EDTA, 0.1% SDS, 1% Triton X-100 and protease inhibitors 1X for 30 minutes in ice. After centrifugation at 14,000 rpm for 10 min at 4°C, supernatants were collected and analyzed.

Protein concentration was measured by the Bradford method (Sigma Aldrich), according to the manufacturer's instructions and using bovine serum albumin fraction V (BSA) as standard.

1.2.7. Western blot analysis

Proteins from total cellular lysis were resuspended in 1x Laemmli sample buffer (400 mM Tris-HCl pH 6.8, glycerol 5% v/v, 2% SDS v/v, 0.01 % wt/v Bromophenol blue and 0.4M β -mercaptoethanol), separated by SDS-PAGE, and electro-transferred to Immobilon-PVDF membranes (Millipore) with transfer buffer solution (CAPS 1X; methanol 20%). PVDF membranes were incubated in blocking solutions (PBS containing 0.1% Tween-20 and 3% BSA) at room temperature for 1 hour and incubated with primary antibodies overnight at 4°C.

Primary antibodies were diluted in blocking solution as follows: Rabbit angiogenin (ANG) polyclonal antibody (OriGene Technologies Inc, 1:500), Rabbit β -actin polyclonal antibody (Sigma Aldrich, 1:1000). After washing, the membranes were incubated with horseradish peroxidase (HRP) conjugated goat anti-mouse or anti-rabbit IgG (1:10000) (ImmunoReagents Inc.).

1.2.8. Densitometric analysis

Densitometric analysis was performed with the software ImageJ. To reduce signal to-background ratio, area which determines the signal intensity was also measured for the background, which was near to the signal of interest. Appropriate background intensity was subtracted from each signal intensity. Each analysis was performed in triplicate.

1.2.9. Cell viability assay

For the biocompatibility evaluation of rANG, rANG_{6xHis} or rANG(Q₃₁Q₃₂)_{6xHis}, 5 x 10³ cells were seeded in 96-well plate and after 24 hours of growth, increasing amounts of recombinant proteins were added.

Cells viability was assessed after 24 hours by MTT method (Kumar et al., 2018), a colorimetric assay for measuring cell metabolic activity based on the ability of NADPH-dependent cellular oxidoreductase enzymes to reduce the tetrazolium dye MTT to its insoluble formazan, which has a purple colour. After treatment, cells were briefly washed with 1X PBS, 0,5 mg/mL MTT dissolved in DMEM without phenol red were added, and then incubated in the dark for 3 hours at 37°C in a 5% CO₂ atmosphere.

Resulting formazan crystals were finally solubilized with dimethyl sulfoxide (DMSO) and, after a further incubation at 37°C for at least 10 minutes, analysed at 570 nm by means a Multi-Mode Microplate Reader (Synergy™ H4).

1.2.10. DCFH-DA assay

The ROS quantification assay was carried out by using the DCFH-DA (2',7'-Dichlorofluorescein diacetate) a non-fluorescent probe. After the diffusion into the cell, it is deacetylated by cellular esterases to a non-fluorescent compound, which is later oxidized by ROS into 2', 7' – dichlorofluorescein (DCF). DCF is highly fluorescent and is detected by fluorescence spectroscopy. 2 x 10⁴ cells were plated into 96-well plated and incubated at 37°C in a 5% CO₂ atmosphere for 1 night. Then, after removing the medium, the cells in the plates were washed with PBS 1X buffer, opportunely treated, and then incubated with 20 µM DCFH-DA diluted in PBS 1X, at 37°C for 40 min. After the incubation time the fluorescence of the cells from each well was measured and recorded in the excitation/ emission wavelengths of 485-532 nm, by means a Multi-Mode Microplate Reader (Synergy™ H4).

1.2.11. Real-Time quantitative PCR (RT-qPCR)

Gene expression was evaluated in HaCat cells by Real-Time quantitative PCR. In brief, 3×10^5 cells were plated and after 24 h exposed to treatments (see paragraph 1.2.5). Total RNA was then isolated using TRIzol™ Reagent (Invitrogen™) according to the manufacturer's instructions. Extracted RNA was spectrophotometrically quantified by Nanodrop 8000 (Thermo-Scientific) and then retro-transcribed to cDNA with SuperScript™ IV VILO™ Master Mix (Invitrogen™) according to the manufacturer's protocol. RT-PCRq was performed by using SYBR GREEN PCR MASTER MIX (Invitrogen™) in the StepOnePlus™ Real-Time PCR System (Applied Biosystems™). The expression of each gene detected was normalized with respect to GAPDH gene (housekeeping gene control).

Table 1.1. Primer sequences associated to selected genes.

Genes	Forward	Reverse
GAPDH	5'-CACCACACTGAATCTCCCCT-3'	5'-TGGTTGAGCACAGGGTACTT- 3'
ANG	5'-CACTTCCTGACCCAGCACTA-3'	5'-ATGTCTTTGCAGGGTGAGGT-3'
HSPA6	5-TGCAAGAGGAAAGCCTTAGGGACA-3'	5'-TTTGCTCCAGCTCCCTCT TCTGAT-3'

1.2.12. Immunofluorescence

Immunofluorescence analyses were performed on $2,5 \cdot 10^4$ HaCaT cells that were seeded on coverslips and cultured for 24 hours.

After treatments (see paragraph 1.2.5), cells were fixed in 4% paraformaldehyde (PFA) for 15 minutes, permeabilized in 0,1% TRITON-X100 for 5 minutes and blocked with 1% BSA for 20 minutes. Then cells were incubated over-night with primary antibodies suitably diluted as indicated by the manufacturer in BSA 1%. Primary antibodies used were: mouse 26-2F Angiogenin

1.2. Materials and Methods

mAb (eBioscienceTM, InvitrogenTM), mouse 6x-His Tag mAb (InvitrogenTM), rabbit PABPC1 pAb (Sigma-Aldrich).

After washing in PBS, the secondary antibodies used were Alexa488 conjugated goat anti-rabbit (InvitrogenTM) or Cy3 conjugated goat anti-mouse F(ab')₂ (1:500 dilution) (Jackson ImmunoResearch Laboratories).

Then the secondary antibody used was added for 1 hour. For nuclear staining the cells were then incubated with DAPI (Molecular Probes, Invitrogen, Italy) 1:1000 in PBS for 5 min at room temperature. After washing, coverslips were mounted in Mowiol® 4-88. Confocal microscopy was performed using Zeiss Confocal Microscope LSM 700 at 63x magnification.

1.2.13. Cell cycle analysis

Cell cycle analysis was carried out exploiting a propidium iodide staining. Propidium iodide is a fluorescent intercalating agent that can be used for the DNA content measurement, a method that employs flow cytometry to distinguish cells in different phases of the cell cycle.

Briefly, $2.5 \cdot 10^5$ cells were plated and after 24 h exposed to treatments (see paragraph 2.2.4), then cells were collected and resuspended in 500 μ L of hypotonic buffer (0.1% Triton X-100, 0.1% sodium citrate, 50 μ g/mL iodide propidium, RNase A). Cells were then incubated in the dark for 30 min and samples were acquired on a FACS-Calibur flow cytometer using the Cell Quest software (Becton Dickinson) and ModFitLT version 3 software (Verity).

1.2.14. Statistical analysis

Data were analyzed with GraphPad Prism, version 5.0 software (GraphPad Inc., San Diego, CA) by using Student's t-test. A p-value of 0.05 or less was considered statistically significant (* $p < 0.05$, ** $p < 0.01$, *** $p < 0.001$ or **** $p < 0.0001$).

Chapter 1.3. Results

1.3.1. Expression of endogenous ANG and its localization in HaCaT cells

As above described, a series of recently publications has further extended the biological activity of ANG from enabling cell growth and proliferation to sustaining survival under adverse conditions, through its ability to cleave tRNAs and to contribute to SGs recruitment (Yamasaki et al., 2009). In this regard, more and more reports highlight the protective role of ANG in different cell types but, surprisingly, none of these focus on epidermal cells, central elements of the largest human organ, continuously subject to a plethora of stressful stimuli (Kruk & Duchnik, 2014).

For this purpose, the main objective of this part of the PhD project was focused on the evaluation of the potential role of ANG in the stress response of skin cells and for this reason HaCaT cells were chosen as experimental system.

First approach was focused on the analysis of expression level of endogenous ANG. As shown in **Figure 1.9 (panels A and B)**, analyses performed by Real Time quantitative PCR (RT-qPCR) and western blotting on HaCaT cells subjected to various growth conditions, indicate that endogenous ANG, both at transcriptional and translational level, does not undergo substantial changes.

These evidences, never highlighted to date in any scientific report, allowed us to hypothesize that HaCaT cells, under the growth conditions tested, constitutively synthesize ANG and that an its hypothetical stress induced role is closely related to its intracellular re-localization.

Therefore, in order to follow the cellular localization of endogenous ANG in HaCaT cells in the same growth conditions above mentioned, an immunofluorescence analysis was carried out.

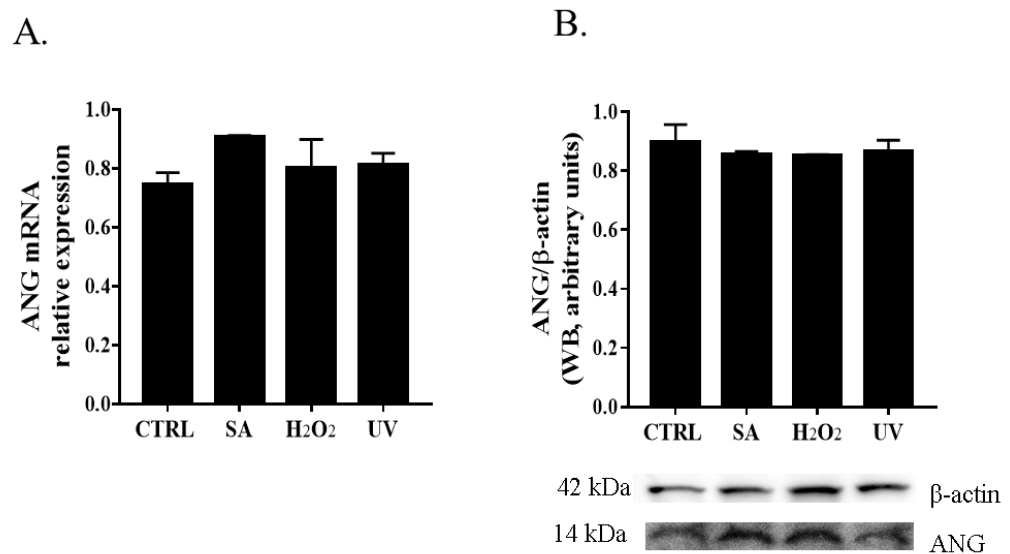


Figure 1.9. ANG analysis in HaCaT cells cultured in different growth conditions: (A) expression analysis of angiogenin mRNA by RT-qPCR; (B) Western blot analysis. CTRL: cells cultured in physiological conditions; SA: cells treated with 500 μ M sodium arsenite; H₂O₂: cells treated with 1 mM hydrogen peroxide; UV: cells subjected to UV irradiation (see material and methods). A *p*-value of 0.05 or less was considered statistically significant (* *p* < 0.05, ** *p* < 0.01, *** *p* < 0.001 or **** *p* < 0.0001).

As shown in **Figure 1.10**, in HaCaT cells cultured in physiological conditions (CTRL), ANG was localized both in cytosol and nuclei, accordingly to what commonly reported for ANG in other cells (Pizzo et al., 2013). Interestingly, when cells were subjected to oxidative stress by SA or H₂O₂, ANG changed dramatically its subcellular localization clearly colocalizing with cytoplasmic loci positive to immunostaining with PABP (*Poly-A Binding Protein*), a specific marker of SGs. This data, reported for the first time in skin cells, clearly suggests that ANG, by a significant intracellular repositioning, could be involved in the recruitment of SGs induced by oxidizing stimuli.

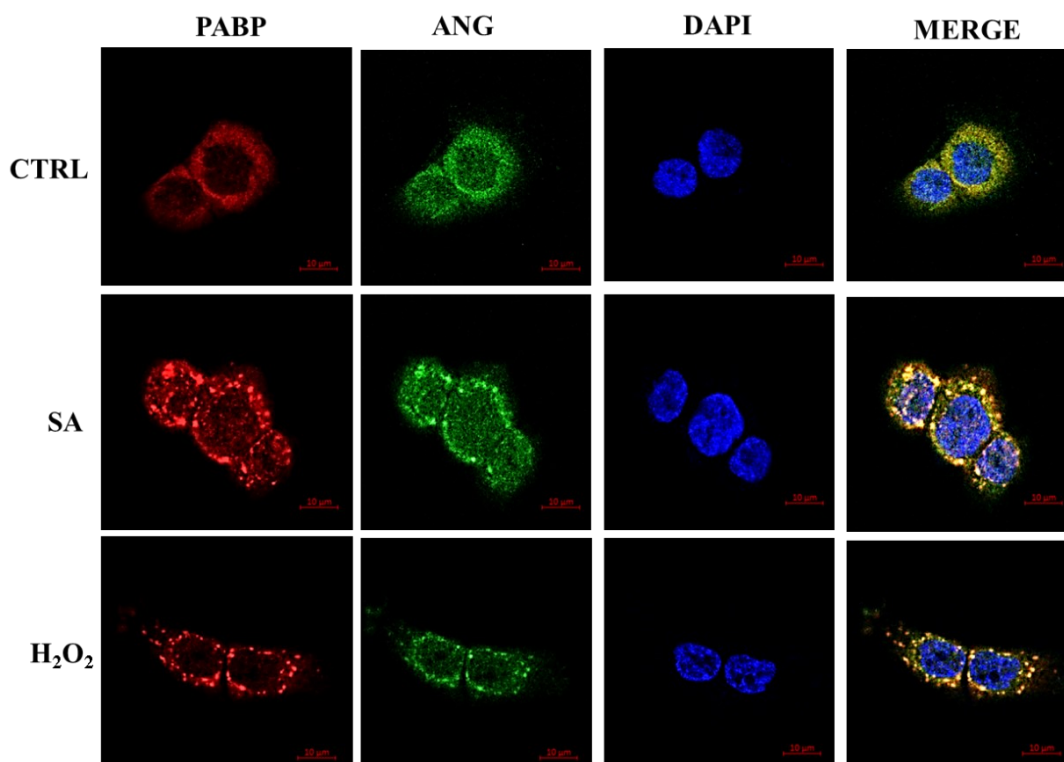


Figure 1.10. Immunofluorescence analysis in HaCaT cells cultured in different growth conditions. PABP (red), ANG (green) and blue staining (DAPI) for nuclei. CTRL: cells cultured in physiological conditions; SA: cells treated with 500 μ M sodium arsenite; H₂O₂: cells treated with 1 mM hydrogen peroxide.

This trend was also highlighted in an alternative experiment in which HaCaT cells were subjected to thermal stress (T₄₅) and to a lesser extent if the same cells were subjected to ultraviolet irradiation (UV) (see **Figure 1.11**). As shown in Figure 3, under stress induced by UV ionization, ANG has undergone a relocation, though not distinctly coincident to the SGs formation as PABP signal was not fully associated with cytoplasmic foci. On the contrary, the thermal stress, obtained incubating the cells at 45°C for 1h, induced a clear colocalization between ANG and PABP, underlining also in this case a strong repositioning of ANG during the stress response.

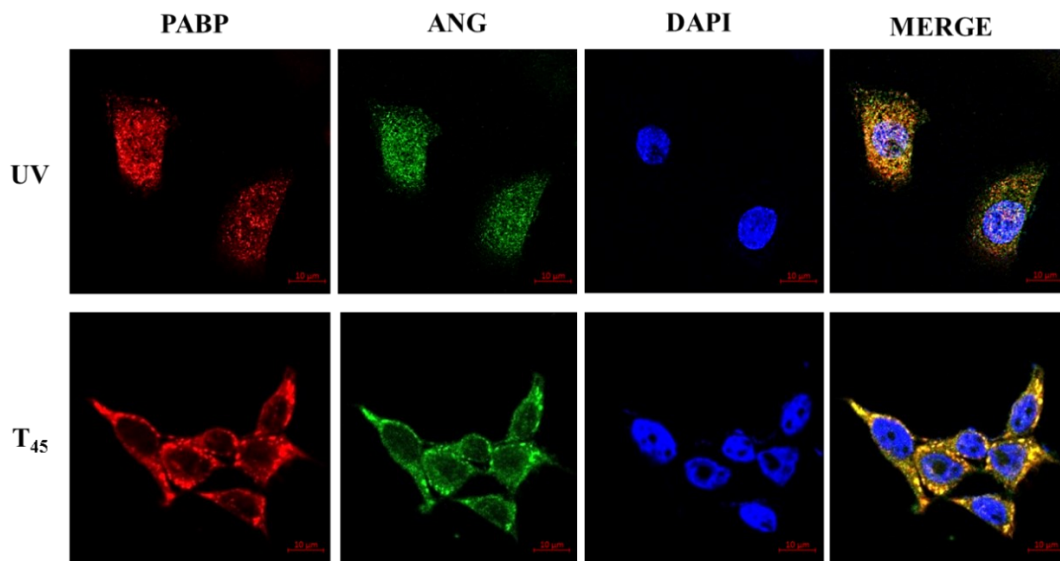


Figure 1.11. Immunofluorescence analysis in HaCaT cells cultured in different growth conditions. PABP (red), ANG (green) and DAPI (blue), used for staining of nuclei. UV: cells subjected to irradiation for 1 h in PBS (details are indicated in material and methods section); T₄₅: cells incubated at 45°C for 1 h.

The results of these immunofluorescence analyses, in line with previous data, corroborate the hypothesis that the stress-induced role of ANG also in HaCaT cells is predominantly carried out in the cytosol where it will probably exercise its catalytic activity to mediate hydrolysis of tRNAs.

Recent studies have also clearly established that ANG may represent a paracrine “help me” signal secreted from stressed cells that stimulates defense mechanisms in adjacent cells (Prehn & Jirstrom, 2020; Skorupa et al., 2012). Furthermore, in different cell types it has been widely verified that ANG can be taken up by sub-confluent cells from the extracellular matrix and translocate in the nucleus where it can contribute to ribosome biogenesis (Kishimoto et al., 2004).

Taken all these premises together and considering that to date skin cells have never been studied in relation to the properties of ANG, next procedures described in this study was exclusively based on exogenous proteins, produced in recombinant form (rANGs), designed to better outline the contribute of this special enzyme in HaCaT cell stress response.

1.3.2. Effects of rANG on viability and homeostasis of HaCaT cells

Exploiting a strategy already established in our research group, rANG (in **Figure 1.12** it is possible to observe its primary structure and its three-dimensional model) was produced in *E. coli* cells (see material and methods) and purified to homogeneity (Pizzo et al., 2006).

Subsequently, before proceeding to verify the potential protective effects of the protein on HaCaT cells, rANG was preliminary analysed to check its acquisition of a correct conformation (see **Figure 1.12a**), its catalytic activity (**Table 1.2**), and its biocompatibility (see **Figure 1.12b**).

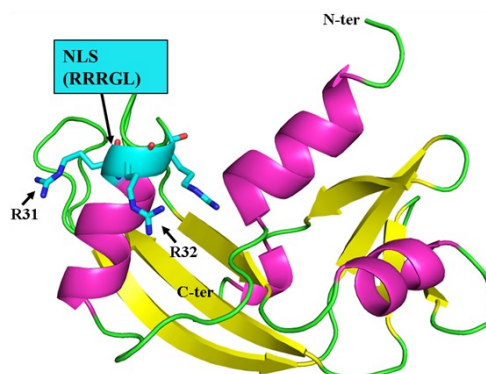
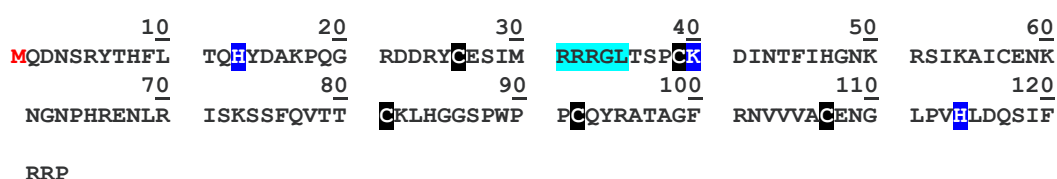


Figure 1.12. Amino acid sequence of rANG (PDB: 1ANG) and its predictive protein model obtained with the molecular visualization system PyMOL (<https://pymol.org>). Prokaryotic initial formyl methionine is highlighted in red; catalytic residues are highlighted in blue; Nuclear Localization Sequence (NLS) is highlighted in turquoise; cysteine residues are highlighted in black.

Table 1.2. Catalytic efficiency of rANG. RNase A was used as control

	k_{cat}/K_M ($\text{M}^{-1}\text{s}^{-1}$)
RNase A	$4.6 \pm 0.5 \cdot 10^7$
rANG	$5.2 \pm 0.3 \cdot 10^3$

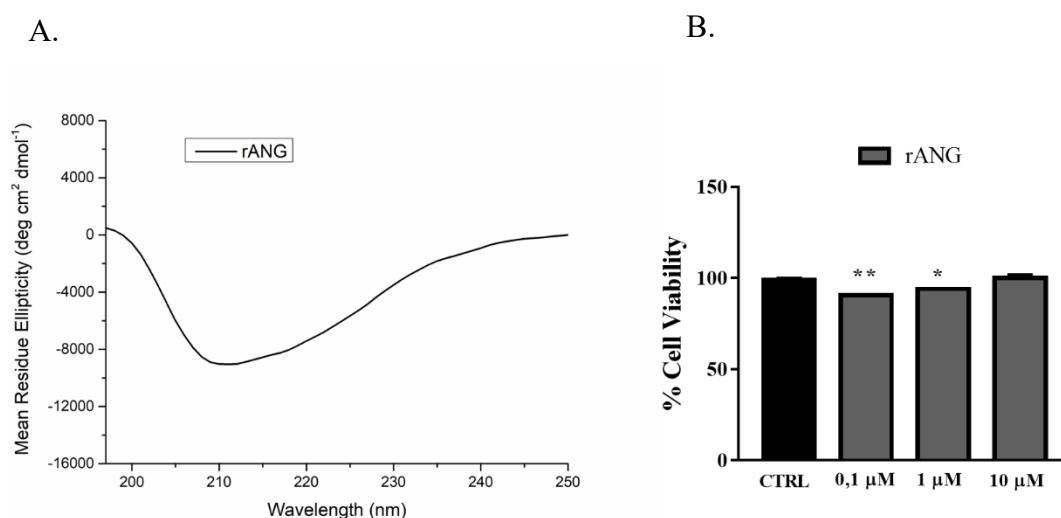


Figure 1.13. Conformational and biocompatibility analysis of rANG. *A. Structural analysis of rANG and its variants: A. Far-UV CD spectra recorded at 10°C in 10 mM Tris-HCl pH 7.4, using a protein concentration of 0.2 mg ml⁻¹. B. Cell viability assay by MTT. Three increasing doses of rANG were tested on HaCaT cells for 24 hours. A p-value of 0.05 or less was considered statistically significant (* $p < 0.05$, ** $p < 0.01$, *** $p < 0.001$ or **** $p < 0.0001$).*

As shown in **Table 1.2**, purified rANG was catalytically active (as expected about 10^4 lesser active than RNase A) (Pizzo et al., 2008), able to assume a correct conformation (see **Figure 1.12a**) in which it is evident a α/β conformation typical of other members of Superfamily, and not toxic on HaCaT cells, even when administered at high concentrations (see **Figure 1.12b**). All these checks allowed us subsequently to verify, by three alternative approaches, the potential involvement of rANG in the cellular stress response of HaCaT cells subjected to

1.3. Results

oxidative stress induced by SA. All tests were carried out using the same growth conditions: pre-treatment of HaCaT cells with 2 μ M rANG for 1 h and then a stress stimulus by administration of 500 μ M SA for 1h.

It should be noted that the concentration of rANG (2 μ M), chosen for these experiments, was not stress inducing because it did not induce SGs recruitment, the latter taken in consideration in this work as cell stress sensors (see in **Figure 1.14**).

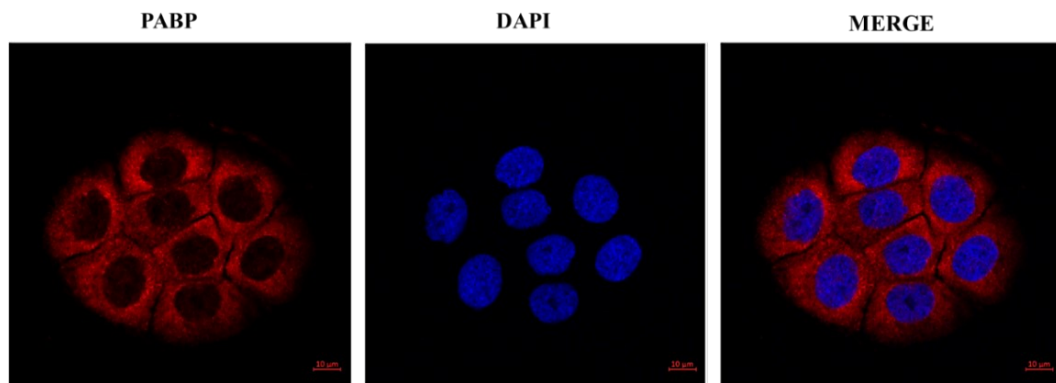


Figure 1.14. *Immunofluorescence analysis of HaCaT treated with 2 μ M of rANG. PABP (red); DAPI (blue), used for staining of nuclei.*

First test performed on HaCaT cells pre-treated with rANG was carried out by RT-qPCR and revealed an attenuated expression of HSPA6 (a stress induced Heat Shock Protein) if compared to that of cells subjected to same perturbation but not preliminarily pre-treated with rANG (**Figure 1.15**).

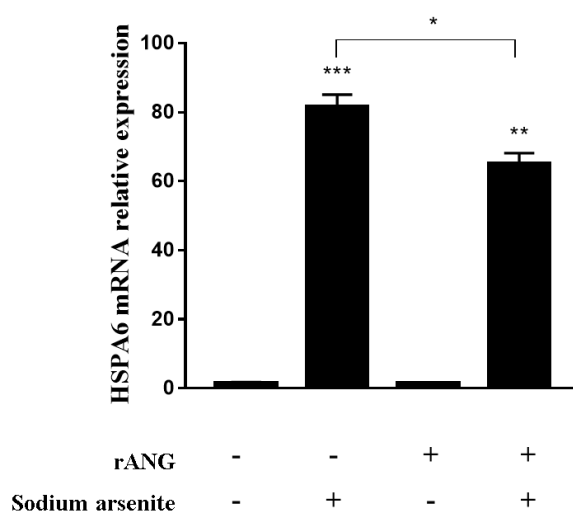


Figure 1.15. Real-Time qPCR analysis of the expression of HSPA6 gene. (-) untreated cells; (+) pre-treatment of cells with 2 μ M of rANG or 500 μ M sodium arsenite. A p -value of 0.05 or less was considered statistically significant (* $p < 0.05$, ** $p < 0.01$, *** $p < 0.001$ or **** $p < 0.0001$).

This protective trend shown by rANG was confirmed also in the second experimental approach in which intracellular ROS level analysis of HaCaT cells was measured by using a DCFH-DA assay (see Material and Methods). This test has allowed us to detect that the increasing level of ROS, normally detected in HaCaT cells subjected to oxidative stress with SA, was virtually absent in the same cells if the latter were pre-treated with rANG (Figure 1.16).

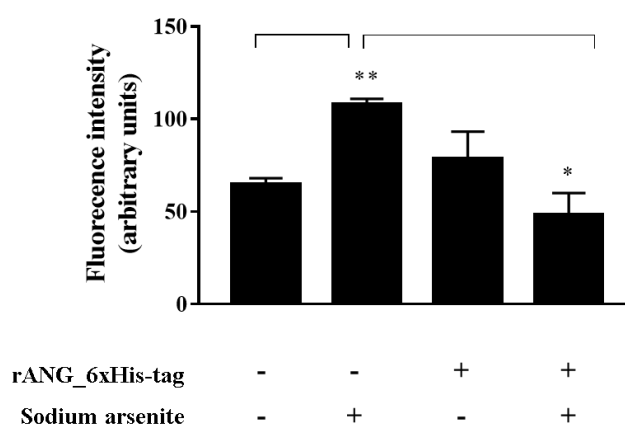


Figure 1.16. DCFH-Da assay performed in HaCaT cells subjected to oxidative stress. (-) untreated cells; (+) pre-treatment of cells with 2 μ M of rANG or 500 μ M sodium arsenite. A p -value of 0.05 or less was considered statistically significant (* $p < 0.05$, ** $p < 0.01$, *** $p < 0.001$ or **** $p < 0.0001$).

The positive effects induced by the pre-treatment of HaCaT cells with rANG were also detected in the third experimental approach. In this case, flow cytometry analysis allowed us to highlight that treatment of the cells with the recombinant protein determined a restoration of their cell cycle, even comparable to that of unstressed cells. In fact, as can be observed in **Figure 1.17**, SA stress induced an enrichment in the number of cells in stalled G1 phase, completely absent in stressed conditions of cells pre-treated with rANG.

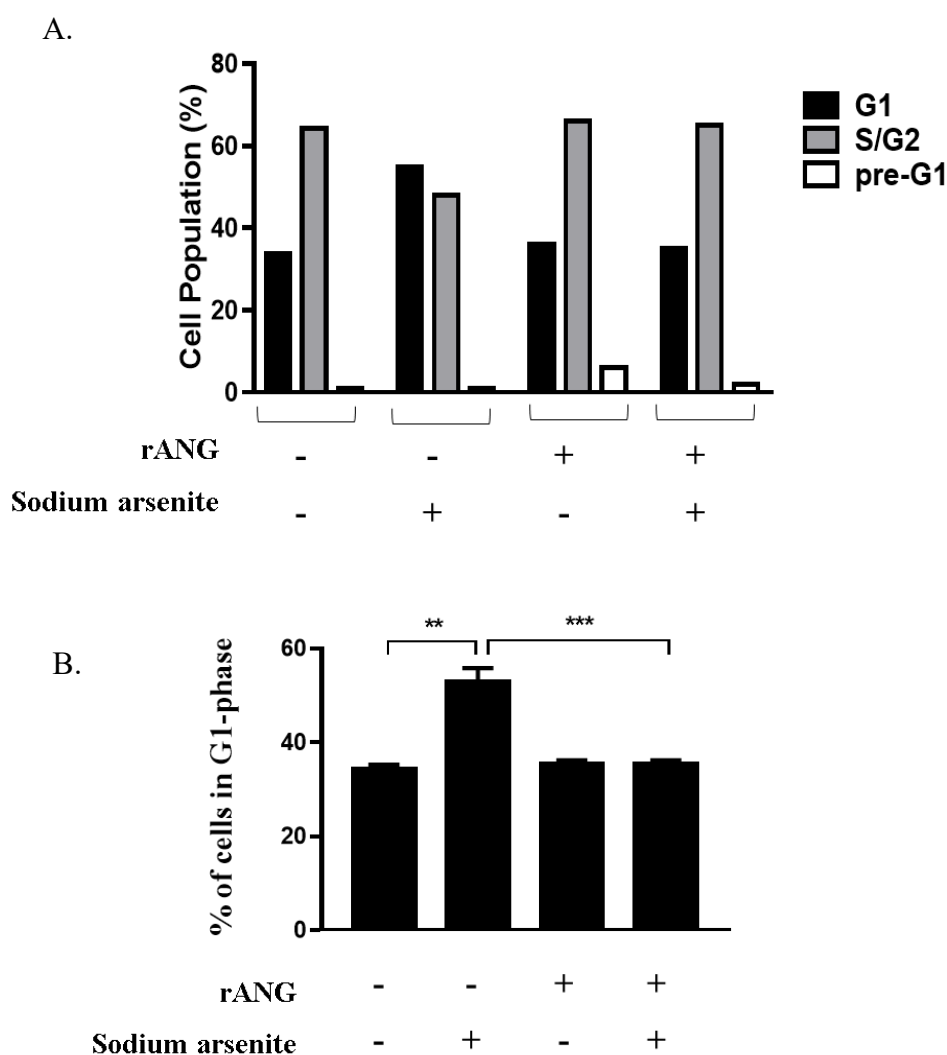


Figure 1.17. Cell cycle analysis. A. Distribution of the cell population among G1, S/G2 and pre-G1 phases of the cell cycle. B. Comparison of the percentage of cells subjected to different treatments, in phase G1. (-) untreated cells; (+) pre-treatment of cells with 2 μ M of rANG or 500 μ M sodium arsenite. A p-value of 0.05 or less was considered statistically significant (* $p < 0.05$, ** $p < 0.01$, *** $p < 0.001$ or **** $p < 0.0001$).

1.3.3. Design, production and characterization of two new rANG variants

These promising protective abilities induced us to design a strategy to verify if rANG was able to exert its properties once internalized or outside of HaCaT cells.

Therefore, in this regard, it was decided to design a different version of rANG that would allow to discriminate the recombinant protein from the endogenous one. This version was designed with the insertion of a His_{6x} tag in the C-term region of ANG following the rationale that the resulting protein could be discriminated from the endogenous ANG by the specific immunoreactivity of His tag. Furthermore, in order to avoid that the presence of the His tag could negatively influence the folding and/or the catalytic efficiency of the protein, a linker composed by the sequence K-L-A-A-A-L-E able to assume an ordered and flexible α -helical conformation, was inserted between the native sequence of ANG and the His_{6x} tag. The complete strategy to obtain this variant, known as rANG_{6xHis}, is depicted in **Figure 1.18**.

Furthermore, based on the results associated to the strong relocation of endogenous ANG in the stress response and to better define whether the cytosolic localization of the protein is decisive for its protective role, an alternative variant of rANG was designed. On this regard, starting from the strategy adopted for rANG_{6xHis} and described in **Figure 1.18**, the new variant was designed by altering the nuclear localization sequence of ANG. In detail, the residues R₃₁ and R₃₂ of rANG_{6xHis} have been replaced by the residues Q₃₁ and Q₃₂. The sequence of this new variant, known as rANG(Q₃₁Q₃₂)_{6xHis}, and its three-dimensional model are shown in the **Figure 1.19**.

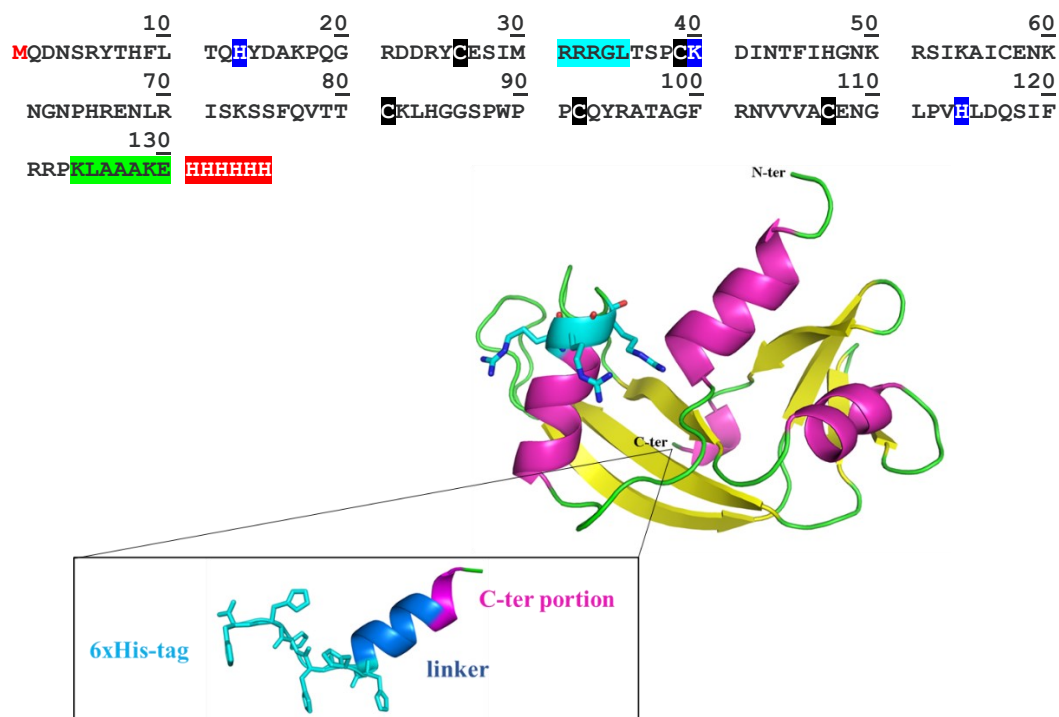


Figure 1.18. Amino acid sequence of *rANG*_{6xHis} and its predictive protein model obtained with the molecular visualization system PyMOL (<https://pymol.org>). Prokaryotic initial formyl methionine is highlighted in red; catalytic residues are highlighted in blue; nuclear Localization Sequence (NLS) is highlighted in turquoise; the linker peptide that separate the protein from the His tag is highlighted in green; cysteine residues are indicated in bold; His_{6x} tag is highlighted in red.

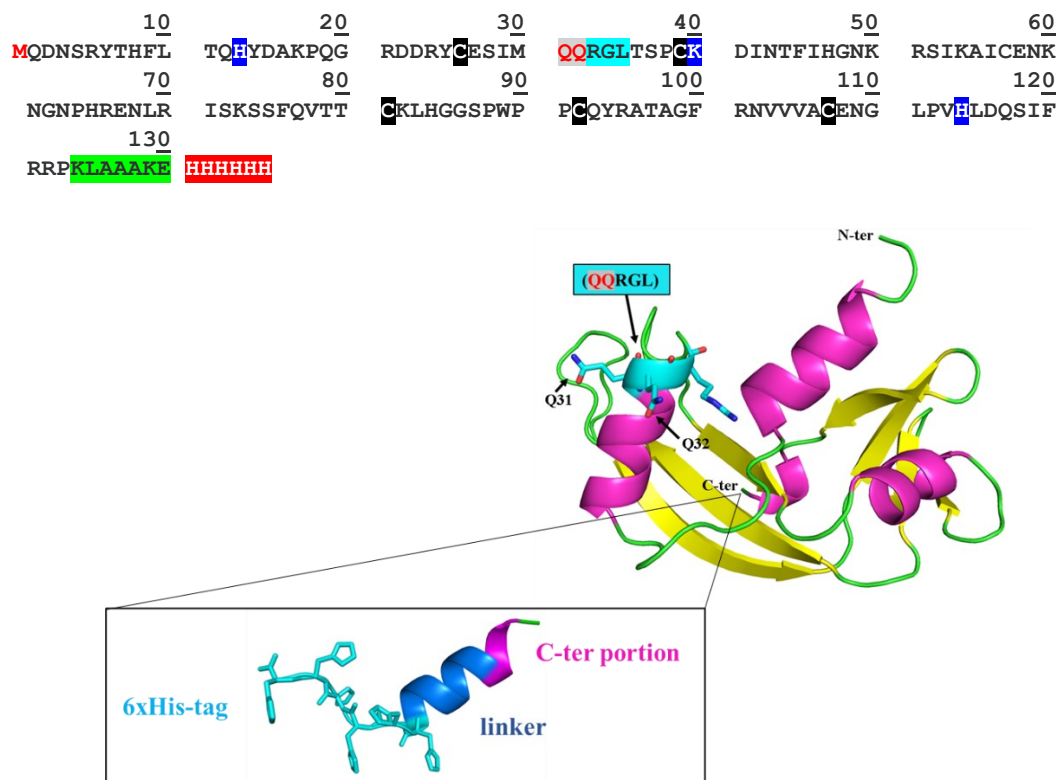


Figure 1.19. *Amino acid sequence of rANG(Q₃₁Q₃₂)_{6xHis} and its predictive protein model obtained with the molecular visualization system PyMOL (<https://pymol.org>). Prokaryotic initial formyl methionine is highlighted in red; catalytic residues are highlighted in blue; nuclear Localization Sequence (NLS) is highlighted in turquoise; aminoacidic substitutions are in red on a grey background; the linker peptide that separate the protein from the His tag is highlighted in green; cysteine residues are indicated in bold; His_{6x} tag is highlighted in red.*

Both recombinant variants were produced and purified to homogeneity as described in Materials and Methods. In a similar way to rANG, also for these two variants preliminary tests before of the assays on cells were carried out; furthermore, as these new proteins were never to date structurally studied, we carried out also a basic chemical-physical characterization of their structures.

The catalytic efficiency of rANG_{6xHis} and rANG(Q₃₁Q₃₂)_{6xHis} was estimated and compared to that of rANG and RNase A by monitoring the cleavage of the same

fluorogenic substrate already previously described. As shown in **Table 1.3**, rANG(Q₃₁Q₃₂)_{6xHis} presented a catalytic efficiency comparable to that of rANG whereas rANG_{6xHis} showed a slightly lower catalytic activity however in a range typical for angiogenins.

Table 1.3. Catalytic efficiency of rANG and of its two variants. RNaseA was used as control.

	$k_{\text{cat}}/K_M \text{ (M}^{-1}\text{)}$
RNase A	$4.6 \pm 0.5 \cdot 10^7$
rANG	$5.2 \pm 0.3 \cdot 10^3$
rANG _{6xHis}	$3.7 \pm 0.2 \cdot 10^2$
rANG(Q ₃₁ Q ₃₂) _{6xHis}	$2.2 \pm 0.2 \cdot 10^3$

The folded state of rANG_{6xHis} and rANG(Q₃₁Q₃₂)_{6xHis} was investigated in solution by circular dichroism (CD) spectroscopy using rANG as control. As shown in **Figure 1.20**, the inspection of the far-UV CD spectra indicated that the two mutants retained the secondary structure of the parent protein. Thermal unfolding curves were also obtained in the temperature range 10–90°C, by following the CD signal at 222 nm (**Figure 1.21**).

CD spectra, recorded at 10 °C before heating and after cooling, indicated reversible thermal unfolding for all proteins (**Figure 1.22**). The T_d of rANG was 59°C, while that of rANG_{6xHis} and rANG(Q₃₁Q₃₂)_{6xHis} were slightly lower, but still close to the characteristics of the reference protein (**Table 1.4**).

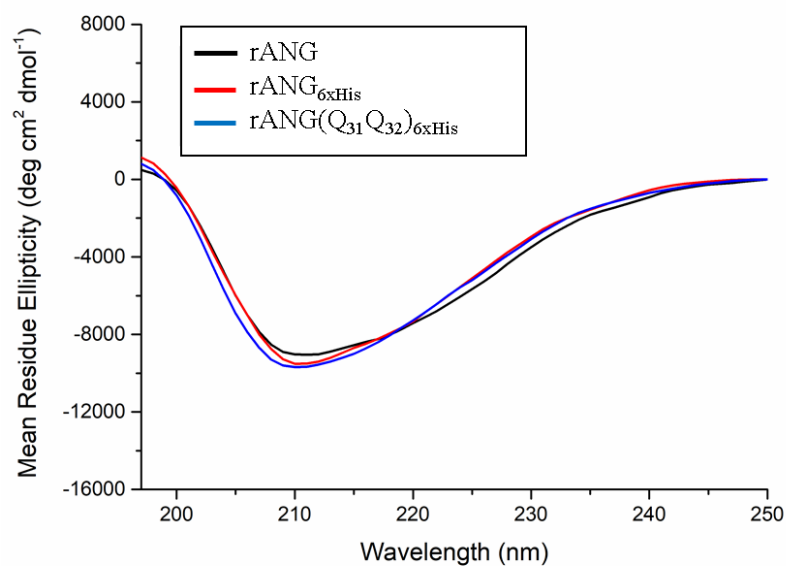


Figure 1.20. Structural analysis of rANG and of its variants. Far-UV CD spectra recorded at 10°C in 10 mM Tris-HCl pH 7.4, using a protein concentration of 0.2 mg ml⁻¹.

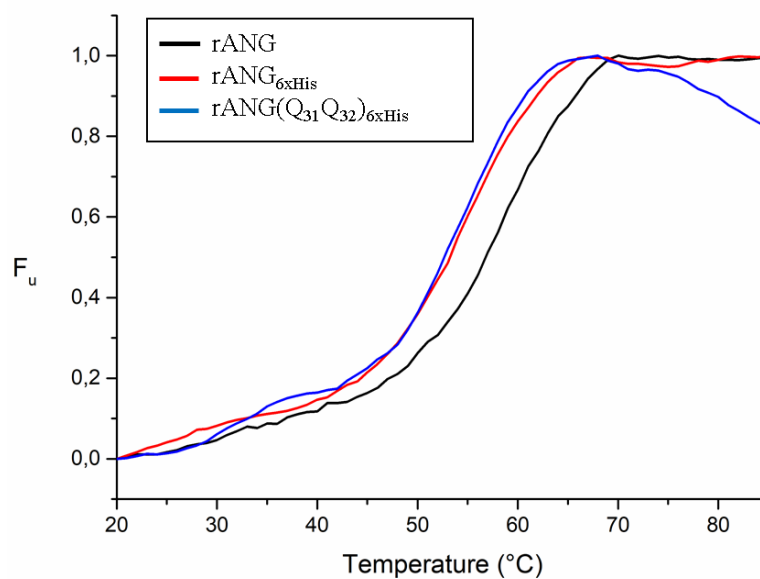


Figure 1.21. Thermal unfolding curves. Thermal denaturation profiles, as followed by monitoring changes in the molar ellipticity at 222 nm as a function of temperature, of rANG and of its variants.

Table 1.4. Denaturation temperatures of rANG and of its two variants. The values obtained were compared to T_d value of RNase A.

	T_d (°C)
RNase A	64
rANG	59
rANG _{6xHis}	56
rANG(Q ₃₁ Q ₃₂) _{6xHis}	54

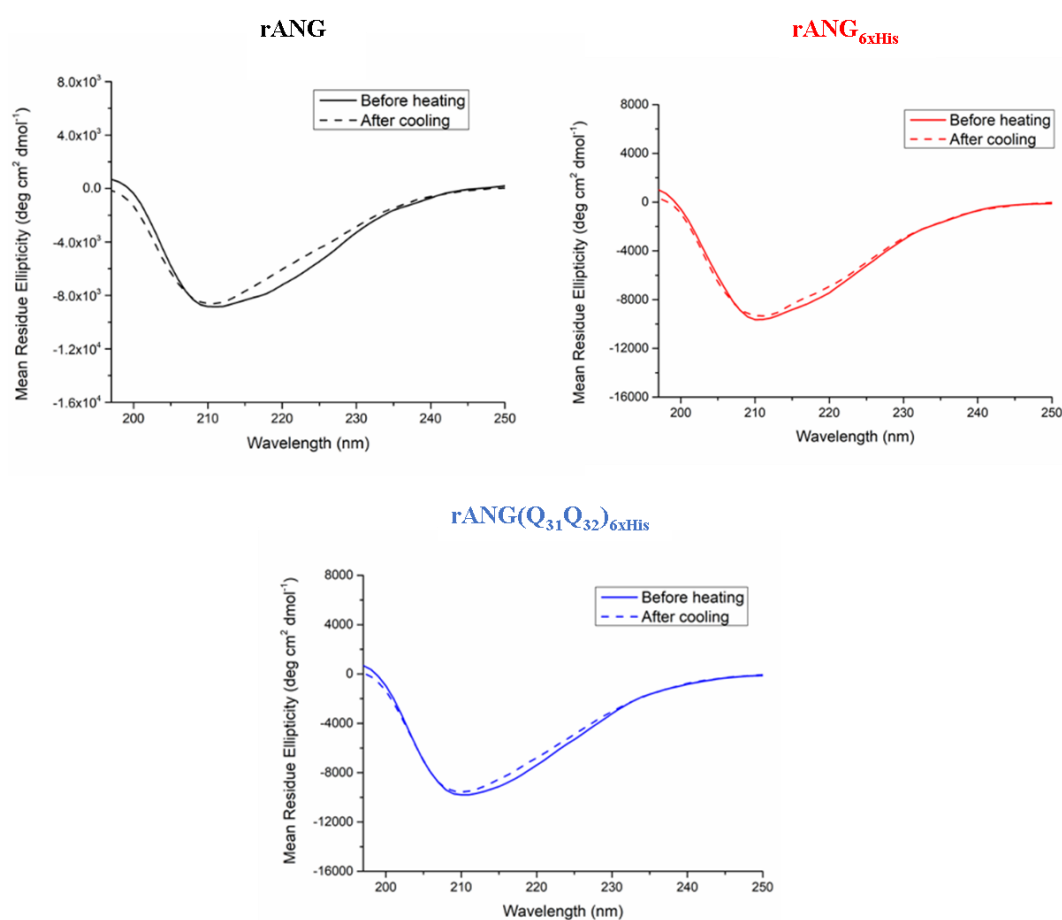


Figure 1.22. Reversible thermal denaturation analysis. Measurements were carried out in 20 mM Mes/NaOH pH 6, 100 mM NaCl, using a protein concentration of 0.1 mg/ml.

Once it was established that both proteins were correctly structured and catalytically active, we proceeded to evaluate their biocompatibility on HaCaT, as shown in **Figure 23**. As expected, also the two variants did not show significant toxicity on HaCaT cells even at high doses.

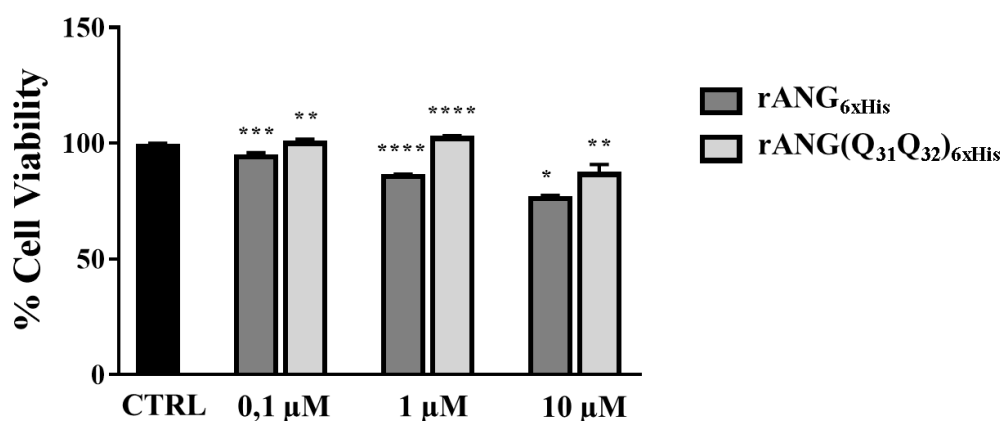
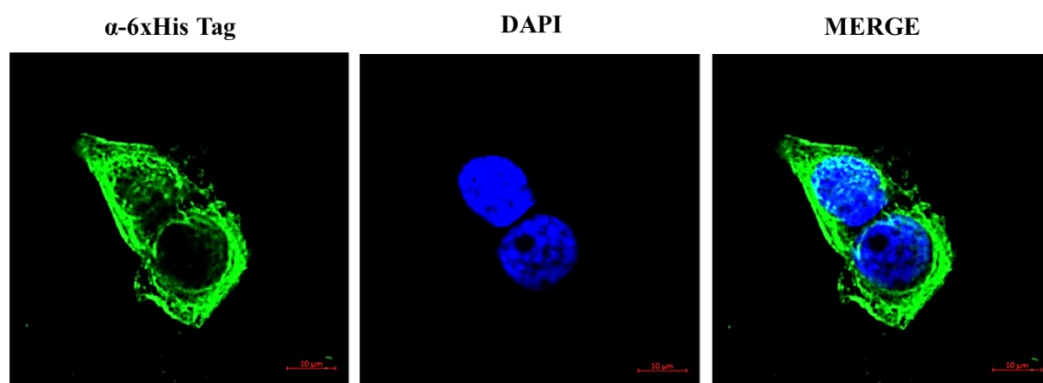


Figure 1.23. *rANG* variants biocompatibility with HaCaT cells. Cell viability was analysed by MTT assay after 24 hours of treatment with three increasing doses of rANG_{6xHis} or rANG(Q₃₁Q₃₂)_{6xHis}. A *p*-value of 0.05 or less was considered statistically significant (* *p* < 0.05, ** *p* < 0.01, *** *p* < 0.001 or **** *p* < 0.0001).

The ability of angiogenin variants to be internalized by HaCaT cells was assessed by immunofluorescence. The analysis carried out by using confocal microscopy and administrating 2 μM of recombinant proteins, have shown that rANG_{6xHis} seems to be localized both in cytoplasm and nucleus (**Figure 1.24 panel A**), as also evidenced by the z-stack where the co-localization among rANG_{6xHis} and the nuclear dye is notable (**Figure 1.24 panel B**).

A.



B.

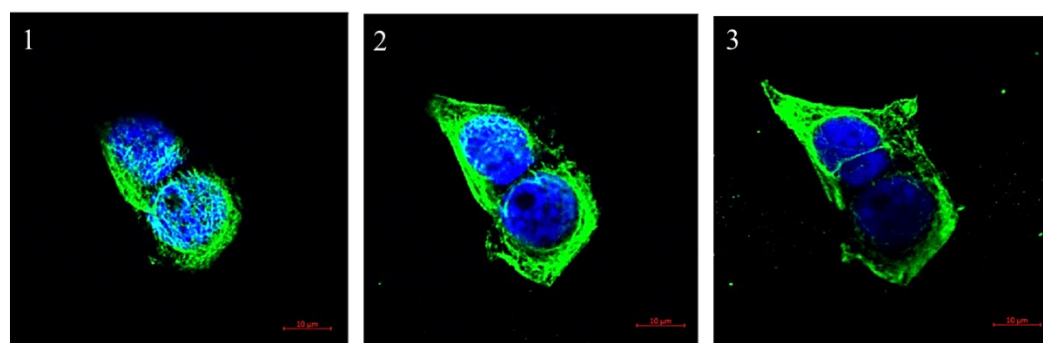
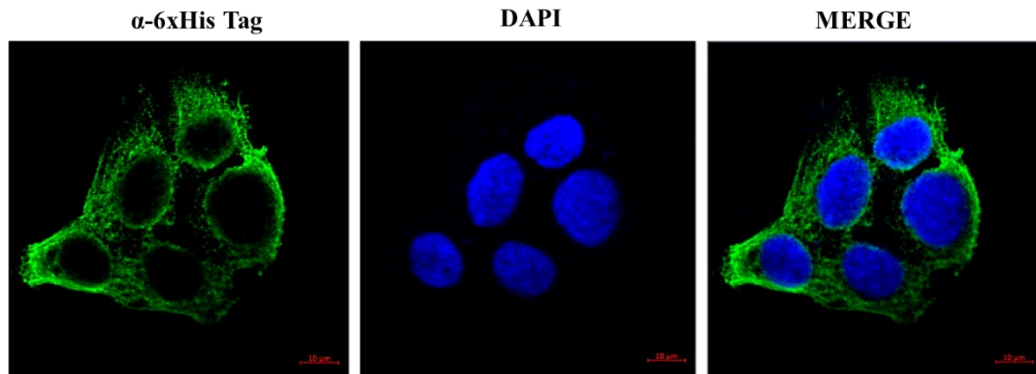


Figure 1.24. *Internalization in HaCaT cells of rANG_{6xHis} tested by immunofluorescence (A) and Z-stack analysis (B). rANG_{6xHis} (green); nuclear staining (DAPI – blue).*

On the other hand, rANG(Q₃₁Q₃₂)_{6xHis}, the variant of rANG characterized by two aminoacidic substitutions in the NLS, showed a predominant cytoplasmic localization (**Figure 1.25 panel A**), as demonstrated by z-stack analysis, in which there were a weak co-localization with the nuclear dye (**Figure 1.25 panel B**).

A.



B.

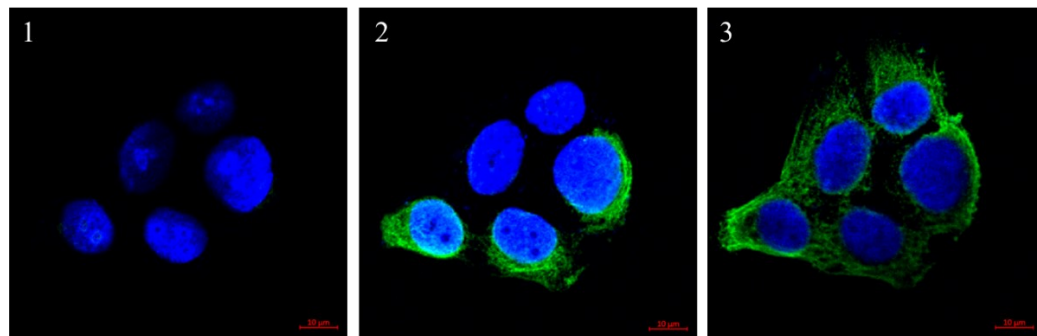


Figure 1.25. *Internalization in HaCaT cells of rANG(Q₃₁Q₃₂)_{6xHis} tested by immunofluorescence (A) and Z-stack analysis (B). rANG(Q₃₁Q₃₂)_{6xHis} (green); nuclear staining (DAPI – blue).*

Once it was established that HaCaT cells were able to internalize the two types of variants, we proceeded to verify whether these proteins were in turn able to manifest the same properties of the reference protein.

On this regard, HaCaT cells pre-treated with 2μM of rANG_{6xHis} or 2μM of rANG(Q₃₁Q₃₂)_{6xHis} and then subjected to stress with SA were analyzed following the same three procedures above described for rANG.

As shown in **Figure 1.26**, both variants were able to significantly influence the expression of the HSPA6 gene under oxidative stress conditions (analyzed by Real-Time qPCR), thus corroborating the idea that ANG can perform a potential cytoprotective role.

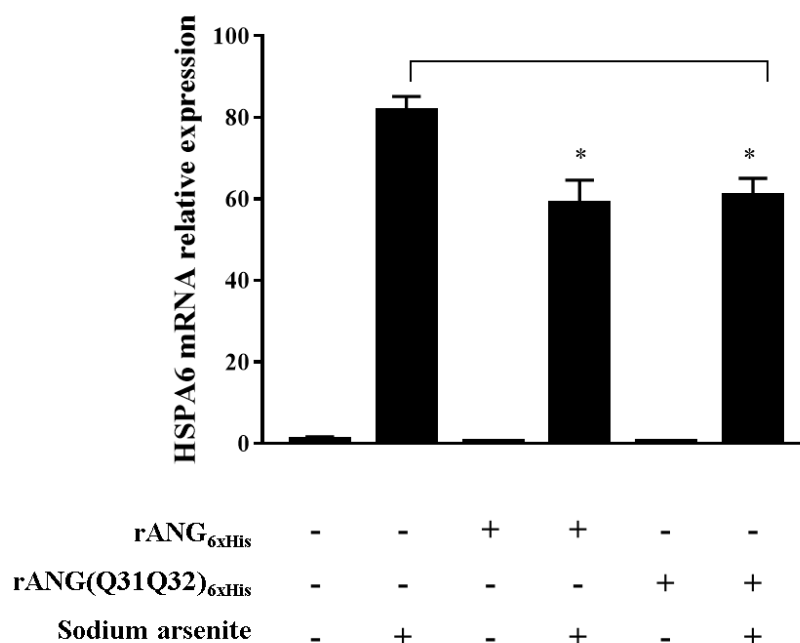


Figure 1.26. Effects of ANG variants on HSPA6 gene expression in HaCaT cells subjected to oxidative stress by sodium arsenite. (-) untreated cells; (+) pre-treatment of cells with 2 μ M of rANG_{6xHis}, rANG(Q31Q32)_{6xHis} or 500 μ M sodium arsenite. A *p*-value of 0.05 or less was considered statistically significant (* *p* < 0.05, ** *p* < 0.01, *** *p* < 0.001 or **** *p* < 0.0001).

The same experimental conditions were used also to execute the analysis of the cellular level of ROS in pre-treated HaCaT cells (with 2 μ M of rANG_{6xHis} or rANG(Q31Q32)_{6xHis}) when treated with SA.

As above mentioned, the non-fluorescent probe DCFH-DA, upon de-esterification and oxidation by intracellular ROS, shows a fluorescence emission increased under oxidative stress induced by SA; interestingly, as shown in **Figure 1.27**, the fluorescence was greatly attenuated in stressed HaCaT cells pre-treated with one of the two variants, highlighting once again the ability of ANG in promoting a more vigorous stress response.

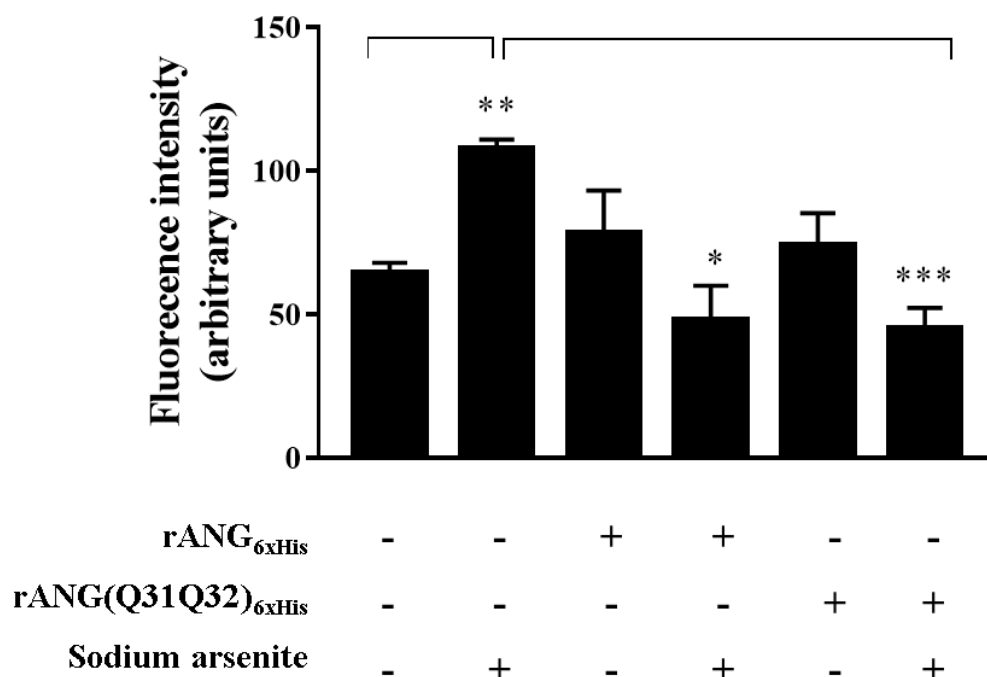


Figure 1.27. *Determination of cellular ROS by DCFH-DA assay in HaCaT cells, pre-treated rANG_{6xHis} or rANG(Q₃₁Q₃₂)_{6xHis} and then subjected to oxidative stress by sodium arsenite. (-) untreated cells; (+) pre-treatment of cells with 2 μ M of rANG_{6xHis}, rANG(Q₃₁Q₃₂)_{6xHis} or 500 μ M sodium arsenite. A p-value of 0.05 or less was considered statistically significant (* $p < 0.05$, ** $p < 0.01$, *** $p < 0.001$ or **** $p < 0.0001$).*

Chapter 1.4. Discussion and Conclusions

1.4. Discussion and Conclusions

The lack of experimental evidence in the skin regarding the expression of ANG as well as of its biological functions in this organ, have prompted us to undertake this pilot work.

ANG is widely known for several functions (Lyons et al., 2017), however, among them, the most interesting both for its recent discovery and for the new implications that it can cause is undoubtedly its role as a stress-induced RNase.

The epidermis is the outermost of the three layers that comprise the skin and for this reason also the most exposed to stressful stimuli from the external environment. For this reason, we have started a pioneering study aimed at the preliminary verification of the expression and localization of ANG in external skin cells subjected to different growth conditions. In order to do this, the HaCaT cell line was chosen as experimental model system as it simulates the most superficial state of the epidermis (Colombo et al., 2017) thus meeting our needs.

The first result collected allowed us to highlight that in HaCaT cells ANG is expressed both at the transcriptional and translational level and that this expression does not change if the cells were subjected to different growth conditions (physiological conditions or chemically/physically induced oxidative stress conditions) (**Figure 1.9**).

Interestingly this finding, highlighted for the first time in a skin cell line, is coincident with other studies in which ANG carries out its biological functions related to stress exclusively downstream of its intracellular re-localization (Giacomelli et al., 2015).

Indeed, it is widely ascertained that in physiological conditions ANG is localized both in nucleus and cytoplasm linked to its inhibitor (RNH1); only in the nucleoli ANG is free to promote the expression of rDNA and hence the ribosomes biogenesis (Lyons et al., 2017). Instead, in stressful conditions, ANG bypasses RNH1 control and it concentrates primarily in the cytosol, where it promotes the tRNAs cleavage into tiRNAs and contributes to stress granules (SGs) recruitment (Lyons et al., 2016).

In this work, we found that also in HaCaT cells, both in physiological conditions and when they are subjected to stressful perturbations, endogenous ANG assumes a similar behaviour (in terms of intracellular localization). In detail, our

1.4. Discussion and Conclusions

data clearly indicate that in stressed HaCaT cells endogenous ANG strongly tends to colocalize with the stress granules and thus for the first time was highlighted a potential involvement of ANG on SGs recruitment also in the stressed skin cells (**Figures 1.10 and 1.11**).

These evidences have then prompted us to undertake a new phase of the study aimed to better characterize the stress-induced role of ANG. Starting from the evidences by which we did not detect differences on the expression of endogenous ANG (**Figure 1.9**) and exploiting some reports in which ANG was studied as a paracrine factor (Prehn & Jirström, 2020; Skorupa et al., 2012), we performed a series of tests using recombinant proteins.

In a first phase, we verified by three alternative approaches that HaCaT cells pre-treated with recombinant ANG were always able to counteract vigorously oxidizing conditions (**Figures 1.15-1.17**). In the wave of these promising results, in a second phase we focused our efforts on two recombinant ANG variants:

- rANG_{6xHis}, designed with a His-tag inserted in C-term region and produced to verify a possible internalization in HaCaT cells;
- rANG(Q₃₁Q₃₂)_{6xHis}, designed with an altered NLS to detect a possible link between ANG stress induced role and a more marked cytosolic intracellular localization.

Both recombinant ANG variants were firstly characterized for their catalytic and structural properties as well as for their biocompatibility and then assayed following the same procedures performed on parental rANG.

Interestingly all results collected with these variants confirmed what reported for rANG, including the verification that both proteins were internalized, with a different tendency to accumulate in the cells (**Figures 1.24 and 1.25**), and that both were able to move towards growing SGs in stressed cells (**Figure 1.28**).

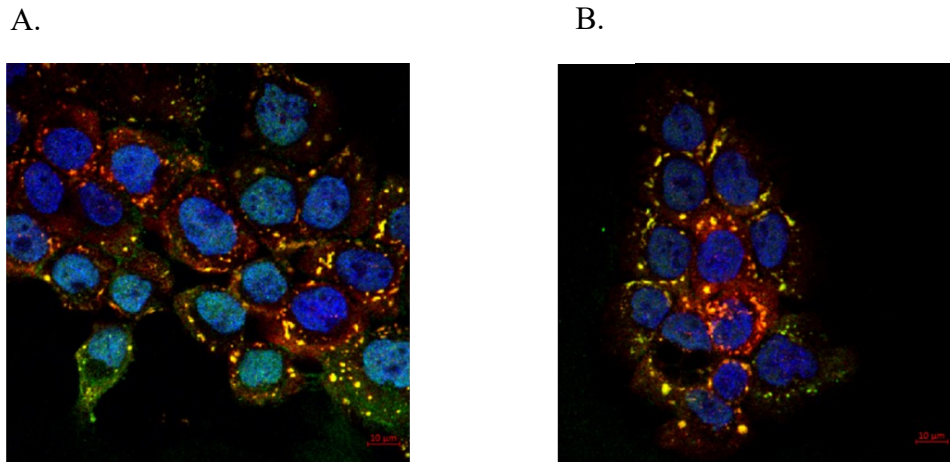


Figure 1.28. Immunofluorescence analysis of HaCaT cells subjected to oxidative stress with sodium arsenite. A. Pre-treated cells with 2 μ M of rANG_{6xHis} and then subjected to stress with 500mM SA. B. Pre-treated cells with 2 μ M of rANG(Q₃₁Q₃₂)_{6xHis} and then subjected to stress with 500mM. PABP (red), 6xHis (green) and blue staining (DAPI) for nuclei.

All these evidences clearly open a new scenario, in which ANG seems to exert a leading role in containing the response to skin stress by actively contributing to the restoration of homeostasis. However, the way forward is still quite long because there are several considerations to make.

In the first instance, the administered recombinant proteins were produced in bacteria and thus devoid of possible post-translational modifications. This issue could be a key point, especially considering that some residues (S28, Y36, S37 and S8) are susceptible to phosphorylation and could be important in the relationship with RNH1 that usually enormously constrains the functionality of ANG in the cell. The solution to this problem could be easily solved by planning transfection experiments, thus producing an endogenous recombinant protein fully suitable to undergo the canonical post-translational modifications.

A second point to consider concerns the internalization of ANG which in our experimental system has been induced at 2 μ M whereas *in vivo* it should be carefully reconsidered, both in terms of doses and of real availability on the skin.

1.4. Discussion and Conclusions

Moreover, also the internalization process could be different as the cells of an organized epithelium show modifications at the membrane level that instead are absent in membranes of cells grown *in vitro* on a plate. Also in this case, further tests need to be performed to calibrate how ANG is internalized in target cells.

A further consideration to be made concerns the catalytic activity of ANG which appears to be fundamental for the processing of tRNAs. In our experimental model, RNase activity of ANG on tRNAs has not been analyzed but it represents a fundamental objective if we concretely want to place ANG as a stress-induced skin protein, and therefore as a potential therapeutic platform for designing novel targeted anti-stress agents.

On the basis of all these observations, however, it must be considered that this is a pilot work that had as its main aim the preliminary investigation of the functional attitudes of ANG in a tissue district, such as the skin, never explored to date for this enzyme.

In conclusion, although preliminary, our results would seem to add a further contribution to the understanding of ANG's potential, effectively corroborating the idea that the human proteome is an inexhaustible platform for the inspiration and the design of new therapeutic agents (ANG and its variants, why not?) but, above all, an essential source from which to draw in order to understand the sophisticated mechanisms that regulate cellular homeostasis.

1.5. Bibliography

1.5. Bibliography

- Arimoto, K., Fukuda, H., Imajoh-Ohmi, S., Saito, H., & Takekawa, M. (2008). Formation of stress granules inhibits apoptosis by suppressing stress-responsive MAPK pathways. *Nature Cell Biology* 2008 10:11, 1011), 1324–1332. <https://doi.org/10.1038/ncb1791>
- Aulas, A., Fay, M. M., Lyons, S. M., Achorn, C. A., Kedersha, N., Anderson, P., & Ivanov, P. (2017). Stress-specific differences in assembly and composition of stress granules and related foci. *Journal of Cell Science*, 130(5), 927. <https://doi.org/10.1242/JCS.199240>
- Baird, S. D., Turcotte, M., Korneluk, R. G., & Holcik, M. (2006). Searching for IRES. *RNA*, 12(10), 1755–1785. <https://doi.org/10.1261/RNA.157806>
- Buchan, J. R., & Buchan, R. (2014). mRNP granules. *Http://Dx.Doi.Org/10.4161/15476286.2014.972208*, 11(8), 1019–1030. <https://doi.org/10.4161/15476286.2014.972208>
- Bushati, N., & Cohen, S. M. (2007). microRNA Functions. *Http://Dx.Doi.Org/10.1146/Annurev.Cellbio.23.090506.123406*, 23, 175–205. <https://doi.org/10.1146/ANNUREV.CELLBIO.23.090506.123406>
- Colombo, I., Sangiovanni, E., Maggio, R., Mattozzi, C., Zava, S., Corbett, Y., Fumagalli, M., Carlino, C., Corsetto, P. A., Scaccabarozzi, D., Calvieri, S., Gismondi, A., Taramelli, D., & Dell’Agli, M. (2017). HaCaT Cells as a Reliable In Vitro Differentiation Model to Dissect the Inflammatory/Repair Response of Human Keratinocytes. *Mediators of Inflammation*, 2017. <https://doi.org/10.1155/2017/7435621>
- Cox, D. J., Strudwick, N., Ali, A. A., Paton, A. W., Paton, J. C., & Schröder, M. (2011). Measuring signaling by the unfolded protein response. *Methods in Enzymology*, 491, 261–292. <https://doi.org/10.1016/B978-0-12-385928-0.00015-8>
- Donnelly, N., Gorman, A. M., Gupta, S., & Samali, A. (2013). The eIF2 α kinases: their structures and functions. *Cellular and Molecular Life Sciences : CMLS*, 70(19), 3493–3511. <https://doi.org/10.1007/S00018-012-1252-6>

1.5. Bibliography

- Elkordy, A., Mishima, E., Niizuma, K., Akiyama, Y., Fujimura, M., Tominaga, T., & Abe, T. (2018). Stress-induced tRNA cleavage and tiRNA generation in rat neuronal PC12 cells. *Journal of Neurochemistry*, 146(5), 560–569. <https://doi.org/10.1111/JNC.14321>
- Elkordy, A., Rashad, S., Shehabeldeen, H., Mishima, E., Niizuma, K., Abe, T., & Tominaga, T. (2019). tiRNAs as a novel biomarker for cell damage assessment in in vitro ischemia-reperfusion model in rat neuronal PC12 cells. *Brain Research*, 1714, 8–17. <https://doi.org/10.1016/J.BRAINRES.2019.02.019>
- Emara, M. M., Ivanov, P., Hickman, T., Dawra, N., Tisdale, S., Kedersha, N., Hu, G. F., & Anderson, P. (2010). Angiogenin-induced tRNA-derived stress-induced RNAs promote stress-induced stress granule assembly. *Journal of Biological Chemistry*, 285(14), 10959–10968. <https://doi.org/10.1074/jbc.M109.077560>
- Ferguson, R., Holloway, D. E., Chandrasekhar, A., Acharya, K. R., & Subramanian, V. (2019). The catalytic activity and secretion of zebrafish RNases are essential for their in vivo function in motor neurons and vasculature. *Scientific Reports* 2019 9:1, 9(1), 1–15. <https://doi.org/10.1038/s41598-018-37140-2>
- Fett, J. W., Strydom, D. J., Lobb, R. R., Alderman, E. M., Bethune, J. L., Riordan, J. F., & Vallee, B. L. (1985). Isolation and characterization of angiogenin, an angiogenic protein from human carcinoma cells. *Biochemistry*, 24(20), 5480–5486. <https://doi.org/10.1021/BI00341A030>
- Fulda, S., Gorman, A. M., Hori, O., & Samali, A. (2010). Cellular Stress Responses: Cell Survival and Cell Death. *International Journal of Cell Biology*, 2010. <https://doi.org/10.1155/2010/214074>
- Giacomelli, C., Trincavelli, M. L., Satriano, C., Hansson, Ö., la Mendola, D., Rizzarelli, E., & Martini, C. (2015). ♦Copper (II) ions modulate Angiogenin activity in human endothelial cells. *The International Journal of Biochemistry & Cell Biology*, 60, 185–196. <https://doi.org/10.1016/J.BIOCEL.2015.01.005>
- Gilks, N., Kedersha, N., Ayodele, M., Shen, L., Stoecklin, G., Dember, L. M., & Anderson, P. (2004). Stress granule assembly is mediated by prion-like

1.5. Bibliography

- aggregation of TIA-1. *Molecular Biology of the Cell*, 15(12), 5383–5398. <https://doi.org/10.1091/MBC.E04-08-0715>
- Good, A. L., & Stoffers, D. A. (2020). Stress-Induced Translational Regulation Mediated by RNA Binding Proteins: Key Links to β -Cell Failure in Diabetes. *Diabetes*, 69(4), 499–507. <https://doi.org/10.2337/DBI18-0068>
- Hardie, D. G. (2007). AMP-activated/SNF1 protein kinases: conserved guardians of cellular energy. *Nature Reviews Molecular Cell Biology* 2007 8:10, 8(10), 774–785. <https://doi.org/10.1038/nrm2249>
- Harding, H. P., Novoa, I., Zhang, Y., Zeng, H., Wek, R., Schapira, M., & Ron, D. (2000). Regulated Translation Initiation Controls Stress-Induced Gene Expression in Mammalian Cells. *Molecular Cell*, 6(5), 1099–1108. [https://doi.org/10.1016/S1097-2765\(00\)00108-8](https://doi.org/10.1016/S1097-2765(00)00108-8)
- Hay, N., & Sonenberg, N. (2004). Upstream and downstream of mTOR. *Genes & Development*, 18(16), 1926–1945. <https://doi.org/10.1101/GAD.1212704>
- Himanen, S. v., & Sistonen, L. (2019). New insights into transcriptional reprogramming during cellular stress. *Journal of Cell Science*, 132(21). <https://doi.org/10.1242/JCS.238402/224639>
- Hooper, L. v., Stappenbeck, T. S., Hong, C. v., & Gordon, J. I. (2003). Angiogenins: a new class of microbicidal proteins involved in innate immunity. *Nature Immunology*, 4(3), 269–273. <https://doi.org/10.1038/NI888>
- Ibaragi, S., Yoshioka, N., Kishikawa, H., Hu, J. K., Sadow, P. M., Li, M., & Hu, G. F. (2009). Angiogenin-Stimulated rRNA Transcription Is Essential for Initiation and Survival of AKT-Induced Prostate Intraepithelial Neoplasia. *Molecular Cancer Research*, 7(3), 415–424. <https://doi.org/10.1158/1541-7786.MCR-08-0137>
- Ibaragi, S., Yoshioka, N., Li, S., Hu, M. G., Hirukawa, S., Sadow, P. M., & Hu, G. F. (2009). Neamine Inhibits Prostate Cancer Growth by Suppressing Angiogenin-Mediated rRNA Transcription. *Clinical Cancer Research*, 15(6), 1981–1988. <https://doi.org/10.1158/1078-0432.CCR-08-2593>

1.5. Bibliography

- Ivanov, P., Emara, M. M., Villen, J., Gygi, S. P., & Anderson, P. (2011). Angiogenin-Induced tRNA Fragments Inhibit Translation Initiation. *Molecular Cell*, 43(4), 613–623. <https://doi.org/10.1016/j.molcel.2011.06.022>
- Iwawaki, T., Hosoda, A., Okuda, T., Kamigori, Y., Nomura-Furuwatari, C., Kimata, Y., Tsuru, A., & Kohno, K. (2001). Translational control by the ER transmembrane kinase/ribonuclease IRE1 under ER stress. *Nature Cell Biology* 2001 3:2, 3(2), 158–164. <https://doi.org/10.1038/35055065>
- Jain, S., Wheeler, J. R., Walters, R. W., Agrawal, A., Barsic, A., & Parker, R. (2016a). ATPase-Modulated Stress Granules Contain a Diverse Proteome and Substructure. *Cell*, 164(3), 487–498. <https://doi.org/10.1016/J.CELL.2015.12.038>
- Katz, M. J., Gándara, L., de Lella Ezcurra, A. L., & Wappner, P. (2016). Hydroxylation and translational adaptation to stress: some answers lie beyond the STOP codon. *Cellular and Molecular Life Sciences* 2016 73:9, 73(9), 1881–1893. <https://doi.org/10.1007/S00018-016-2160-Y>
- Keegan, L. P., Gallo, A., & O’Connell, M. A. (2001). The many roles of an RNA editor. *Nature Reviews Genetics* 2001 2:11, 2(11), 869–878. <https://doi.org/10.1038/35098584>
- Kieran, D., Sebastia, J., Greenway, M. J., King, M. A., Connaughton, D., Concannon, C. G., Fenner, B., Hardiman, O., & Prehn, J. H. M. (2008). Control of Motoneuron Survival by Angiogenin. *Journal of Neuroscience*, 28(52), 14056–14061. <https://doi.org/10.1523/JNEUROSCI.3399-08.2008>
- Kishimoto, K., Liu, S., Tsuji, T., Olson, K. A., & Hu, G. F. (2004). Endogenous angiogenin in endothelial cells is a general requirement for cell proliferation and angiogenesis. *Oncogene* 2005 24:3, 24(3), 445–456. <https://doi.org/10.1038/sj.onc.1208223>
- Kültz, D. (2005). MOLECULAR AND EVOLUTIONARY BASIS OF THE CELLULAR STRESS RESPONSE CELLULAR STRESS: WHAT IS THE THREAT AND HOW DO CELLS RESPOND? *Annu. Rev. Physiol*, 67, 225–257. <https://doi.org/10.1146/annurev.physiol.67.040403.103635>

1.5. Bibliography

- Kumar, P., Nagarajan, A., & Uchil, P. D. (2018). Analysis of Cell Viability by the MTT Assay. *Cold Spring Harbor Protocols*, 2018(6), 469–471. <https://doi.org/10.1101/PDB.PROT095505>
- Kwon, S., Zhang, Y., & Matthias, P. (2007). The deacetylase HDAC6 is a novel critical component of stress granules involved in the stress response. *Genes & Development*, 21(24), 3381–3394. <https://doi.org/10.1101/GAD.461107>
- Leung, A. K. L., Vyas, S., Rood, J. E., Bhutkar, A., Sharp, P. A., & Chang, P. (2011). Poly(ADP-ribose) regulates stress responses and microRNA activity in the cytoplasm. *Molecular Cell*, 42(4), 489–499. <https://doi.org/10.1016/J.MOLCEL.2011.04.015>
- Li, S., & Hu, G. F. (2012). Emerging role of angiogenin in stress response and cell survival under adverse conditions. In *Journal of Cellular Physiology* (Vol. 227, Issue 7, pp. 2822–2826). <https://doi.org/10.1002/jcp.23051>
- Li, S., Sheng, J., Hu, J. K., Yu, W., Kishikawa, H., Hu, M. G., Shima, K., Wu, D., Xu, Z., Xin, W., Sims, K. B., Landers, J. E., Brown, R. H., & Hu, G. F. (2013). Ribonuclease 4 protects neuron degeneration by promoting angiogenesis, neurogenesis, and neuronal survival under stress. *Angiogenesis*, 16(2), 387–404. <https://doi.org/10.1007/S10456-012-9322-9/FIGURES/11>
- Li, Y., Corradetti, M. N., Inoki, K., & Guan, K. L. (2004). TSC2: filling the GAP in the mTOR signaling pathway. *Trends in Biochemical Sciences*, 29(1), 32–38. <https://doi.org/10.1016/J.TIBS.2003.11.007>
- Liu, B., & Qian, S. B. (2014). Translational reprogramming in stress response. *Wiley Interdisciplinary Reviews. RNA*, 5(3), 301. <https://doi.org/10.1002/WRNA.1212>
- Lu, L., Li, J., Moussaoui, M., & Boix, E. (2018). Immune Modulation by Human Secreted RNases at the Extracellular Space. *Frontiers in Immunology*, 9(MAY), 1. <https://doi.org/10.3389/FIMMU.2018.01012>
- Lu, P. D., Jousse, C., Marciniak, S. J., Zhang, Y., Novoa, I., Scheuner, D., Kaufman, R. J., Ron, D., & Harding, H. P. (2004). Cytoprotection by pre-emptive

- conditional phosphorylation of translation initiation factor 2. *The EMBO Journal*, 23(1), 169–179. <https://doi.org/10.1038/SJ.EMBOJ.7600030>
- Lyons, S. M., Achorn, C., Kedersha, N. L., Anderson, P. J., & Ivanov, P. (2016). YB-1 regulates tiRNA-induced Stress Granule formation but not translational repression. *Nucleic Acids Research*, 44(14), 6949–6960. <https://doi.org/10.1093/NAR/GKW418>
- Lyons, S. M., Fay, M. M., Akiyama, Y., Anderson, P. J., & Ivanov, P. (2017). RNA biology of angiogenin: Current state and perspectives. *RNA Biology*, 14(2), 171–178. <https://doi.org/10.1080/15476286.2016.1272746>
- Mahboubi, H., & Stochaj, U. (2017). Cytoplasmic stress granules: Dynamic modulators of cell signaling and disease. *Biochimica et Biophysica Acta. Molecular Basis of Disease*, 1863(4), 884–895. <https://doi.org/10.1016/J.BBADIS.2016.12.022>
- McCormick, C., & Khaperskyy, D. A. (2017). Translation inhibition and stress granules in the antiviral immune response. In *Nature Reviews Immunology* (Vol. 17, Issue 10, pp. 647–660). Nature Publishing Group. <https://doi.org/10.1038/nri.2017.63>
- Moroianu, J., & Riordan, J. F. (1994). Nuclear translocation of angiogenin in proliferating endothelial cells is essential to its angiogenic activity. *Proceedings of the National Academy of Sciences of the United States of America*, 91(5), 1677–1681. <https://doi.org/10.1073/PNAS.91.5.1677>
- Nakagawa, K., Lokugamage, K. G., & Makino, S. (2016). Viral and Cellular mRNA Translation in Coronavirus-Infected Cells. *Advances in Virus Research*, 96, 165–192. <https://doi.org/10.1016/BS.AIVIR.2016.08.001>
- Ohn, T., Kedersha, N., Hickman, T., Tisdale, S., & Anderson, P. (2008). A functional RNAi screen links O-GlcNAc modification of ribosomal proteins to stress granule and processing body assembly. *Nature Cell Biology*, 10(10), 1224. <https://doi.org/10.1038/NCB1783>

1.5. Bibliography

- Palmer, K. A., Scheraga, H. A., Riordan, J. F., & Vallee, B. L. (1986). A preliminary three-dimensional structure of angiogenin. *Proceedings of the National Academy of Sciences of the United States of America*, 83(7), 1965. <https://doi.org/10.1073/PNAS.83.7.1965>
- Park, J., Kim, J. T., Lee, S. J., & Kim, J. C. (2020). The Anti-Inflammatory Effects of Angiogenin in an Endotoxin Induced Uveitis in Rats. *International Journal of Molecular Sciences*, 21(2). <https://doi.org/10.3390/IJMS21020413>
- Pizzo, E., Sarcinelli, C., Sheng, J., Fusco, S., Formiggini, F., Netti, P., Yu, W., D'Alessio, G., & Hu, G. F. (2013). Ribonuclease/angiogenin inhibitor 1 regulates stress-induced subcellular localization of angiogenin to control growth and survival. *Undefined*, 126(18), 4308–4319. <https://doi.org/10.1242/JCS.134551>
- Pizzo, E., Varcamonti, M., di Maro, A., Zanfardino, A., Giancola, C., & D'Alessio, G. (2008). Ribonucleases with angiogenic and bactericidal activities from the Atlantic salmon. *The FEBS Journal*, 275(6), 1283–1295. <https://doi.org/10.1111/J.1742-4658.2008.06289.X>
- Prehn, J. H. M., & Jirström, E. (2020). Angiogenin and tRNA fragments in Parkinson's disease and neurodegeneration. *Acta Pharmacologica Sinica* 2020 41:4, 41(4), 442–446. <https://doi.org/10.1038/s41401-020-0375-9>
- Protter, D. S. W., & Parker, R. (2016). Principles and Properties of Stress granules. *Trends in Cell Biology*, 26(9), 668. <https://doi.org/10.1016/J.TCB.2016.05.004>
- Reiling, J. H., & Sabatini, D. M. (2006). Stress and mTOR signaling. *Oncogene* 2006 25:48, 25(48), 6373–6383. <https://doi.org/10.1038/sj.onc.1209889>
- Sack, R. A., Conradi, L., Krumholz, D., Beaton, A., Sathe, S., & Morris, C. (2005). Membrane array characterization of 80 chemokines, cytokines, and growth factors in open- and closed-eye tears: angiogenin and other defense system constituents. *Investigative Ophthalmology & Visual Science*, 46(4), 1228–1238. <https://doi.org/10.1167/IOVS.04-0760>

1.5. Bibliography

- Samuel, C. E. (2001). Antiviral actions of interferons. *Clinical Microbiology Reviews*, 14(4), 778–809. <https://doi.org/10.1128/CMR.14.4.778-809.2001/ASSET/00C86B9D-C501-4944-86BB-21BCC773A58A/ASSETS/GRAPHIC/CM0410036006.JPEG>
- Scadden, A. D. J. (2007). Inosine-Containing dsRNA Binds a Stress-Granule-like Complex and Downregulates Gene Expression In trans. *Molecular Cell*, 28(3), 491–500. <https://doi.org/10.1016/J.MOLCEL.2007.09.005>
- Shapiro, R., Riordan, J. F., & Vallee, B. L. (1986). Characteristic ribonucleolytic activity of human angiogenin. *Biochemistry*, 25(12), 3527–3532. <https://doi.org/10.1021/BI00360A008>
- Shapiro, R., & Vallee, B. L. (1987). Human placental ribonuclease inhibitor abolishes both angiogenic and ribonucleolytic activities of angiogenin. *Proceedings of the National Academy of Sciences*, 84(8), 2238–2241. <https://doi.org/10.1073/PNAS.84.8.2238>
- Sheng, J., & Xu, Z. (2016). Three decades of research on angiogenin: a review and perspective. *Acta Biochimica et Biophysica Sinica*, 48(5), 399–410. <https://doi.org/10.1093/ABBS/GMV131>
- Sheng, J., Yu, W., Gao, X., Xu, Z., & Hu, G. F. (2014). Angiogenin stimulates ribosomal RNA transcription by epigenetic activation of the ribosomal DNA promoter. *Journal of Cellular Physiology*, 229(4), 521–529. <https://doi.org/10.1002/JCP.24477>
- Skorupa, A., King, M. A., Aparicio, I. M., Dussmann, H., Coughlan, K., Breen, B., Kieran, D., Concannon, C. G., Marin, P., & Prehn, J. H. M. (2012). Motoneurons Secrete Angiogenin to Induce RNA Cleavage in Astroglia. *The Journal of Neuroscience*, 32(15), 5024. <https://doi.org/10.1523/JNEUROSCI.6366-11.2012>
- Slotkin, W., & Nishikura, K. (2013). Adenosine-to-inosine RNA editing and human disease. *Genome Medicine*, 5(11), 1–13. <https://doi.org/10.1186/GM508/FIGURES/4>

1.5. Bibliography

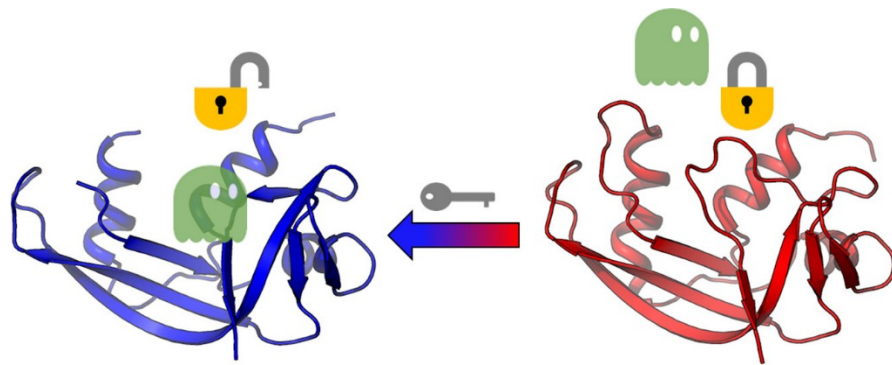
- Tao, E. W., Cheng, W. Y., Li, W. L., Yu, J., & Gao, Q. Y. (2020). tiRNAs: A novel class of small noncoding RNAs that helps cells respond to stressors and plays roles in cancer progression. *Journal of Cellular Physiology*, 235(2), 683–690. <https://doi.org/10.1002/JCP.29057>
- Tello-Montoliu, A., Patel, J. v., & Lip, G. Y. H. (2006). Angiogenin: a review of the pathophysiology and potential clinical applications. *Journal of Thrombosis and Haemostasis : JTH*, 4(9), 1864–1874. <https://doi.org/10.1111/J.1538-7836.2006.01995.X>
- Thiyagarajan, N., & Acharya, K. R. (2012). Crystal structure of human angiogenin with an engineered loop exhibits conformational flexibility at the functional regions of the molecule. *FEBS Open Bio*, 3, 65–70. <https://doi.org/10.1016/J.FOB.2012.12.003>
- Thompson, D. M., Lu, C., Green, P. J., & Parker, R. (2008). tRNA cleavage is a conserved response to oxidative stress in eukaryotes. *RNA*, 14(10), 2095. <https://doi.org/10.1261/RNA.1232808>
- Tourrière, H., Chebli, K., Zekri, L., Courselaud, B., Blanchard, J. M., Bertrand, E., & Tazi, J. (2003). The RasGAP-associated endoribonuclease G3BP assembles stress granules. *Journal of Cell Biology*, 160(6), 823–831. <https://doi.org/10.1083/JCB.200212128>
- Tsuji, T., Sun, Y., Kishimoto, K., Olson, K. A., Liu, S., Hirukawa, S., & Hu, G. F. (2005). Angiogenin Is Translocated to the Nucleus of HeLa Cells and Is Involved in Ribosomal RNA Transcription and Cell Proliferation. *Cancer Research*, 65(4), 1352–1360. <https://doi.org/10.1158/0008-5472.CAN-04-2058>
- van Es, M. A., Schelhaas, H. J., van Vught, P. W. J., Ticozzi, N., Andersen, P. M., Groen, E. J. N., Schulte, C., Blauw, H. M., Koppers, M., Diekstra, F. P., Fumoto, K., Leclerc, A. L., Keagle, P., Bloem, B. R., Scheffer, H., van Nuenen, B. F. L., van Blitterswijk, M., van Rheenen, W., Wills, A. M., ... van den Berg, L. H. (2011). Angiogenin variants in Parkinson disease and

1.5. Bibliography

- amyotrophic lateral sclerosis. *Annals of Neurology*, 70(6), 964–973.
<https://doi.org/10.1002/ANA.22611>
- Wang, Q., Miyakoda, M., Yang, W., Khillan, J., Stachura, D. L., Weiss, M. J., & Nishikura, K. (2004). Stress-induced Apoptosis Associated with Null Mutation of ADAR1 RNA Editing Deaminase Gene *. *Journal of Biological Chemistry*, 279(6), 4952–4961. <https://doi.org/10.1074/JBC.M310162200>
- Wen, J., Huang, Z., Li, Q., Chen, X., Qin, H., & Zhao, Y. (2021). Research progress on the tsRNA classification, function, and application in gynecological malignant tumors. *Cell Death Discovery* 2021 7:1, 7(1), 1–9.
<https://doi.org/10.1038/s41420-021-00789-2>
- Wullschleger, S., Loewith, R., & Hall, M. N. (2006). TOR Signaling in Growth and Metabolism. *Cell*, 124(3), 471–484.
<https://doi.org/10.1016/J.CELL.2006.01.016>
- Yamasaki, S., & Anderson, P. (2008). Reprogramming mRNA translation during stress. *Current Opinion in Cell Biology*, 20(2), 222.
<https://doi.org/10.1016/J.CEB.2008.01.013>
- Yoshida, H., Matsui, T., Yamamoto, A., Okada, T., & Mori, K. (2001). XBP1 mRNA Is Induced by ATF6 and Spliced by IRE1 in Response to ER Stress to Produce a Highly Active Transcription Factor. *Cell*, 107(7), 881–891.
[https://doi.org/10.1016/S0092-8674\(01\)00611-0](https://doi.org/10.1016/S0092-8674(01)00611-0)

Part 2

*The structural features of an ancient ribonuclease
from *Salmo salar* reveal
an intriguing case of auto-inhibition*



Chapter 2.1. Introduction

2.1.1. Vertebrate-secreted RNase Superfamily

Vertebrate-secreted RNase Superfamily is nowadays one of the best characterized family of enzymes and comprises proteins involved in host defense with specific cytotoxic and immune-modulatory properties (D'Alessio, 2011).

The genes encoding these RNases are all phylogenetically linked and all encoding for secreted proteins able to display, in addition to ribonucleolytic properties, surprising different physiological functions as selective toxicity, angiogenesis, host defense, immunosuppression, biogenesis of ribosomes, stress response etc. (H. H. Lee et al., 2019; Leland et al., 2002; Monti et al., 2009)

The study of the archetype of this Superfamily, RNase A, completely changed the understanding of protein chemistry and significantly contributed to set the foundation of modern biology, providing a useful model for innovative methodologies in the structural and functional protein study (Beintema & Kleineidam, 1998).

Phylogenetic studies revealed (Beintema et al., 1997) that many RNases present in a variety of organisms, from amphibians to reptiles, birds, mammals, were structurally and functionally close to RNase A, reason why was initially conceived the Superfamily knows as “RNase A Superfamily”, from the first described archetypical RNase. Subsequently, further homologous members have been found also in fishes and thus this extended group has been definitely renamed as Vertebrate-secreted RNase Superfamily.

All members share specific structural features, listed below:

1. A consensus region, also known as “RNase signature”, composed by the sequence CKxxNTF
2. A reading frame contained in a single exon;
3. A catalytic activity carried out by the cooperation of two His and 1 Lys (His12, His 119 and Lys 41 in RNase A);
4. A common catalytic mechanism in which the action of the two histidines in the active site removes a proton from the 2'-OH of the pyrimidine, causing the formation of a cyclic 2',3'-phosphate. Phosphate cyclization releases the portion of the RNA chain that is 3' to the pyrimidine, resulting in cleavage of the RNA strand. The cyclized phosphate is then hydrolyzed creating a 2'-

OH and 3'-phosphate on the 3'-terminal ribose of the cleaved RNA. The reaction mechanism requires the 2'-OH on the nucleotide recognized by the nuclease to facilitate the attack and subsequent cleavage of the phosphate backbone (Cuchillo et al., 1997)

5. A α/β structure arranged in a kidney shape commonly by three α -helix stretches and a four stranded antiparallel β -sheet (**Figure 2.1**). All members of the Superfamily are monomeric, with the exception of the dimeric protein BS-RNase (Bovine Seminal RNase).



Figure 2.1. *Crystal structure of wild-type bovine pancreatic Ribonuclease A (PDB. 3DH5).*

2.1.2. Fish RNases

For a long time, it has been debated whether homologs of archetypal RNase A were present only in tetrapods.

The increasing availability of annotated genomes has led to clarify that members of the Superfamily were present also in fish (to date, only in bony fish) (Figure 2.2).

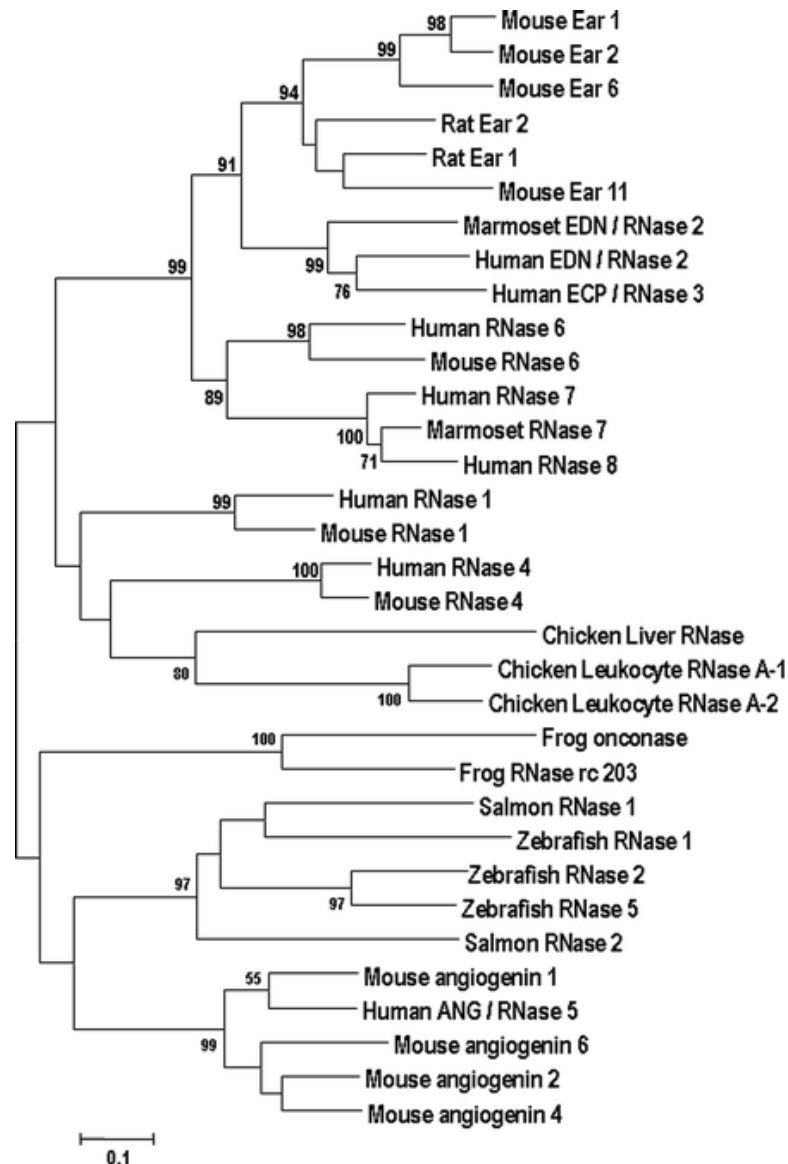


Figure 2.2. *Phylogenetic tree documenting relationships among various vertebrate secretory (RNase A) ribonucleases. Neighbor-joining tree constructed with encoded amino acid sequences, using algorithms within MEGA 4.0 (Rosenberg, 2011).*

The first recombinant fish RNases was obtained and studied, first from zebrafish (*Danio rerio*) (Cho & Zhang, 2007; Kazakou et al., 2008; Pizzo et al., 2011), then from Atlantic salmon (*Salmo salar*) (Pizzo et al., 2008).

The main properties of the fish RNases studied so far are basically related to the low ribonucleolytic activity and the angiogenic/bactericidal activity, the latter likely associated to an ancestral hypothetical role of these proteins as part of host-defense mechanisms (Cho & Zhang, 2007). Consistent with this hypothesis, is the finding of high level of RNases in gut and liver of zebrafish (Hooper et al., 2003) and Atlantic salmon (Pizzo et al., 2008), suggestive of their involvement in innate immunity.

The similarity of fish RNases with other angiogenins, in particular with human ANG (described above), is related not only to the function but is also structural. In effect, all identified fish RNases share with ANG six cysteine residues, involved in the formation of three disulphide bridges as well as all fish RNase share with ANG the same partial obstruction of the active site (Pizzo et al., 2011), a peculiar structural feature directly related to the lower ribonucleolytic activity of this proteins.

2.1.3. Mechanisms of RNases enzymatic regulation

Various mechanisms in biological systems operate to avoid unwanted activation of a specific enzyme activity. This is often achieved through a direct interaction with an effector that limits the entrance of the substrate in the active site. In some cases, a rather flexible portion from the same enzyme adopts a position that limits or fully prevents the enzymatic activity by intramolecular clashes. This auto-inhibition may be relieved by the interaction with an appropriate external factor that activates a conformational change making the active site accessible to the substrate.

Both kinds of inhibition mechanisms have been described for components of the vertebrate RNase Superfamily (Beintema et al., 1997; Pizzo & D'Alessio, 2007; Raines, 1998).

The catalytic site of vertebrate RNases includes a P1 subsite, that houses the hydrolysable phosphodiester group and is composed by two histidines and a lysine (catalytic triad), and two subsites, B1 and B2, that preferentially bind a pyrimidine

and a purine base, respectively (Parés et al., 1991). Except for these conserved residues, vertebrate RNases are quite divergent, with sequence identities varying from 20% to nearly 100%.

RNase A is characterized by an α/β architecture that embodies four intrachain disulphides. The protein is a highly efficient enzyme that can reach a value of $k_{\text{cat}}/K_{\text{M}}$ even greater than $10^7 \text{ M}^{-1} \text{ s}^{-1}$ for the best substrates, but is severely inhibited by some small oligonucleotides and, in particular, by RNH1, a very potent protein inhibitor (Kobe & Deisenhofer, 1996). On the other hand, auto-inhibition is observed in other members of vertebrate RNases, which present a folding very similar to that of RNase A. These proteins have a very low ribonucleolytic activity that is associated with some other specific functions, which turns out to be explicitly dependent on the enzymatic activity (Matousek et al., 1995; Pizzo & D'Alessio, 2007). Outstanding examples are onconase (Wu et al., 1993) and angiogenin (Vliegthart et al., 2002).

Onconase from *Rana pipiens* has a three-dimensional folding very close to the pancreatic enzyme (Mosimann et al., 1994; Rutkoski & Raines, 2008), with an additional disulphide bond that tethers the C-terminus to the body of the molecule.

Despite the strict similarity of the overall architecture, onconase is capable to escape the interaction with RNH1 (Matousek et al., 1995), and displays low affinity towards oligonucleotides and low catalytic activity (J. E. Lee & Raines, 2003). These effects are probably caused by a remarkable reduction of the skeleton flexibility considered to play an important role in the functional behaviour of the pancreatic enzyme (Holloway et al., 2011; Merlino et al., 2005)

Similarly, to onconase, human ANG, has a folding that closely matches that of RNase A. In this case, its low activity has been mainly ascribed to a partial obstruction of the B1 subsite by the side chain of Gln117 (Leonidas et al., 2002; Riordan, 1997; Russo et al., 1994), whose orientation seems to be dictated by a turn of a 3_{10} helix that encompasses the segment 118–121. A similar obstruction of the B1 subsite has also been observed in murine angiogenin (mANG) (Holloway et al., 2005), as well as in the closely associated monomeric ribonucleases from *Danio rerio* (Kazakou et al., 2008; Pizzo et al., 2006, 2011). In all these cases, however, the presence of a 3_{10} helix was not observed.

2.1.4. Salmon RNases

Salmo salar belongs to Protoacanthopterygii, an ancient group of Teleostei, appeared over 100 million years ago. In this organism, one of the most exploited species worldwide in sports, fishing industry and as major farmed for food sector, two monomeric RNases, SS-RNase-1 (SS1) and SS-RNase-2 (SS2), have been identified and studied (Pizzo et al., 2008). These ancient RNases, probably the oldest members of the Superfamily identified to date, embody three disulphide bridges and are identified by their ability to stimulate the growth of blood vessels and a very low catalytic activity, albeit essential to their angiogenic function. An analysis of the protein stability indicates that SS2 is much more stable than SS1 and even more stable than RNase A (Pizzo et al., 2008). Furthermore, SS2 is the most active of the two salmon ribonucleases and of the most active fish ribonucleases studied so far, although much less active than RNase A (Pizzo et al., 2008).

The crystallographic structure of SS2 was determined at 1.89 Å resolution by Professor Sica and her team (Department of Chemical Sciences, University of Naples “Federico II”). Crystals belong to P21 space group and contain two molecules (A and B) in the asymmetric unit, correlated by a non-crystallographic twofold axis (**Figure 2.3a**).

The protein adopts the characteristic “V” shaped fold of vertebrate RNases, in which the two lobes V1 and V2 have a multiple strand β -sheet organization and form a cleft housing the catalytic centre. Considering the structure-based alignment (**Figure 2.3b**), the expected catalytic triad of SS2 comprises His13, Lys40 and His113, while other phosphate-binding interactions are provided by the side-chain amide group of Gln12 and the main chain N atom of Tyr114.

The crystallographic structure of SS2 as well as the analysis of its sequence compared to those of ANG and RNaseA, reveal that the active site is partially obstructed by a downstream pentapeptide that represents an anomalous insertion with respect to the sequences of vertebrate RNases.

As usually observed in other RNases, the active site residues His13 and Lys40 are well ordered, and their conformation (see **Figure 2.4**) is very similar to the corresponding residues of RNase A (His12 and Lys41).

In particular, the imidazole ring of His13 is firmly held in place by a strong hydrogen bond with the carbonyl oxygen of Thr44 (see **Figure 2.4a**), an interaction highly conserved within the members of the Superfamily, and the side chain of Lys40 is hydrogen bonded to Asn43. Altogether, the conserved residues His13, Asn43, Thr44, lining the B1 subsite, correlate well with the corresponding residues of RNase A (His12, Asn44, Thr45). Interestingly, in SS2 the charged side chain of Lys42, that replaces Val43, points towards the B1 subsite (see **Figure 2.4b**), making more positive the expected binding site of the pyrimidine bases.

In addition, the replacement of two polar residues Asp83 and Ser123 in the pancreatic enzyme by the hydrophobic residues Ile79 and Ile122 with bulkier side chains, narrows the entrance of the B1 subsite and considerably modifies the electrostatic surface potential in this region.

Mostly intriguing, the remaining part of the active site is obstructed by the segment Val118-Ile120, a well-structured peptide anchored to the protein body by several interactions. In particular, the main chain of residues 118 and 119 is located well inside the region occupied by the ribose ring in the B1 subsite, as reported in the structure of RNase A complexed with 2'-deossicitidilil (3'-5')-2'-deossiadenosine dinucleotide (pdb: 1RPG) or in the complex of the closely related bovine seminal ribonuclease with uridylyl-2',5'-adenosine (pdb: 11BA). The side chain of Asp119 is salt bridged to that of Lys42 (see **Figure 2.4 b**) and mimics part of the pyrimidine ring in a manner that is reminiscent of human ANG, in which a similar obstruction is contributed by Gln117 (Leonidas et al., 1999). As result, the key residues His113-Tyr114-Asp115 (His119-Phe120-Asp121 in RNase A), which are expected to constitute the necessary completion of the active site, are displaced from their canonical position. These residues and the following pentapeptide (Gly116-Ile120) form a loop located between the V1 and V2 arms of the protein skeleton (see **Figure 2.5**).

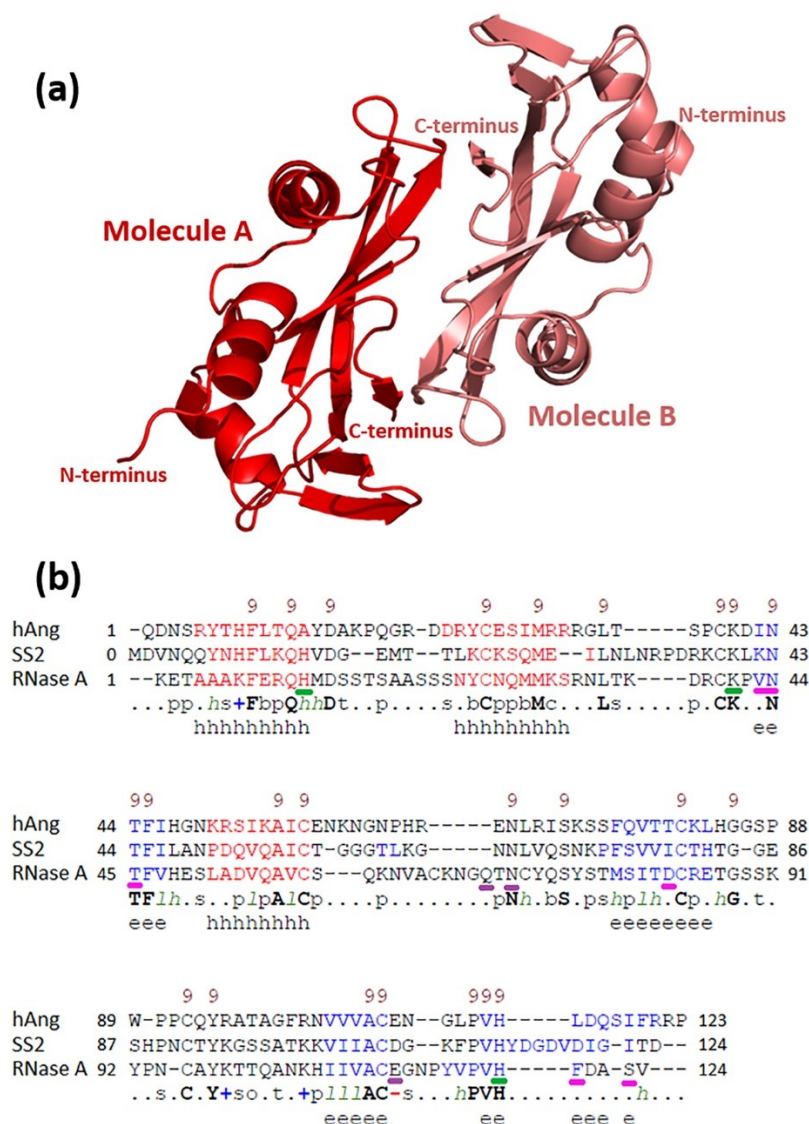


Figure 2.3. Crystal structure of SS2. The two molecules, A and B, in the asymmetric unit are coloured in red and pink, respectively. (b) Structure-based sequence alignment. The coordinates of SS2, RNase A (pdb: 1KF5) and human angiogenin (hAng, pdb: 1B1J) were aligned with PROMALS3D (Pei et al., 2008). Alpha-helix is coloured in red, and beta-strand is in blue. The first line in each block shows conservation indices. The last two lines show consensus amino acid sequence and consensus predicted secondary structures. Consensus predicted secondary structure symbols are: alpha-helix, h; beta-strand, e. Consensus amino acid symbols are: conserved amino acids, bold and uppercase letters; aliphatic (I, V, L), ; hydrophobic (W, F, Y, M, L, I, V, A, C, T, H), h; alcohol (S, T), o; polar residues (D, E, H, K, N, Q, R, S, T), p; tiny (A, G, C, S), t; small (A, G, C, S, V, N, D, T, P), s; bulky residues (E, F, I, K, L, M, Q, R, W, Y), b; positively charged (K, R, H), +; negatively charged (D, E), -; charged (D, E, K, R, H), c. The residues that form the P1, B1 and B2 subsites in RNase A are underlined in green, magenta, and violet, respectively.

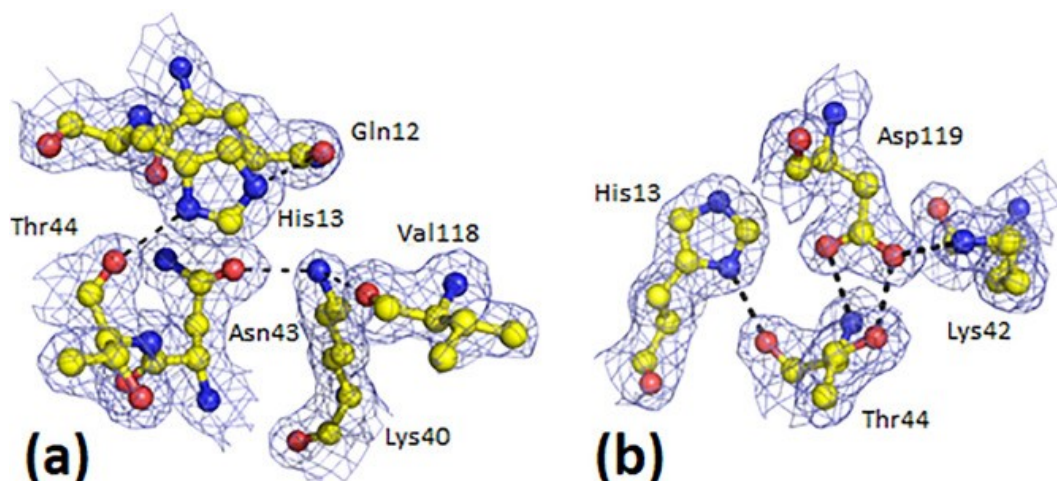


Figure 2.4. *Electron density map of SS2. (a) P1 and (b) B1 subsites.*

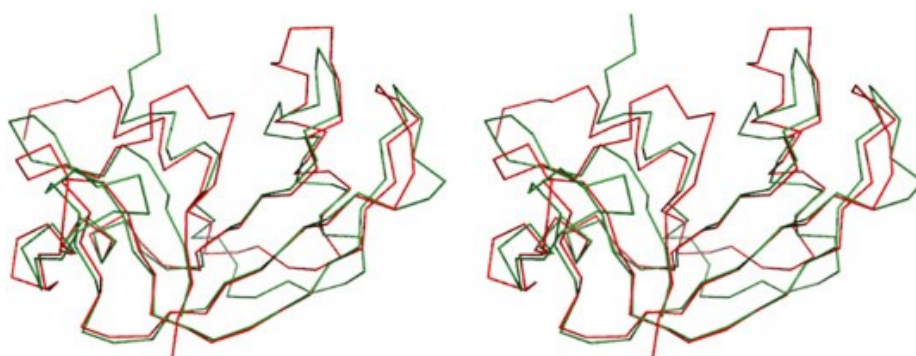


Figure 2.5. *Stereo view of SS2 superposed on RNase A (pdb: 1KF5). SS2 (red); RNase A (green).*

Interestingly, the three residues Gly121, Ile122 and Thr123, downstream to the pentapeptide, adopt a β -conformation and contribute to the formation of the four stranded C-terminal β -sheet, in a manner similar to the terminal residues of RNase A and some other members of RNases (**Figure 2.6**). Thus, the sequence Gly116-Ile120 apparently behaves as a disturbing insertion in a regular RNase structure.

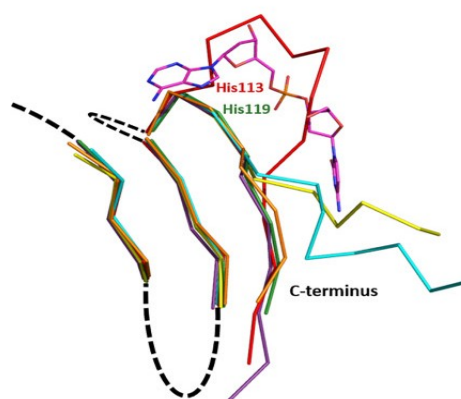


Figure 2.6. Drawing of SS2 selected regions. The picture includes the two β -sheet segments Asn67-Ser71 and Lys101-Ala105 (well conserved in all RNases), and Pro111-Asp124 C-terminus (red), superposed on the structural conserved residues of RNase A (pdb: 1KF5, green), ZF-RNase 1 (pdb: 2VQ8, yellow), ZF-RNase 3 (pdb: 2VQ9, violet), onconase (pdb: 1ONC, orange) and hAng (pdb: 1B1J, cyan). The dashed lines indicate the connecting regions of the β strands. The putative position of the oligonucleotide d(CpA) derived from the superposition of SS2 on RNase A-d(CpA) complex (pdb: 1RPG) is also shown (magenta), together with the position of the C-terminal active histidine (His119 in RNase A and His113 in SS2).

It is worth noting that in all known structures of angiogenins, the active site residues occupy the canonical location, and the partial obstruction of the active site is caused by the displacement with respect to RNase A of few residues at the C-terminus (**Figure 2.6**) that places the Gln117 side chain in the region of the B1 subsite (Russo et al., 1994). This structural feature is also observed in two monomeric ribonucleases from zebrafish, ZF1 (pdb: 2VQ8, 3LJD) and ZF5 (pdb: 3LJE) (Pizzo et al., 2011). Interestingly, in ZF3 (pdb: 2VQ9), the most active member among the zebrafish ribonucleases, the C-terminus closely follows the folding of RNase A (**Figure 2.6**).

Despite the enhanced impairment of the active site organization described above, in SS2 the purine subsite B2 appears only slightly perturbed with respect to the pancreatic enzyme. Residues Asn66, Asn67, Asp107 occupy positions rather similar to Gln69, Asn71, Gln111, which in the pancreatic enzyme play an important role in the stabilization of the complex of the enzyme with the substrate analogue, forming hydrogen bonds with the purine base (Raines, 1998; Zegers et al., 1994).

2.1.5. Aims

The crystallographic structure of SS2 clearly suggests that the obstruction of the active site by the segment Gly116-Ile120 and the resulting displacement of the His113-Tyr114-Asp115 segment is the major reason of its low enzymatic activity. The obstruction of the active site is much greater than that observed in angiogenins, where the accessibility to the active site is limited to the B1 subsite and is caused by a modified position of the C-terminus (**Figure 2.6**).

In angiogenins a rather simple reorganization of this segment is required to obtain an unobstructed site. In SS2 the recovery of an appreciable enzymatic activity might be obtained either by an exposed conformation of the invading pentapeptide (**Figure 2.7a**) that would allow the His113-Tyr114-Asp115 segment to gain the proper position or, alternatively, by a sliding of the last ten residues along the chain axis (**Figure 2.7b**), which eliminates the chain loop and might favour the incorporation of the peptide Gly116-Asp117-Val118 in the four stranded β -sheet that is characteristic of RNase A structure.

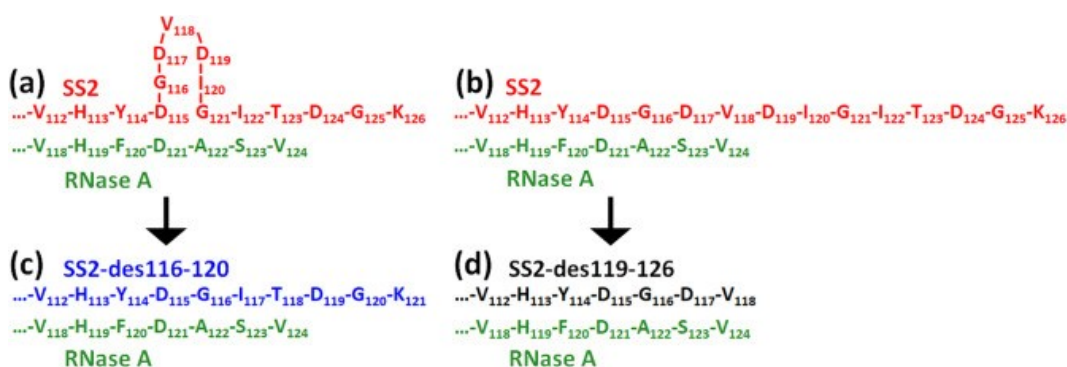


Figure 2.7. Schemes of the possible SS2 activation mechanisms.

Alignments of selected sequences of SS2 (red) and RNase A (green), bulging out of Gly116-Ile120 segment (a) and sliding of Asp119-Lys126 segment (b). Mutants designed to confirm the two mechanisms: SS2-des116–120 (c) and SS2-des119–126 (d).

On the basis of these considerations, the main aim of this part of PhD thesis was focused on the preparation and characterization of two deletion mutants: SS2-des116–120, in which the chain segment that in the wild-type protein obstructs the active site has been removed (**Figure 2.7c**), and SS2-des119–126, in which the elimination of the last eight residues of the chain might favour the chain sliding (**Figure 2.7d**).

Chapter 2.2. Materials and Methods

2.2.1. Recombinant plasmids encoding for of SS2 mutants

Recombinant vector encoding for wild-type SS2 has been already described (Pizzo et al., 2008), while recombinant vector pET-22b(+) (**Figure 2.8**) containing the open reading frames encoding the two mutants, SS2-des116–120 and SS2-des119–126, were prepared by the Custom Cloning Service of GenScript® Biotech Company (Leiden, Netherlands). The multiple alignment of coding sequences of SS2, SS2-des116–120 and SS2-des119–126 is reported in **Figure 2.9**.

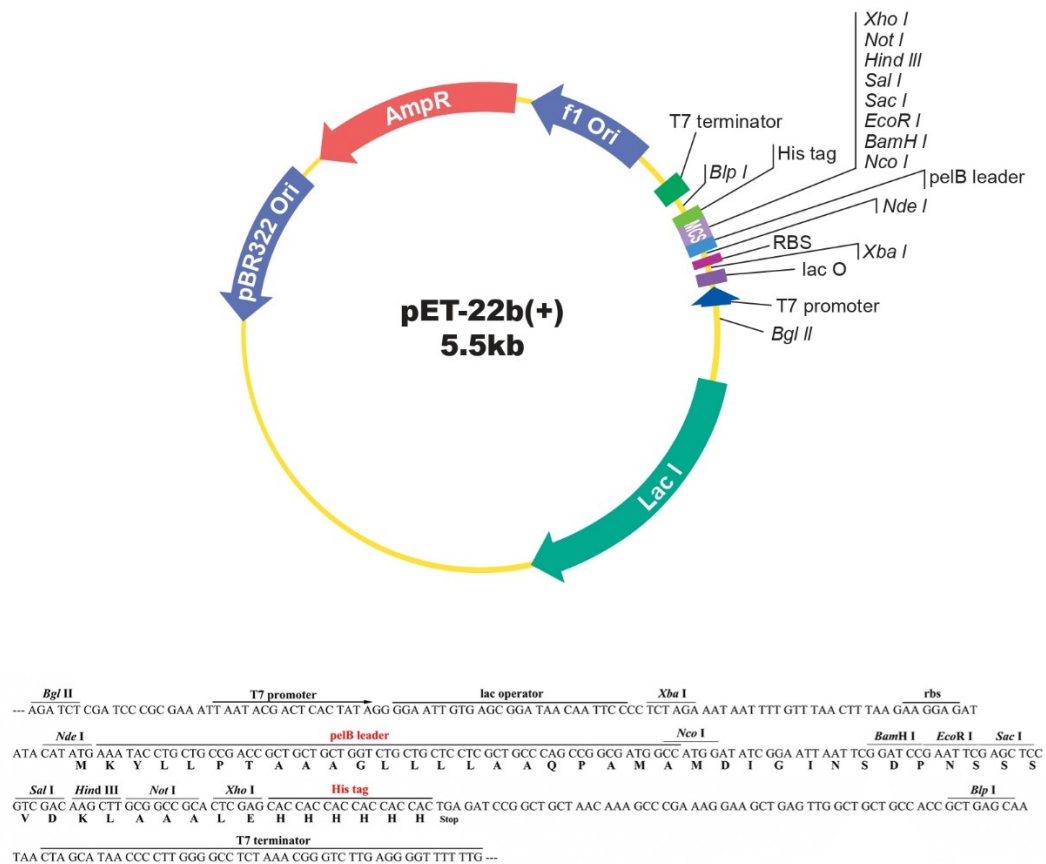


Figure 2.8. *pET-22b(+)* vector map and corresponding multiple cloning site region (MCS).

2.2. Materials and Methods

SS2	GACGTCAACCAACAATATAATCACTTCCTAAAACAACACGTCGATGGGGAAATGACGACC
SS2-des116-120	GACGTCAACCAACAATATAATCACTTCCTAAAACAACACGTCGATGGGGAAATGACGACC
SS2-des119-126	GACGTCAACCAACAATATAATCACTTCCTAAAACAACACGTCGATGGGGAAATGACGACC
SS2	CTGAAGTGTAAGAGTCAGATGGAAATCTTGAATTTGAACAGGCCTGATAGAAAATGCAAA
SS2-des116-120	CTGAAGTGTAAGAGTCAGATGGAAATCTTGAATTTGAACAGGCCTGATAGAAAATGCAAA
SS2-des119-126	CTGAAGTGTAAGAGTCAGATGGAAATCTTGAATTTGAACAGGCCTGATAGAAAATGCAAA
SS2	TTGAAGAACACCTTCATCTTGGCCAATCCAGATCAGGTCCAAGCCATCTGCACTGGTGGT
SS2-des116-120	TTGAAGAACACCTTCATCTTGGCCAATCCAGATCAGGTCCAAGCCATCTGCACTGGTGGT
SS2-des119-126	TTGAAGAACACCTTCATCTTGGCCAATCCAGATCAGGTCCAAGCCATCTGCACTGGTGGT
SS2	GGCACACTGAAGGGAAACAATCTGGTTCAAAGCAACAAACCCTTCAGTGTAGTCATATGT
SS2-des116-120	GGCACACTGAAGGGAAACAATCTGGTTCAAAGCAACAAACCCTTCAGTGTAGTCATATGT
SS2-des119-126	GGCACACTGAAGGGAAACAATCTGGTTCAAAGCAACAAACCCTTCAGTGTAGTCATATGT
SS2	ACACATACAGGTGGGGAGTCCCATCCCAATTGTACATACAAGGGATCTTCGGCCACTAAG
SS2-des116-120	ACACATACAGGTGGGGAGTCCCATCCCAATTGTACATACAAGGGATCTTCGGCCACTAAG
SS2-des119-126	ACACATACAGGTGGGGAGTCCCATCCCAATTGTACATACAAGGGATCTTCGGCCACTAAG
SS2	AAAGTTATCATTGCTTGTGATGGAAAATTTCCAGTGCACTATGATGGT GATGTTGATATT
SS2-des116-120	AAAGTTATCATTGCTTGTGATGGAAAATTTCCAGTGCACTATGATGGT-----
SS2-des119-126	AAAGTTATCATTGCTTGTGATGGAAAATTTCCAGTGCACTATGATGGTATGTTGA----
SS2	GGC ATCACGGATGGAAAGTGAA
SS2-des116-120	---ATCACGGATGGAAAGTGAA
SS2-des119-126	-----

Figure 2.9. Multiple alignment between coding sequence of parent SS2 and SS2 variants. Nucleotides removed to obtain SS2-des116-120 are typed in red and highlighted in yellow; underlined characters refer to nucleotides absent in SS2-des119-126.

2.2.2. Production of RNases from *Salmo salar*

Heterologous production of salmon RNases was carried out following the procedures already described (Pizzo et al., 2008). Briefly, all three recombinant vectors were used to transform competent *E. coli* strain BL21(DE3) (Invitrogen™). Cells were grown at 37 °C to an A_{600 nm} = 0.6, treated with 0.4 mM isopropyl-1-thio-d-galactopyranoside and grown overnight. Expressed recombinant proteins were purified by inclusion bodies, the latter isolated after centrifugation and subsequent sonication of bacterial lysates. Inclusion bodies were then first washed and then denatured in 5.0 M guanidine hydrochloride, 100 mM Tris-HCl pH 7.4, 0.1 M reduced glutathione and finally renatured, diluting 20-fold the denaturing agent in 0.1 M Tris acetate pH 8.4, containing 0.5 M L-Arginine and 0.001 M

oxidized glutathione. All three salmon RNases were finally purified by RP-HPLC, following a previously described procedure (Pizzo et al., 2006)

2.2.3. Analysis of RNA extracted from *Salmo salar* tissue

Muscle tissue from *Salmo salar* was cryogenically grinded using liquid nitrogen and mechanical pressure, and then immediately stored at -80°C . RNA extraction in TRIzol™ (Invitrogen™) has been performed on 100 mg of grinded tissue; total RNA obtained was quantified using NanoDrop Spectrophotometer.

Total RNA was retro-transcribed to cDNA using SuperScript™ IV VILO Master MIX (Invitrogen™) and the cDNA obtained was then used for a PCR amplification using the following oligonucleotide primers: forward 5'-GACGTCAACCAACAATATAATCAC-3' and reverse 5'-TTCACCTTCCATCCGTGATGCC-3'. Resulting PCR products were purified from agarose gel by PureLink™ Quick Gel Extraction Kit (Invitrogen™), quantified and then sequenced with Sanger method by Eurofins Genomics Service (<https://eurofinsgenomics.com/en/home/>).

2.2.4. Circular Dichroism analysis

Circular dichroism (CD) spectra were recorded with a Jasco J-715 spectropolarimeter equipped with a Peltier temperature controller. Far-UV measurements were carried out at protein concentration of 0.2 mg ml^{-1} in 10 mM Tris-HCl pH 7.4, at 10°C , using a cell with an optical path length of 0.1 cm. Spectra, registered with 50 nm min^{-1} scanning speed, 2 s response time, 1 nm data pitch, and 2.0 nm bandwidth, were obtained averaging three scans.

Thermal unfolding curves were obtained by following the CD signal at 222 nm, in the $10\text{--}90^{\circ}\text{C}$ range, at heating rate of $1.0^{\circ}\text{C min}^{-1}$. The denaturation temperatures (T_d) were determined through analysis of the first derivative of the melting profiles. The reversibility of the transition was checked by lowering the temperature to 10°C and re-scanning.

2.2.5. Ribonucleolytic activity assays

Ribonucleolytic activity studies were performed on the fluorogenic substrate 5'-/6FAM/mAmArCmAmA/3Dab/-3' synthesized by Integrated DNA Technologies, Inc. (IDT) (Ferguson et al., 2019). Fluorescence measurements were performed in a low volume quartz cuvette with 1 cm optical path length under magnetic stirring at 20 °C using a Fluoromax-4 spectrofluorometer equipped with a Peltier thermostatic cell holder. The variation of the emission signal induced by substrate cleavage was monitored at $\lambda_{em} = 520$ nm (slit width = 3 nm) using an excitation wavelength $\lambda_{ex} = 495$ nm (slit width = 2 nm) with an acquisition time of 0.5 s. Each measurement was performed in triplicate in 10 mM Tris-HCl pH 7.4, 0.001% w/v Tween-20, 100 nM 5'-/6FAM/ mAmArCmAmA/3Dab/-3', 200 pM RNase A or 45 nM SS2 RNase (parent or mutants). To obtain a stable signal in the absence of the enzyme, fluorescence was recorded during a 5 min equilibration period. The catalytic reactions were initialized upon the addition of the enzymes and then were monitored for ~15 min until the complete cleavage of the substrate. The quantum yield increase registered upon the phosphodiester bond cleavage is due to the contemporary removal from the substrate of a quencher group. The variation of the emission intensity with time was used to calculate the k_{cat}/K_M value by the following equation:

$$\frac{k_{cat}}{K_M} = \left(\frac{\left(\frac{\Delta F}{\Delta t} \right)}{(F_{max} - F_0)} \right) 1/[E]$$

where $\Delta F/\Delta t$ is the slope of the straight line that fits the initial velocity of the enzymatic activity with $R^2 \geq 0.99$, F_{max} and F_0 are the fluorescence acquired after the complete cleavage of the substrate and in the absence of enzyme, respectively, and $[E]$ is the concentration of the enzyme used during the experiment.

Chapter 2.3. Results

2.3.1. SS2 gene expression analysis in *Salmo salar* muscle tissue

Previous studies on SS2 (Pizzo et al., 2008) were carried out on a recombinant version of the protein obtained on the basis of a putative transcript (accession number NM_001141089) extracted from a salmonid expressed sequence tag (EST) database (Adzhubei et al., 2007). In order to verify the real existence of SS2 in *Salmo salar*, before investigating the protein structural and functional properties, we performed an analysis on total RNA extracted from the animal. Briefly, *Salmo salar* muscle tissue was frozen in liquid nitrogen, powdered, and finally subjected to RNA extraction in a suitable lysis buffer. Total extracted RNA was then retro-transcribed using random primers, amplified by PCR adopting specific oligonucleotides (see materials and methods), purified and finally subjected to sequencing that clearly indicated that a transcript fully congruent with the sequence deduced in silico was produced in *Salmo salar*.

2.3.2. CD and thermal stability of SS2 and its mutants

The folded state of SS2 and its two deletion mutants was investigated in solution by circular dichroism (CD) spectroscopy. The inspection of the far-UV CD spectra indicates that the two mutants retain the secondary structure of the parent protein (**Figure 2.10 panel A**), although a decrease in signal intensity was observed.

Thermal unfolding curves were also obtained in the temperature range 10–90 °C, by following the CD signal at 222 nm (**Figure 2.10 panel B**). CD spectra, recorded at 10 °C before heating and after cooling, indicate reversible thermal unfolding for all proteins (**Figure 2.11**).

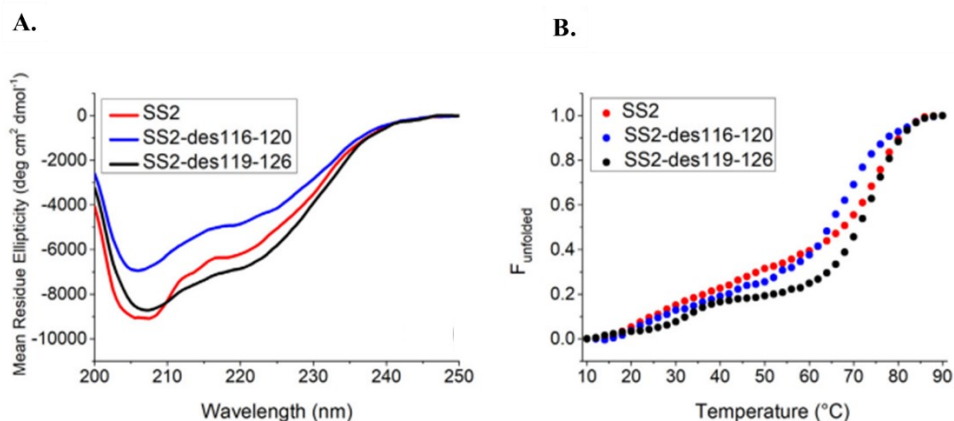


Figure 2.10. *A. Far-UV CD spectra recorded at 10 °C B. thermal denaturation profiles, as followed by monitoring changes in the molar ellipticity at 222 nm as a function of temperature, of SS2 and its deletion mutants. Measurements were carried out in 10 mM Tris-HCl pH 7.4, using a protein concentration of 0.2 mg ml⁻¹.*

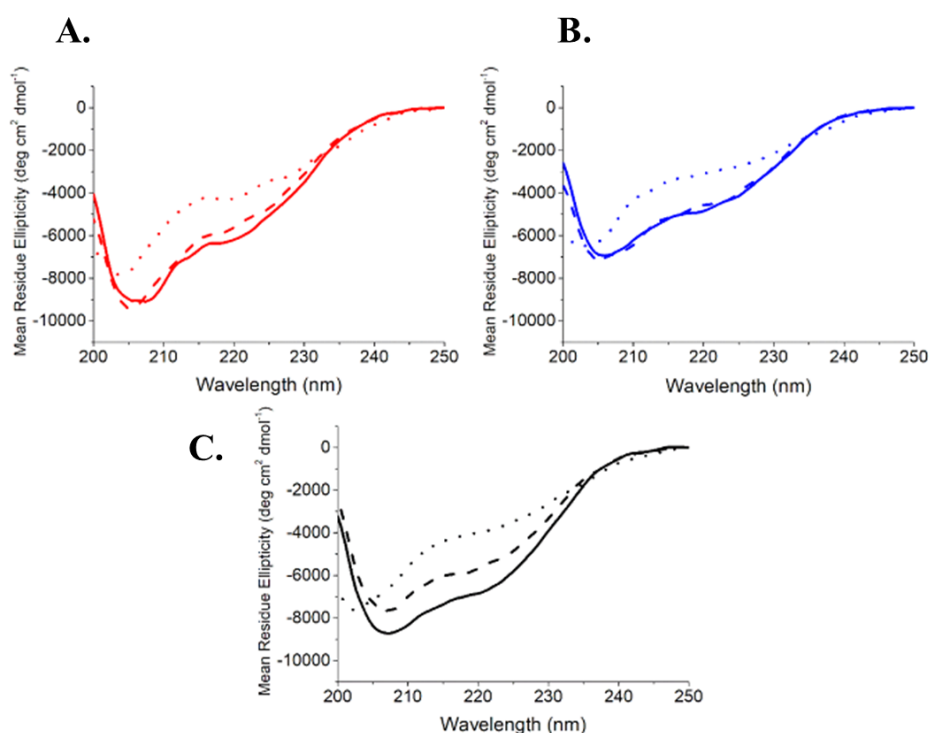


Figure 2.11. *Superimposition of the CD spectra, registered at 10 °C before heating (plane line), at 90 °C (dotted line) and at 10 °C after cooling (dashed line), of SS2 (A), SS2-des116-120 (B) and SS2-des119-126 (C). Spectra were recorded at 10 °C in 10 mM Tris-HCl pH 7.4, using a protein concentration of 0.2 mg ml⁻¹.*

The T_d of SS2 is 76 °C, while that of SS2-des116–120 is about 8 °C lower (**Table 1**), a result that can most likely be attributed to the lack of stabilizing interactions of the missing pentapeptide. Interestingly, the T_d of the mutant SS2-des119–126 is only slightly lower than that of the native enzyme, suggesting that the stabilizing interactions of the extra residues observed in the native enzyme are still present in this derivative, and that the sliding of the C-terminus has not occurred. It should be noted that the last three residues Gly116- Asp117-Val118 of the chopped terminus could be less prone to adopt the position of the corresponding residues Gly121-Ile122-Thr123 in the native enzyme. Indeed, the replacement of isoleucine by an aspartic acid introduces a charged side chain in a strong hydrophobic environment provided by Val77, Ile79, Ala98, Val102.

Table 2.1. Denaturation temperature of SS2 and its two mutants. The T_d values were compared with that of RNase A.

	T_d (°C)
RNase A	64
SS2	76
SS2-des116-120	68
SS2-des119-126	74

2.3.3. Catalytic activity assays

The catalytic efficiency of SS2 and of its deletion variants was estimated and compared to that of RNase A by monitoring the time courses for cleavage of the fluorogenic 5'-/6FAM/mAmArCmAmA/3Dab/-3', an oligonucleotide tailored for angiogenins (Ferguson et al., 2019), in which the cleavable bond joins a cytidine and an adenine residue. The increase of the fluorescence emission at 520 nm, upon excitation at 495 nm, was used to follow the progress of the catalytic reaction. The catalytic efficiency values (k_{cat}/K_M), determined as described in experimental

section, indicate that the substrate cleavage is ~ 180 -fold more efficient in the presence of RNase A in comparison to SS2 and SS2-des119–126 (**Table 2.2**). These results agree with the much less effective catalytic activity of the angiogenins with respect to that of RNase A. Interestingly, SS2-des116–120 cleaves the substrate two-fold faster than the parent protein (**Table 2.2**).

Table 2.2. Ribonucleolytic activity of SS2 and its two mutants compared with that of RNase A.

	$k_{\text{cat}}/K_{\text{M}}$ ($\text{M}^{-1}\text{s}^{-1}$)
RNase A	$(6.3 \pm 0.4) \cdot 10^7$
SS2	$(3.5 \pm 0.3) \cdot 10^5$
SS2-des116-120	$(6.2 \pm 0.3) \cdot 10^5$
SS2-des119-126	$(3.5 \pm 0.3) \cdot 10^5$

2.3.4. Crystal structure of SS2-des116–120

An extensive search of crystallization conditions was performed on both SS2 deletion mutants. Positive results were obtained only in the case of SS2-des116–120, whose crystal structure was refined at 2.88 Å resolution.

With respect to the native enzyme, the most prominent difference of the mutant is localized in the region of the C-terminus, where the deletion of the five residues allows the rearrangement of the segment His113-Asp115 that reconstitutes the integrity of the active site. Indeed, its overall architecture is now practically superimposable to that of the pancreatic enzyme with the catalytically important residues His13, Lys40, His113, Asp115 replacing His12, Lys41, His119 and Asp121 of RNase A. The His13 imidazole ring is hydrogen bonded to Thr44 and to a water molecule, which in turn is hydrogen bonded to Gln12, and Lys40 interacts with Asn43 (**Figure 2.12**).

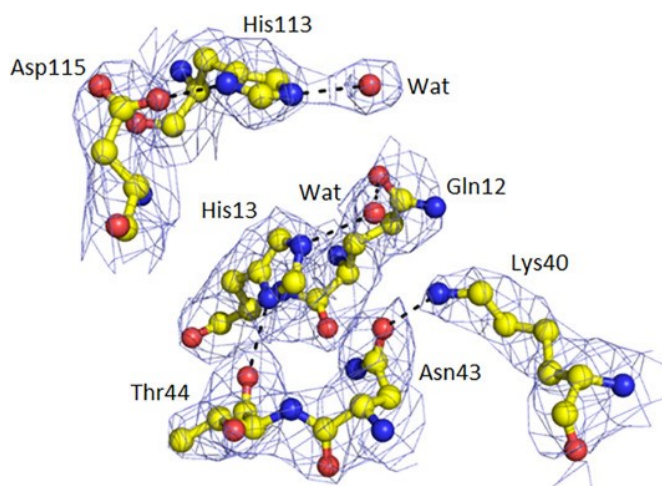


Figure 2.12. *Electron density map at the P1 subsite of the mutant SS2-des116–120.*

In addition, His113 adopts a conformation that is similar to the productive conformation of RNase A His119, in which the imidazole group is hydrogen bonded to the carboxylate group of Asp121 (Borkakoti et al., 1982; Wlodawer et al., 1983). In SS2-des116–120 the corresponding intrachain bond between His113 and Asp115 is observed only for the A and C molecules, whereas in B and D the side chain of Asp115 adopts a different conformation required to fulfil the Asp115-Asp115 hydrogen bond geometry at the AB interface (**Figure 2.13**).

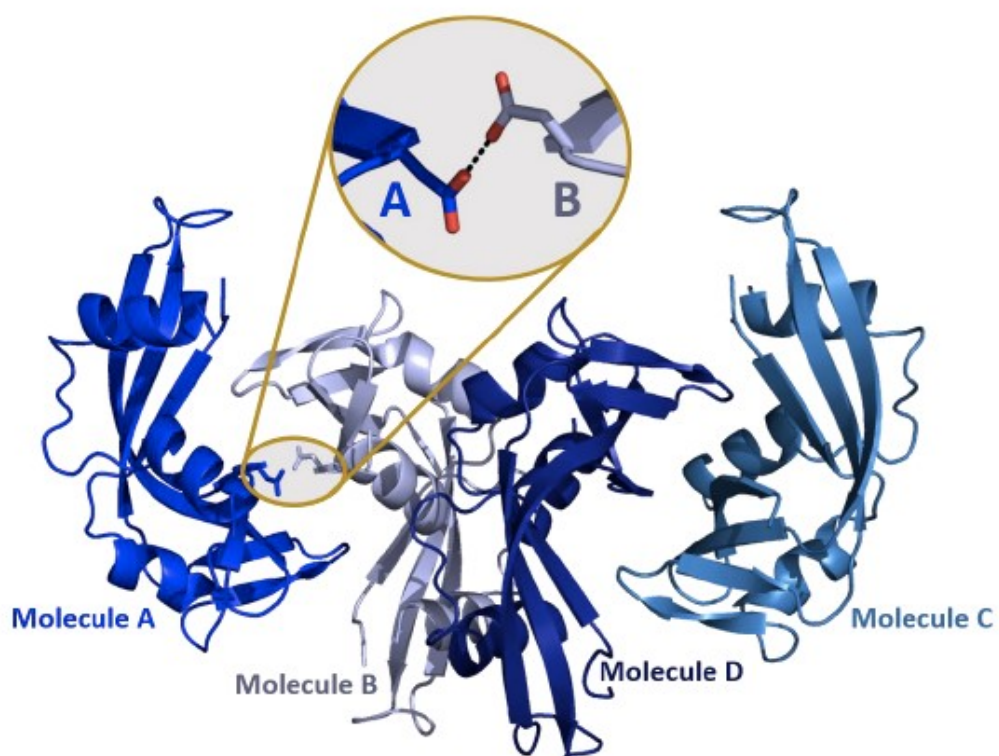


Figure 2.13. *Cartoon representation of the four SS2-des116-120 molecules (A, B, C and D) in the asymmetric unit. At the AB interface the Asp115-Asp115 hydrogen bond is highlighted.*

Chapter 2.4. Discussion and Conclusions

2.4. Discussion and Conclusions

Crystallographic results of SS2, have revealed a novel auto-inhibition mechanism never identified before in vertebrate RNase Superfamily. In this molecule, five residues are inserted between the catalytic important stretch His113 → Asp115 and the triplet Gly121-Ile122-Thr123 that participates to the β -sheet organization of RNase A as well as of other vertebrate RNases.

The extra residues invade the region of the active site displacing the segment His113 → Asp115. On the other hand, the remaining part of the molecule closely follows the three-dimensional organization of RNase A, except for few residues insertion or deletion in some loops that only affect the local conformation.

The structural details suggest that the five-residue peptide might be a disturbing insertion in the usual ribonuclease organization. Indeed, the crystal structure of the mutant SS2- des116–120, in which the pentapeptide has been removed, acquires a three-dimensional structure that matches very well that of RNase A, and displays a reasonable intact active site. The possibility that SS2 could be an artefact of the experimental procedure adopted for the production of the protein was also taken in consideration, in view of the fact that the studied protein had been obtained on the basis of a putative transcript identified in a salmonid expressed sequence tag database.

However, this possibility was ruled out by directly sequencing the cDNA obtained by mRNA extracted from *Salmo salar* muscle tissue, whose resulting sequence is fully congruent with the sequence deduced in silico.

SS2 is endowed with a ribonucleolytic activity that turns out to be of the same order of magnitude manifested by human ANG (Pizzo et al., 2008) and even greater than other fish ribonucleases studied so far (Borkakoti et al., 1982). Moreover, this activity is almost doubled in the mutant SS2-des116–120 (**Table 1.1**), where the pentapeptide is missing.

Thus, on the basis of all these results, it would be interesting to understand the way in which the native enzyme can recover a functional active site and properly bind the substrate. An intriguing mechanism may reside in a sliding of the C-terminus that would remove the invading pentapeptide from the active site and allow the reconstruction of an intact active site. For this reason, the mutant SS2-des119–126 was designed on consideration that the lack of Gly121-Ile122-Thr123

2.4. Discussion and Conclusions

tripeptide, which acts as a hook coupling the C-terminus to the rest of the protein, might facilitate the sliding. Unfortunately, despite numerous trials this mutant could not be crystallized. Further information comes from the denaturation experiments.

The thermal denaturation curves indicate a Td of 76 °C for SS2, revealing a stability for the native protein sensibly higher than that measured for RNase A and angiogenins (Pizzo et al., 2011). According to the crystallographic results, this increased stability is probably caused by the extra residues that partially fill the open space in the active site cleft formed by the two lobes of the β structure organization of the protein and contribute with several interactions to the overall stability of the protein. Among them, an important contribution is provided in both chains of the asymmetric unit by the salt bridge between Asp119 and Lys42.

Interestingly, in all known members of the vertebrate RNase Superfamily Lys42 is replaced by a hydrophobic residue. For the mutant SS2-des116–120, the value of Td is about 8 °C lower than that of SS2 and very close to the value measured for RNase A (Pizzo et al., 2011). In this case, the pentapeptide and in particular Asp119 is missing and Lys42 is exposed to the solvent. Interestingly, the denaturation curve measured on the mutant SS2-des119–126 indicates that the mutant has a Td close to the native enzyme, suggesting that the remaining part of the chopped C-terminus is still able, at least partially, to provide the stabilizing contributions operating in the parent molecule. In other words, this result strongly suggests that the possible sliding of the C-terminus might not have occurred.

In agreement with this conclusion, the observed enzymatic activity of this mutant is hardly affected with respect to the native enzyme. On the basis of the present results, it is reasonable to conclude that the measured enzymatic activity of SS2 should be related to some rearrangement of the extra residues. Still remains the fact that SS2-des116–120, in which the invading peptide has been removed, shows only a rather limited increase in the activity despite the crystallographic structure appears to be fully prepared to bind a nucleotide substrate, apart for small readjustments of few side chains, mostly related to specific packing interactions.

However, further speculation on the importance of various residues must await the identification of the target RNA substrate to better understand the specific role and functionality of this interesting version of vertebrate RNase.

2.4. Discussion and Conclusions

As a final comment, it is worth to stress the peculiarity of the SS2 with respect to all the other members of the Superfamily. Present-day ribonucleases have been supposed to be evolved from ancestral proteins which possess a structural organization stabilized by three intrachain disulphide bonds, and a low ribonucleolytic activity. In some cases, the low activity has been found to be associated to a partial obstruction caused by a residue located near the C-terminus (Holloway et al., 2005; Kazakou et al., 2008; Pizzo et al., 2011; Russo et al., 1994), which in the case of human ANG is also sustained by the presence of a downstream 3_{10} helix (Leonidas et al., 2002).

SS2, a protein much phylogenetically distant with respect to previously studied ribonucleases, also presents an obstructive C-terminus, but in this case the obstruction is considerably more severe.

Indeed, an extra pentapeptide, inserted in an otherwise normal ribonuclease sequence, profoundly occupies the expected substrate binding region, and perturbs the structural relationship between the catalytically important His13 and His113.

2.5. Bibliography

2.5. Bibliography

- Adzhubei, A. A., Vlasova, A. v., Hagen-Larsen, H., Ruden, T. A., Laerdahl, J. K., & Høyheim, B. (2007). Annotated expressed sequence tags (ESTs) from pre-smolt Atlantic salmon (*Salmo salar*) in a searchable data resource. *BMC Genomics*, 8(1), 1–15. <https://doi.org/10.1186/1471-2164-8-209/TABLES/4>
- Beintema, J. J., Breukelman, H. J., Carsana, A., & Furiat, A. (1997). Evolution of Vertebrate Ribonucleases: Ribonuclease A Superfamily. *Ribonucleases*, 245–269. <https://doi.org/10.1016/B978-012588945-2/50009-1>
- Beintema, J. J., & Kleineidam, R. G. (1998). The ribonuclease A superfamily: general discussion. *Cellular and Molecular Life Sciences : CMLS*, 54(8), 825–832. <https://doi.org/10.1007/S000180050211>
- Borkakoti, N., Moss, D. S., Palmer, R. A., & IUCr. (1982). Ribonuclease-A: least-squares refinement of the structure at 1.45 Å resolution. *Urn:Issn:0567-7408*, 38(8), 2210–2217. <https://doi.org/10.1107/S0567740882008346>
- Cho, S., & Zhang, J. (2007). Zebrafish Ribonucleases Are Bactericidal: Implications for the Origin of the Vertebrate RNase A Superfamily. *Molecular Biology and Evolution*, 24(5), 1259–1268. <https://doi.org/10.1093/MOLBEV/MSM047>
- Cuchillo, C. M., Vilanova, M., & Nogués, M. V. (1997). Pancreatic Ribonucleases. *Ribonucleases*, 271–304. <https://doi.org/10.1016/B978-012588945-2/50010-8>
- D'Alessio, G. (2011). *The Superfamily of Vertebrate-Secreted Ribonucleases*. 1–34. https://doi.org/10.1007/978-3-642-21078-5_1
- Ferguson, R., Holloway, D. E., Chandrasekhar, A., Acharya, K. R., & Subramanian, V. (2019). The catalytic activity and secretion of zebrafish RNases are essential for their in vivo function in motor neurons and vasculature. *Scientific Reports 2019 9:1*, 9(1), 1–15. <https://doi.org/10.1038/s41598-018-37140-2>
- Holloway, D. E., Chavali, G. B., Hares, M. C., Subramanian, V., & Acharya, K. R. (2005). Structure of murine angiogenin: features of the substrate- and cell-binding regions and prospects for inhibitor-binding studies. *Urn:Issn:0907-4449*, 61(12), 1568–1578. <https://doi.org/10.1107/S0907444905029616>

- Holloway, D. E., Singh, U. P., Shogen, K., & Acharya, K. R. (2011). Crystal structure of Onconase at 1.1 Å resolution – insights into substrate binding and collective motion. *The FEBS Journal*, 278(21), 4136–4149. <https://doi.org/10.1111/J.1742-4658.2011.08320.X>
- Hooper, L. v., Stappenbeck, T. S., Hong, C. v., & Gordon, J. I. (2003). Angiogenins: a new class of microbicidal proteins involved in innate immunity. *Nature Immunology*, 4(3), 269–273. <https://doi.org/10.1038/NI888>
- Kazakou, K., Holloway, D. E., Prior, S. H., Subramanian, V., & Acharya, K. R. (2008). Ribonuclease A Homologues of the Zebrafish: Polymorphism, Crystal Structures of Two Representatives and their Evolutionary Implications. *Journal of Molecular Biology*, 380(1), 206–222. <https://doi.org/10.1016/J.JMB.2008.04.070>
- Kobe, B., & Deisenhofer, J. (1996). Mechanism of Ribonuclease Inhibition by Ribonuclease Inhibitor Protein Based on the Crystal Structure of its Complex with Ribonuclease A. *Journal of Molecular Biology*, 264(5), 1028–1043. <https://doi.org/10.1006/JMBI.1996.0694>
- Lee, H. H., Wang, Y. N., & Hung, M. C. (2019). Functional roles of the human ribonuclease A superfamily in RNA metabolism and membrane receptor biology. *Molecular Aspects of Medicine*, 70, 106–116. <https://doi.org/10.1016/J.MAM.2019.03.003>
- Lee, J. E., & Raines, R. T. (2003). Contribution of Active-Site Residues to the Function of Onconase, a Ribonuclease with Antitumoral Activity†. *Biochemistry*, 42(39), 11443–11450. <https://doi.org/10.1021/BI035147S>
- Leland, P. A., Staniszewski, K. E., Park, C., Kelemen, B. R., & Raines, R. T. (2002). The ribonucleolytic activity of angiogenin. *Biochemistry*, 41(4), 1343–1350. <https://doi.org/10.1021/BI0117899>
- Leonidas, D. D., Shapiro, R., Allen, S. C., Subbarao, G. v., Veluraja, K., & Acharya, K. R. (1999). Refined Crystal Structures of Native Human Angiogenin and Two Active Site Variants: Implications for the Unique Functional Properties of an Enzyme Involved in Neovascularisation During Tumour Growth.

- Journal of Molecular Biology*, 285(3), 1209–1233.
<https://doi.org/10.1006/JMBI.1998.2378>
- Leonidas, D. D., Shapiro, R., Subbarao, G. v., Russo, A., & Acharya, K. R. (2002). Crystallographic Studies on the Role of the C-Terminal Segment of Human Angiogenin in Defining Enzymatic Potency^{†,‡}. *Biochemistry*, 41(8), 2552–2562. <https://doi.org/10.1021/BI015768Q>
- Matousek, J., Soucek, J., Riha, J., Zankel, T. R., & Benner, S. A. (1995). Immunosuppressive activity of angiogenin in comparison with bovine seminal ribonuclease and pancreatic ribonuclease. *Comparative Biochemistry and Physiology Part B: Biochemistry and Molecular Biology*, 112(2), 235–241. [https://doi.org/10.1016/0305-0491\(95\)00075-5](https://doi.org/10.1016/0305-0491(95)00075-5)
- Merlino, A., Mazzearella, L., Carannante, A., di Fiore, A., di Donato, A., Notomista, E., & Sica, F. (2005). The Importance of Dynamic Effects on the Enzyme Activity: X-RAY STRUCTURE AND MOLECULAR DYNAMICS OF ONCONASE MUTANTS. *Journal of Biological Chemistry*, 280(18), 17953–17960. <https://doi.org/10.1074/JBC.M501339200>
- Monti, D. M., Yu, W., Pizzo, E., Shima, K., Hu, M. G., di Malta, C., Piccoli, R., D'Alessio, G., & Hu, G. F. (2009). Characterization of the angiogenic activity of zebrafish ribonucleases. *FEBS Journal*, 276(15), 4077–4090. <https://doi.org/10.1111/J.1742-4658.2009.07115.X>
- Mosimann, S. C., Ardelt, W., & James, M. N. G. (1994). Refined 1.7 Å X-ray crystallographic structure of P-30 protein, an amphibian ribonuclease with anti-tumor activity. *Journal of Molecular Biology*, 236(4), 1141–1153. [https://doi.org/10.1016/0022-2836\(94\)90017-5](https://doi.org/10.1016/0022-2836(94)90017-5)
- Parés, X., Nogués, M. v., de Llorens, R., & Cuchillo, C. M. (1991). Structure and function of ribonuclease A binding subsites. *Essays in Biochemistry*, 26, 89–103.
- Pei, J., Kim, B. H., & Grishin, N. v. (2008). PROMALS3D: a tool for multiple protein sequence and structure alignments. *Nucleic Acids Research*, 36(7), 2295–2300. <https://doi.org/10.1093/NAR/GKN072>

2.5. Bibliography

- Pizzo, E., Buonanno, P., di Maro, A., Ponticelli, S., de Falco, S., Quarto, N., Cubellis, M. V., & D'Alessio, G. (2006). Ribonucleases and Angiogenins from Fish. *Journal of Biological Chemistry*, 281(37), 27454–27460. <https://doi.org/10.1074/JBC.M605505200>
- Pizzo, E., & D'Alessio, G. (2007). The success of the RNase scaffold in the advance of biosciences and in evolution. *Gene*, 406(1–2), 8–12. <https://doi.org/10.1016/J.GENE.2007.05.006>
- Pizzo, E., Merlino, A., Turano, M., Russo Krauss, I., Coscia, F., Zanfardino, A., Varcamonti, M., Furia, A., Giancola, C., Mazzarella, L., Sica, F., & D'Alessio, G. (2011). A new RNase sheds light on the RNase/angiogenin subfamily from zebrafish. *Biochemical Journal*, 433(2), 345–355. <https://doi.org/10.1042/BJ20100892>
- Pizzo, E., Varcamonti, M., di Maro, A., Zanfardino, A., Giancola, C., & D'Alessio, G. (2008). Ribonucleases with angiogenic and bactericidal activities from the Atlantic salmon. *The FEBS Journal*, 275(6), 1283–1295. <https://doi.org/10.1111/J.1742-4658.2008.06289.X>
- Raines, R. T. (1998). Ribonuclease A. *Chemical Reviews*, 98(3), 1045–1065. <https://doi.org/10.1021/CR960427H>
- Riordan, J. F. (1997). Structure and Function of Angiogenin. *Ribonucleases*, 445–489. <https://doi.org/10.1016/B978-012588945-2/50015-7>
- Rosenberg, H. F. (2011). *Vertebrate Secretory (RNase A) Ribonucleases and Host Defense*. 35–53. https://doi.org/10.1007/978-3-642-21078-5_2
- Russo, N., Shapiro, R., Acharya, K. R., Riordan, J. F., & Vallee, B. L. (1994). Role of glutamine-117 in the ribonucleolytic activity of human angiogenin. *Proceedings of the National Academy of Sciences*, 91(8), 2920–2924. <https://doi.org/10.1073/PNAS.91.8.2920>
- Rutkoski, T., & Raines, R. (2008). Evasion of Ribonuclease Inhibitor as a Determinant of Ribonuclease Cytotoxicity. *Current Pharmaceutical Biotechnology*, 9(3), 185–199. <https://doi.org/10.2174/138920108784567344>

2.5. Bibliography

- Vliegenthart, G. J., Gerken, J. F. G., Dearborn, T. A., Gilkey, D. G., Gray, J. C., Gray, W. R., Hayashi, W. R., Bai, R., Hata, Y., Inoue, T., Iwasaki, S., Inoue, M., Matsumura, S., Inoue, G., Matsumura, M., Iwasaki, G., Kitajima, S., Nomoto, K., Inoue, H., ... Chang, C. J. (2002). Isolation and characterization of angiogenin, an angiogenic protein from human carcinoma cells. *Biochemistry*, 24(20), 5480–5486. <https://doi.org/10.1021/BI00341A030>
- Wlodawer, A., Miller, M., & Sjölin, L. (1983). Active site of RNase: neutron diffraction study of a complex with uridine vanadate, a transition-state analog. *Proceedings of the National Academy of Sciences*, 80(12), 3628–3631. <https://doi.org/10.1073/PNAS.80.12.3628>
- Wu, Y., Mikulski, S. M., Ardelt, W., Rybak, S. M., & Youle, R. J. (1993). A cytotoxic ribonuclease. Study of the mechanism of onconase cytotoxicity. *Journal of Biological Chemistry*, 268(14), 10686–10693. [https://doi.org/10.1016/S0021-9258\(18\)82252-9](https://doi.org/10.1016/S0021-9258(18)82252-9)
- Zegers, I., Maes, D., Dao-Thi, M. -H, Wyns, L., Poortmans, F., & Palmer, R. (1994). The structures of rnaase a complexed with 3'-CMP and d(CpA): Active site conformation and conserved water molecules. *Protein Science*, 3(12), 2322–2339. <https://doi.org/10.1002/PRO.5560031217>

List of Publications (accepted during PhD course)

Publication associated to the PhD thesis

- Sica F, Russo Krauss I, Troisi R, Bosso A, Culurciello R, Carluccio C, Trapani M, Merlino A, Mazzarella L, Pizzo E. The structural features of an ancient ribonuclease from *Salmo salar* reveal an intriguing case of auto-inhibition. Int J Biol Macromol. 2021 Jul 1; 182:659-668. <https://doi.org/10.1016/j.ijbiomac.2021.04.041>

Other publications

- Bosso A, Gaglione R, Di Girolamo R, Veldhuizen EJA, García-Vello P, Fusco S, Cafaro V, Monticelli M, Culurciello R, Notomista E, Arciello A, Pizzo E. Human Cryptic Host Defence Peptide GVF27 Exhibits Anti-Infective Properties against Biofilm Forming Members of the Burkholderia cepacia Complex. Pharmaceuticals (Basel). 2022 Feb 21;15(2):260. <https://doi.org/10.3390/ph15020260>
- Culurciello R, Bosso A, Di Fabio G, Zarrelli A, Arciello A, Carella F, Leonardi L, Pazzaglia L, De Vico G, Pizzo E. Cytotoxicity of an Innovative Pressurised Cyclic Solid-Liquid (PCSL) Extract from *Artemisia annua*. Toxins (Basel). 2021 Dec 11;13(12):886. <https://doi.org/10.3390/toxins13120886>
- Landi N, Ragucci S, Culurciello R, Russo R, Valletta M, Pedone PV, Pizzo E, Di Maro A. Ribotoxin-like proteins from *Boletus edulis*: structural properties, cytotoxicity and in vitro digestibility. Food Chem. 2021 Oct 15;359:129931. <https://doi.org/10.1016/j.foodchem.2021.129931>
- Cimmino F, Catapano A, Trinchese G, Cavaliere G, Culurciello R, Fogliano C, Penna E, Lucci V, Crispino M, Avallone B, Pizzo E, Mollica MP. Dietary Micronutrient Management to Treat Mitochondrial Dysfunction in Diet-Induced Obese Mice. Int J Mol Sci. 2021 Mar 11;22(6):2862. <https://doi.org/10.3390/ijms22062862>

Appendix

Abbreviations

ADAR1	Adenosine Deaminase RNA Specific
ADP	Adenosine diphosphate
AGO	Argonaute 2
AMP	Adenosine monophosphate
AMPK	AMP-activated protein kinase
ANG	angiogenin
APOBEC3G	apolipoprotein B mRNA editing enzyme, catalytic polypeptide-like 3G
ATP	Adenosine triphosphate
BSA	Bovine serum albumin
BS-RNase	Bovine Seminal RNase
CD	Circular dichroism
DAPI	4',6-diamidino-2-phenylindole
DCFH-DA	2',7'-Dichlorofluorescein diacetate
DMEM	Dulbecco's modified Eagle medium
DMSO	dimethyl sulfoxide
dsRNA	Double strand RNA
EDTA	Ethylenediaminetetraacetic acid
eIF	Elongation Initiation factor
ER	Endoplasmic reticulum
FBS	Fetal bovine serum
G3BP	Ras-GAP SH3 domain binding protein
GAPDH	Glyceraldehyde-3-Phosphate Dehydrogenase
GCN2	general control non-depressible-2
GDP	Guanosine diphosphate
GTP	Guanosine triphosphate

HaCaT	immortalized human keratinocytes cell line
HCl	Hydrochloric acid
HDAC6	histone deacetylase 6
HRI	heme-regulated inhibitor kinase
HRP	horseradish peroxidase
HSF1	heat-shock factor 1
HSPA6	Heat Shock Protein Family A (Hsp70) Member 6
HT-29	human colon adenocarcinoma cell line
I-dsRNA	Hyper-edited inosine containing dsRNA
IPTG	isopropyl-1-thio-d-galactopyranoside
IREb	ER transmembrane kinase/ribonuclease <i>b</i>
Lsm4	U6 snRNA-associated Sm-like protein LSm4
mAb	Monoclonal antibody
Met-tRNA _i ^{met}	initiator methionine transfer RNA
mRNA	messenger RNA
mRNP	untranslated messenger ribonucleoproteins
mTOR	mammalian target of rapamycin
mTORC1	mTOR complex 1
mTORC2	mTOR complex 2
MTT	3- (4,5-dimethylthiazol-2-yl) -2,5-diphenyltetrazolium bromide
NLS	Nuclear localization sequence
Nrf2	Nuclear factor erythroid 2-related factor 2
pAb	Polyclonal antibody
PABP	PolyA-binding protein
PBS	Phosphate saline buffer
PDB	Protein Data Bank
PERK	PKR-like endoplasmic reticulum (ER) kinase

PFA	paraformaldehyde
PIKK	phosphatidylinositol kinase-related kinase
PKR	double-stranded RNA dependent protein kinase
PVDF	Polyvinylidene fluoride
RACK1	receptor for activated protein C kinase 1
Rheb	Ras-homolog enriched in brain
RISC	RNA-induced silencing complex
RNH1	ribonuclease/angiogenin inhibitor 1
ROS	Reactive oxygen species
RP-HPLC	Reverse-phase high performance liquid chromatography
S6K1	Ribosomal protein S6 kinase beta-1
S6K2	Ribosomal protein S6 kinase beta-2
SA	Sodium arsenite
SG	Stress granule
SS1	<i>Salmo salar</i> RNase 1
SS2	<i>Salmo salar</i> RNase 2
T _d	denaturation temperature
TFs	transcription factors
TIA-1	TIA1 Cytotoxic Granule Associated RNA Binding Protein
TIAR	TIA-1-related protein
tiRNA	tRNA-derived stress-induced RNAs
tRNA	Transfer RNA
TSC	tuberous sclerosis complex
XBP1	X-box binding protein 1

Reagents

Chemicals	Catalogue n°	Manufacturer
Acetic acid glacial	401424	Carlo Erba Reagents
Ammonium acetate	LC-4757.1	neoFroxx GmbH
anti-6x-HisTag monoclonal antibody	MA1-21315	Invitrogen™
BL21(DE3)	EC0114	Invitrogen™
Bromophenol blue	151340250	Acros Organics
BSA	1126GR100	neoFroxx GmbH
CAPS	A1063,0100	ITW Reagents
DAPI	D21490	Invitrogen™
DCFH-DA	D6883	Sigma-Aldrich
DMEM	ECB7501L	Euroclone®
DMEM w/o phenol red	BE12-917F	Lonza®
DMSO	D5879	Sigma-Aldrich
Donkey anti-rabbit secondary antibody Cy3 conjugate	711-165-152	Jackson Immunoresearch
EDTA	A1103	ITW Reagents
FBS	ECS01801	Euroclone®
Glycerol	A9357	Del-tek
Goat anti-Mouse secondary antibody Alexa Fluor 488	A32723	Invitrogen™
Guanidine hydrochloride	A1499,1000	Applichem

Hydrochloric acid	258148	Sigma-Aldrich
Hydrogen peroxide	31642	Sigma-Aldrich
HRP-conjugated goat anti-mouse IgG	GtxMu-003-DHRPX	ImmunoReagents Inc.
HRP-conjugated goat anti-rabbit IgG	GtxRb-003-DHRPX	ImmunoReagents Inc.
Immobilion® PVDF transfer membrane	IPVH00010	Millipore
Isopropanol	33539	Sigma-Aldrich
L-Arginine	A3709,1000	ITW Reagents
L-glutamine	Euroclone®	Euroclone®
Methanol	412383	Carlo Erba Reagents
Mouse angiogenin (ANG) monoclonal (262F) antibody	14-9762-82	eBioscience™
MTT	M2128	Sigma-Aldrich
Oxidized glutathione	A2243,0005	ITW Reagents
PBS 1X	ECB4004L	Euroclone®
Pen/Strep	ECB3001D	Euroclone®
pET-22b+	Customized	GenScript®
PFA	29447	BDM
Propidium iodide	BMS500PI	Invitrogen™
Protease inhibitor	10190300	ITW Reagents
Rabbit PABPC1 polyclonal antibody	HPA045423	Sigma-Aldrich

Rabbit angiogenin (ANG) polyclonal antibody	TA349217	OriGene Technologies
Rabbit β -actin polyclonal antibody	A2066	Sigma-Aldrich
Reduced glutathione	1392GR025	ITW Reagents
RNase A	R6513	Sigma-Aldrich
SYBR GREEN PCR MASTER MIX	4309155	Invitrogen™
SDS	A0675,500	ITW Reagents
Sodium arsenite	57400	Sigma-Aldrich
SuperScript™ IV VILO™	11756050	Invitrogen™
Trypsin-EDTA 1X in PBS	ECB3052D	Euroclone®
Tris Base	1125KG001	ITW Reagents
Triton-x100	A4975,0500	ITW Reagents
TRIzol™ Reagent	15596026	Invitrogen™
β -mercaptoethanol	M6250	Sigma-Aldrich

Instruments

Instrument	Manufacturer	Model
Bench centrifuge	Thermo Scientific	Heraeus Multifuge X1R
Floor centrifuge	Thermo Scientific	Thermo Scientific™ Sorvall™ LYNX™
Spectrophotometer	Agilent Technologies, Inc.	Cary 100 UV-Vis
Multi-Mode Microplate Reader	BioTek®	Synergy™ H4
Confocal Microscope	Zeiss	LSM 700
Flow cytometer	BD Bioscience	FACSCalibur™ Flow Cytometer
Thermal cycler	Applied Biosystem	GeneAmp PCR System 9700
StepOnePlus™ Real-Time PCR System Scientific	Thermo Fisher	StepOnePlus™
RP-HPLC	Shimatzu	Prominence Shimadzu HPLC-MS
FPLC	Cytiva	ÄKTA pure protein purification system
Spectropolarimeter	JASCO, Inc.	Jasco J-715
Spectrofluorometer	HORIBA, Ltd.	Fluoromax-4
Liofilizator	Thermo Scientific	Heto PowerDry PL6000
Transilluminator	Bio-Rad	ChemiDoc™

Power supply (gel electrophoresis)	Bio-Rad	PowerPac Basic
Semi-Dry transfer cell	Bio-Rad	Trans-Blot
Spectrometer	Thermo Scientific	NanoDrop 8000
Gel chamber	Bio-Rad	Mini Trans-Blot®
Cell Incubator	Thermo Fisher Scientific	HERAcell 150
Sonicator	SONICS Inc.	Vibra-Cell CV334